

# MIXED-SYMMETRY SHELL-MODEL CALCULATIONS IN NUCLEAR PHYSICS

A Dissertation

Submitted to the Graduate Faculty of the  
Louisiana State University and  
Agricultural and Mechanical College  
in partial fulfillment of the  
requirements for the degree of  
Doctor of Philosophy

in

The Department of Physics and Astronomy

by

Vesselin Gueorguiev Gueorguiev  
M.S. Sofia University, 1992  
December, 2002

# Dedication

At the end of my Ph.D. study program, I look back in time and think of the events and people that have taught, encouraged and supported me in my study of physics. I would never forget the events of Summer of 1982 that set the direction of my profession. That year I finished middle school and had to make a decision on a high school. Since I had shown interest in mathematics, physics, and technology, my mother recommended that I apply to the National Natural Science High School in Sofia, Bulgaria. I spent the whole summer reviewing my school books in mathematics and physics. That was the first time in my life that I had to concentrate on a broad range of information, extract the essential elements, and commit them to memory. I discovered the joy and satisfaction of learning, problem solving, and overcoming obstacles through hard work. Due to the quality of the National Natural Science High School and my superior performance, I was accepted in the Sofia University as a physics student where I continued to acquire knowledge in physics and mathematics. I am thankful to my school teachers, many of whom were professors in physics at the Sofia University, for keeping me interested in physics and the natural sciences. My interest in theoretical physics jelled during my final years at the Sofia University where I attended many lectures on various subjects in mathematical and theoretical physics. It was then that I became interested in symmetries and group theory, and especially the newly emerging concept of quantum (deformed) Lie algebras.

The next important event in my life was the choice of a professor for my master thesis. I still remember going from one professor to another looking for someone who was working on quantum algebras. Finally, I met my M.S. advisor, Professor R. P. Roussev at the Institute of Nuclear Research and Nuclear Energy of the Bulgarian Academy of Sciences, Sofia, Bulgaria. After a few short meetings with Professor Roussev and his coworkers, Professors P. P. Raychev and A. I. Gueorguieva, I was given a paper, one of the fundamental papers on the topic, to read and explain. Back then, I did not see this as another test that I had to pass, rather I thought of it as an opportunity to show what I had learned and what I was capable of doing. Not until many years later did I appreciate that this was a defining time for me, one that enabled me to continue working with and learning from Professor Roussev and his colleagues, with all of whom I became a good friend. Working with them was one of the best research experiences in my life. I am very thankful to them for their time, help, interesting conversations, and long hours spent in lengthy calculations and hard work. I am also grateful to many other colleagues at the Institute of Nuclear Research and Nuclear Energy of the Bulgarian Academy of Sciences that I had a chance to meet and work

with. My next opportunity came as a surprise to me. I was not planning on going abroad as I was married to a wonderful wife, I had great colleagues, and I found my work to be very rewarding. But the challenge I faced was not mine alone, it was a problem for Bulgaria as it was for most other eastern European countries – limited opportunities due to political upheaval and difficult economic times.

In the spring of 1994 I met Professor Jerry P. Draayer at the Annual Bulgarian International Workshop on Nuclear Theory, Rila Mountains, Bulgaria. As a result, I guess, of a conversation between Professors J. P. Draayer and A. I. Gueorguieva – a conversation that I know very little about – I was offered the chance to come to Louisiana State University as a Ph.D. student in Professor J. P. Draayer’s group. This was an honor I could not turn down. I am very grateful to my advisor Professor J. P. Draayer who gave me the opportunity to learn and work in a different international culture and environment, and to experience and enjoy interactions with teachers, students, and participants at many workshops and conferences in the United States and abroad. I am also very grateful to Professor J. P. Draayer and his wife Lois for their hospitality and the valuable and pleasant time spent in their home.

I also would like to thank the International Hospitality Foundation, and especially my host family, Professor R. Imlay and his wife Dena Imlay, for their warm hospitality and valuable introduction to the American Culture. I am very grateful to Thomas Beuschel and Kenneth Bernstein, who helped me out in my first days in Baton Rouge; to Jutta Escher, Gabriela Popa and Ivan Chompalov for their continuing support through the years; as well as to the other recent and former graduate students in the Nuclear Theory group at Louisiana State University who contributed to a stimulating work environment. I am also grateful to Professor A. I. Gueorguieva, Dr. Ulrich Eichmann, and Kristina Sviratcheva for their friendship and support.

At last, but not least, I cannot find words and space to write my extreme gratefulness to my beloved wife Petia and our precious children Anna and Alex for their support and understanding, and to my mother, father, and sister, and to my relatives for the support they have provided through the years.

# Acknowledgments

First of all, I wish to express my sincere gratitude to my advisor, Professor Jerry P. Draayer, who suggested my Ph. D. project and provided the necessary environment for its realization through his guidance, patience, and understanding. I would like also to acknowledge the help of Dr. W. E. Ormand and C. Johnson with whom two major topics were studied, the structure of the  $^{24}\text{Mg}$  nucleus, and the  $\text{SU}(3)$  symmetry breaking in the lower  $pf$ -shell; discussions with Professor A. Rau with whom the toy model was worked out; and interesting conversations and discussions with Dr. C. Bahri.

I would like to thank Professors E. Zganjar, R. Haymaker, A. Rau, and C. Johnson from the Department of Physics and Astronomy, and A. Raman, from the Department of Mechanical Engineering, for their comments and suggestions, and for serving on my dissertation committee. I am grateful to the professors and administrative personnel in the Department of Physics and Astronomy for educational, technical, and administrative help, as well as for their friendly and kindly attitude. My thanks go also to my recent and former colleagues and friends in the Nuclear Theory group and in the Department of Physics and Astronomy. I am grateful to the LSU Writing Center for providing help in the preparation of my dissertation manuscript and especially to Dr. Joe Abraham and Lauren Moise.

I wish to acknowledge the financial support from the Department of Physics and Astronomy, a dissertation fellowship from the Louisiana State University Graduate School, a travel grant from the Charles E. Coates Memorial Fund, and the U. S. National Science Foundation support under Grant No. PHY-9970769 and Cooperative Agreement No. EPS-9720652 that includes matching from the Louisiana Board of Regents Support Fund.

# Table of Contents

DEDICATION . . . . .	ii
ACKNOWLEDGMENTS . . . . .	iii
LIST OF TABLES . . . . .	viii
LIST OF FIGURES . . . . .	ix
ABSTRACT . . . . .	xiii
1 INTRODUCTION . . . . .	1
2 THE NUCLEAR SHELL MODEL . . . . .	4
2.1 Magic Numbers in Nuclei . . . . .	4
2.2 The Nuclear Interaction . . . . .	5
2.3 Hamiltonian in Second Quantized Form . . . . .	5
2.4 Spherical Shell Model for Nuclei . . . . .	6
2.4.1 Single-Particle Basis . . . . .	6
2.4.2 Many-Particle Basis . . . . .	7
2.4.3 Configuration Truncation and the M-scheme Basis . . . . .	7
2.5 The SU(3) Shell Model for Nuclei . . . . .	9
2.5.1 Labeling of the States in Elliott's SU(3) Model . . . . .	9
2.5.2 SU(3) Truncation Scheme . . . . .	11
2.5.3 Interactions that Break the SU(3) Symmetry . . . . .	12
3 TOY MODEL OF A TWO-MODE SYSTEM . . . . .	14
3.1 Harmonic Oscillator in a One-Dimensional Box . . . . .	15
3.2 Spectral Structure at Different Energy Scales . . . . .	17
3.3 Toy Model Calculations and Results . . . . .	21
3.3.1 On the Hilbert Space of the Basis Wave Functions . . . . .	21
3.3.2 Discussion of the Toy Model Results . . . . .	26

4	OBLIQUE SHELL-MODEL BASICS . . . . .	33
4.1	Generalized Eigenvalue Problem . . . . .	33
4.2	Geometrical Visualization of the Oblique Basis . . . . .	36
4.3	The Lanczos Algorithm . . . . .	36
4.4	Mixed-Symmetry Basis for the Nuclear Shell Model . . . . .	38
4.4.1	Spherical Basis for Single-Particle Excitations . . . . .	38
4.4.2	SU(3) Basis for Collective Excitations . . . . .	39
5	<sup>24</sup> Mg MIXED-SYMMETRY CALCULATIONS . . . . .	47
5.1	Structure of the Model Spaces . . . . .	47
5.1.1	Model Space Dimensions . . . . .	48
5.1.2	Visualizing the Oblique Basis for <sup>24</sup> Mg . . . . .	48
5.2	Spectral Characteristics . . . . .	49
5.2.1	Ground-State Energy . . . . .	49
5.2.2	Energy and Angular Momentum of the Low Lying States . . . . .	50
5.3	Overlaps with the Full <i>sd</i> -shell Calculation . . . . .	50
6	STUDY OF LOWER <i>pf</i> -SHELL NUCLEI . . . . .	59
6.1	<sup>44</sup> Ti Oblique-Basis Results . . . . .	60
6.1.1	Model Space Dimensions . . . . .	60
6.1.2	Ground-State Energy . . . . .	61
6.1.3	Energy Spectrum of the Low Lying States . . . . .	61
6.1.4	Overlaps with the Exact Calculation . . . . .	62
6.2	Set Up for the Study of the SU(3) Breaking . . . . .	62
6.2.1	Interaction Hamiltonian . . . . .	62
6.2.2	Computational Procedures . . . . .	65
6.3	Measuring Symmetry Breaking Using $C_2$ of SU(3) . . . . .	67
6.3.1	Spectral Distribution . . . . .	67
6.3.2	Moments of the Spectral Distributions. . . . .	70
6.3.3	Coherent Spectral Structure . . . . .	70
6.3.4	Enhanced Electromagnetic Transitions. . . . .	73
7	SUMMARY AND DISCUSSIONS . . . . .	79
	BIBLIOGRAPHY . . . . .	83
A	ON THE WAVE FUNCTION SPREAD AND LOCALIZATION . . . . .	90
B	VARIATIONALLY-IMPROVED BASIS METHOD . . . . .	96
C	ON THE LOSS OF HERMITICITY . . . . .	99
D	COHERENT BEHAVIOR, QUASI-SYMMETRIES AND QUASI-LABELS . . . . .	101

E	GUIDE TO THE OBLIQUE-BASIS PACKAGE . . . . .	103
E.1	Generating Basis States . . . . .	104
E.2	Generating Interaction Files . . . . .	105
E.3	Running the Main Routines . . . . .	105
VITA	. . . . .	107

# List of Tables

5.1	Labels and $M_J = 0$ dimensions for various $^{24}\text{Mg}$ calculations. The leading SU(3) irrep is denoted by (8,4) while (8,4)&(9,2) implies that (9,2) irreps have also been included. The SM( $n$ ) spaces correspond to spherical shell-model partitions with $n$ valence particles excited out of the $d_{5/2}$ shell into the $s_{1/2}$ and $d_{3/2}$ levels. . . . .	48
6.1	Labels and $M_J = 0$ dimensions for various $^{44}\text{Ti}$ oblique calculations. . . . .	60
6.2	Space dimensions for the $m$ -scheme calculations in the full $pf$ -shell model space. We have used even parity and even isospin basis states with no restrictions on the total angular momentum $J$ except for the $M_J = 0$ case where only states with even $J$ values have been selected. . . . .	66

# List of Figures

2.1	Three-dimensional view of the $(\lambda, \mu)$ $SU(3)$ irrep. . . . .	10
3.1	Two-mode toy system. The structure of the interaction potential of a particle in a one-dimensional box subject to a harmonic oscillator restoring force towards the center of the box. . . . .	18
3.2	Spectral structure of the two-mode system for $m = \hbar = 2L/\pi = 1$ and $\omega = 4$ . . . . .	19
3.3	Spreading of the wave functions for the harmonic oscillator (blue) and particle in a box (red). . . . .	22
3.4	Harmonic-oscillator trial wave functions adjusted with respect to the one-dimensional box problem: (a) adjusted according to the potential width $E_n^{1Dbox} = \omega_n^2 L^2/2 \Rightarrow \omega_n = \frac{\hbar}{L^2} (1 + 2n)$ , (b) nodally adjusted, (c) boundary adjusted using $\Psi(q) \rightarrow \Psi(q) - \Psi(L)(1 + q/L)/2 - \Psi(-L)(1 - q/L)/2$ . . . . .	25
3.5	Absolute deviations from the exact energy eigenvalues for $\omega = 16$ , $L = \pi/2$ , $\hbar = m = 1$ as a function of $n$ . Blue circles represent deviation of the exact energy eigenvalue from the corresponding harmonic oscillator eigenvalue ( $\Delta E = E_n^{exact} - E_n^{HO}$ ), the red diamonds are the corresponding deviation from the energy spectrum of a particle in a 1D box ( $\Delta E = E_n^{exact} - E_n^{1D}$ ), and the green squares are the first-order perturbation theory results. . . . .	27
3.6	Relative deviations from the exact energy eigenvalues for $\omega = 16$ , $L = \pi/2$ , $\hbar = m = 1$ as a function of $n$ . The blue circles represent deviation of the exact energy eigenvalue from the corresponding harmonic oscillator eigenvalue ( $\Delta E/E = 1 - E_n^{HO}/E_n^{exact}$ ), the red diamonds are the corresponding relative deviation from the energy spectrum of a particle in a 1D box ( $\Delta E/E = 1 - E_n^{1D}/E_n^{exact}$ ), and the green squares are the first-order perturbation theory results. . . . .	28
3.7	Non-zero components of the 105th exact eigenvector in the basis of a free particle in a one-dimensional box. Parameters of the Hamiltonian are $\omega = 16$ , $L = \pi/2$ , $\hbar = m = 1$ . . . . .	29
3.8	Non-zero components of the third harmonic oscillator eigenvector as expanded in the basis of a free particle in a one-dimensional box. Parameters of the Hamiltonian are $\omega = 16$ , $L = \pi/2$ , $\hbar = m = 1$ . . . . .	30

3.9	Coherent structure with respect to the non-zero components of the 25th, 27th and 29th exact eigenvector in the basis of a free particle in a one-dimensional box. Parameters of the Hamiltonian are $\omega = 16$ , $L = \pi/2$ , $\hbar = m = 1$ . . . . .	32
4.1	Three-dimensional view of the $(\lambda, \mu)$ $SU(3)$ irrep together with the action of the $SU(3)$ step operators. . . . .	41
4.2	Ordering scheme of the single-particle levels. . . . .	42
4.3	Action of the $SU(3)$ generators on the single particle levels. The diagram on the left shows that applying an $SU(3)$ generator to a single-particle state results in another single-particle state. The diagram on the right shows the action of the six non-diagonal generators of $SU(3)$ . The vertical solid lines represent the action of the $SU(2)$ subgroup that enters the $SU(3) \supset SU(2) \otimes U(1)$ chain. . . . .	43
4.4	Highest weight state of the leading $(3, 3)$ irrep for $N = 6$ and $S = 1$ in the $sd$ -shell. . . . .	45
4.5	Highest weight state of the leading $(6, 0)$ irrep for $N = 6$ and $S = 0$ in the $sd$ -shell. . . . .	45
5.1	Orthogonality of the basis vectors in the oblique geometry. The $SU(3)$ space consists of $(8,4)$ & $(9,2)$ basis vectors with the shell-model spaces (SM( $n$ )) with $n=2$ and 4) indicated by a horizontal line. (a) SM(2) and the natural $SU(3)$ basis vectors and (b) SM(4) and the natural $SU(3)$ basis vectors. In the latter case (b), there are five $SU(3)$ vectors that lie in the SM(4) space. . . . .	49
5.2	Calculated ground-state energy for $^{24}\text{Mg}$ . Ground-state energy as a function of the various model spaces. Note the dramatic increase in binding (3.3 MeV) in going from SM(2) to SM(2)+two $SU(3)$ irreps, $(8,4)$ & $(9,2)$ , (a 0.5% increase in the dimensionality of the model space). Enlarging the space from SM(2) to SM(4) (a 54% increase in the dimensionality of the model space) adds 4.2 MeV in binding energy. . . . .	51
5.3	Structure of the energy levels for $^{24}\text{Mg}$ for different calculations. Pure $m$ -scheme spherical basis calculations are on the left-hand side of the graph; pure $SU(3)$ basis calculations are on the right-hand side; the spectrum from the FULL space calculation is in the center. . . . .	52
5.4	Energy levels for $^{24}\text{Mg}$ as calculated for different oblique bases. The SM(4) basis calculation is included for comparison. . . . .	53
5.5	Overlaps of the pure spherical and $SU(3)$ with the FULL states. The first four bars represent the SM(0), SM(1), SM(2), and SM(4) calculations, the next two bars represent $SU(3)$ calculations, etc. . . . .	54
5.6	Overlaps of the oblique-basis states with the exact states (set I). Inset SM contains the overlaps for the pure spherical shell-model basis states only. Inset SM+(8,4) contains the overlaps of the SM basis enhanced by the leading $SU(3)$ irrep (8,4). Inset SM+(8,4)&(9,2) has the (9,2) irreps included as well. . . . .	56

5.7	Overlaps of the oblique-basis states with the exact states (set II). Each inset represents a particular SM(n)-type calculation, showing how the overlaps change along the corresponding oblique-basis calculation. . . . .	57
5.8	Representative overlaps of pure SM(n), pure SU(3), and oblique-basis results with the exact full <i>sd</i> -shell eigenstates. A number within a bar denotes the state with the overlap shown by the bar if it is different from the number for the exact full-space calculation shown on the abscissa. For example, for SM(2) the third eigenvector overlaps the most with the fourth exact eigenstate, not the third, while the fifth SM(2) eigenvector has the overlap shown with the third exact eigenstate. . . . .	58
6.1	Ground-state energy for $^{44}\text{Ti}$ as a function of the various model spaces. The SU(3) irreps used are (12,0) and (10,1). . . . .	61
6.2	Structure of the energy levels for $^{44}\text{Ti}$ for different calculations. . . . .	63
6.3	$^{44}\text{Ti}$ wave function overlaps of pure spherical, SU(3), and oblique states with the FULL states. The first four bars in the upper graph represent the SM(0), SM(1), SM(2), and SM(3) calculations, the next two bars represent the SU(3) calculations, etc. Representative overlaps of pure SM(n), pure SU(3), and oblique-basis results with the exact full <i>pf</i> -shell eigenstates are shown in the lower graph. . . . .	64
6.4	Strength distribution of $C_2$ of $SU(3)$ in yrast states of $^{44}\text{Ti}$ for realistic single-particle energies with Kuo-Brown-3 two-body interaction ( <i>KB3</i> ). . . . .	68
6.5	Strength distribution of $C_2$ of $SU(3)$ in yrast states of $^{44}\text{Ti}$ for degenerate single-particle energies with Kuo-Brown-3 two-body interaction ( <i>KB3p-f</i> ). . . . .	69
6.6	Average $C_2$ values for <i>KB3</i> and <i>KB3p-f</i> interactions in $^{44}\text{Ti}$ . . . . .	71
6.7	Average $C_2$ values for <i>KB3</i> and <i>KB3p-f</i> interactions in $^{48}\text{Ti}$ . . . . .	72
6.8	Coherent structure of the first three yrast states in $^{48}\text{Cr}$ calculated using realistic single-particle energies with Kuo-Brown-3 two-body interaction ( <i>KB3</i> ). On the horizontal axis is $C_2$ of $SU(3)$ with contribution of each $SU(3)$ state to the corresponding yrast state on the vertical axis. . . . .	74
6.9	Coherent mixing and SU(3) breaking and recovery in $^{48}\text{Cr}$ . Inset (a) demonstrates the coherent structure of the yrast states with respect to the spherical shell-model configuration basis ( <i>KB3</i> ); (b) coherent structure of the yrast states with respect to the SU(3) basis ( <i>KB3</i> ); (c) recovery of the SU(3) symmetry within the <i>KB3p-f</i> interaction. . . . .	75
6.10	Relative $B(E2)$ values $\left(\frac{B(E2:J_i \rightarrow J_f)}{B(E2:2^+ \rightarrow 0^+)}\right)$ for $^{44}\text{Ti}$ . The $B(E2 : 2^+ \rightarrow 0^+)$ transition values are $122.69e^2 fm^4$ for the experiment, $104.82e^2 fm^4$ for the <i>KB3</i> interaction, and $138.58e^2 fm^4$ for the <i>KB3p-f</i> case. . . . .	76

6.11	Relative $B(E2)$ values $\left(\frac{B(E2:J_i \rightarrow J_f)}{B(E2:2^+ \rightarrow 0^+)}\right)$ for $^{46}\text{Ti}$ . The $B(E2 : 2^+ \rightarrow 0^+)$ transition values are $199.82e^2 fm^4$ for the experimental data, $181.79e^2 fm^4$ for the updated experimental data, $208e^2 fm^4$ for KB3 interaction, and $299.83e^2 fm^4$ for <i>KB3p-f</i> . . . . .	77
6.12	Relative $B(E2)$ values $\left(\frac{B(E2:J_i \rightarrow J_f)}{B(E2:2^+ \rightarrow 0^+)}\right)$ for $^{48}\text{Ti}$ . The $B(E2 : 2^+ \rightarrow 0^+)$ transition values are $144.23e^2 fm^4$ for the experimental data, $155.5e^2 fm^4$ for the updated experimental data, $202.4e^2 fm^4$ for KB3 interaction, and $445.32e^2 fm^4$ for <i>KB3p-f</i> . . . . .	78
A.1	Ground-state convergence for the harmonic-oscillator problem with $\Omega = 1$ using squeezed basis states. The number of basis states needed for $10^{-4}$ convergence accuracy of the ground-state eigenvalue is shown in green squares. The red circles are for the ground-state eigenfunction. . . . .	92
A.2	Role of the wave function spread. (a) Stretched basis states with $\omega = 0.2$ within the harmonic-oscillator potential $\Omega = 1$ . (b) Consecutive approximations of the harmonic-oscillator ground state (red) using the stretched basis states. (c) Squeezed basis states with $\omega = 4$ within the harmonic-oscillator potential $\Omega = 1$ . (d) Consecutive approximations of the harmonic-oscillator ground state (red) using the squeezed basis states. . . . .	93
A.3	Ground-state convergence for the harmonic-oscillator problem with $\Omega = 1$ using coherent basis states. The number of basis states needed for $10^{-4}$ convergence accuracy of the ground-state eigenvalue is shown with the green squares. The red circles are for the ground-state eigenfunction. . . . .	94
A.4	Role of the wave function localization. (a) Coherent basis states with displacement $\xi = -2$ within the harmonic-oscillator potential $\Omega = 1$ . (b) Consecutive approximations of the harmonic-oscillator ground state (red) using the coherent basis states. . . . .	95

# Abstract

Advances in computer technologies allow calculations in ever larger model spaces. To keep our understanding growing along with this growth in computational power, we consider a novel approach to the nuclear shell model. The one-dimensional harmonic oscillator in a box is used to introduce the concept of an oblique-basis shell-model theory. By implementing the Lanczos method for diagonalization of large matrices, and the Cholesky algorithm for solving generalized eigenvalue problems, the method is applied to nuclei. The mixed-symmetry basis combines traditional spherical shell-model states with SU(3) collective configurations. We test the validity of this mixed-symmetry scheme on  $^{24}\text{Mg}$  and  $^{44}\text{Ti}$ . Results for  $^{24}\text{Mg}$ , obtained using the Wilthenthal USD interaction in a space that spans less than 10% of the full-space, reproduce the binding energy within 2% as well as an accurate reproduction of the low-energy spectrum and the structure of the states – 90% overlap with the exact eigenstates. In contrast, for an  $m$ -scheme calculation, one needs about 60% of the full space to obtain compatible results. Calculations for  $^{44}\text{Ti}$  support the mixed-mode scheme although the pure SU(3) calculations with few irreps are not as good as the standard  $m$ -scheme calculations. The strong breaking of the SU(3) symmetry results in relatively small enhancements within the combined basis. However, an oblique-basis calculation in 50% of the full  $pf$ -shell space is as good as a usual  $m$ -scheme calculation in 80% of the space. Results for the lower  $pf$ -shell nuclei  $^{44-48}\text{Ti}$  and  $^{48}\text{Cr}$ , using the Kuo-Brown-3 interaction, show that SU(3) symmetry breaking in this region is driven by the single-particle spin-orbit splitting. In our study we observe some interesting coherent structures, such as coherent mixing of basis states, quasi-perturbative behavior in the toy model, and enhanced B(E2) strengths close to the SU(3) limit even though SU(3) appears to be rather badly broken. The results suggest that a mixed-mode shell-model theory may be useful in situations where competing degrees of freedom dominate the dynamics, and full-space calculations are not feasible.

# Chapter 1

## Introduction

Selecting the right basis to perform calculations is a very essential step in analyzing any eigenvalue problem; it is especially true for many body quantum mechanical problems. When performing calculations, symmetries are also very important. Each of the fundamental quantities, such as energy ( $E$ ), linear momentum ( $p$ ), and angular momentum ( $L$ ), is conserved due to an exact symmetry of the physical space. It is well known that energy conservation is due to time translational symmetry, linear momentum conservation is due to space translational symmetry, and angular momentum conservation is related to rotational symmetry. Any mathematical description used in physics takes advantage of these symmetries and incorporates them explicitly. For example, in the Lagrangian (Hamiltonian) formalism, the Lagrangian (Hamiltonian) of the system is explicitly invariant with respect to the fundamental symmetries, such as time translation, space translation and space rotation. Most examples of exactly solvable problems come from systems with some type of symmetry [1].

The notion of a stable equilibrium state, which is often related to an energy minimum, is another very important concept in physics. If  $\vec{x}_0$  is an equilibrium point of the Hamiltonian function ( $H$ ) for a classical particle, then  $H$  can conveniently be expressed in a Taylor series around  $\vec{x}_0$ :

$$H = \frac{1}{2m}\vec{p}^2 + \frac{1}{2}k(\vec{x} - \vec{x}_0)^2 + \mathcal{O}(\Delta x^4).$$

This way, the harmonic oscillator described by the Hamilton  $H = \frac{1}{2m}\vec{p}^2 + \frac{1}{2}k\vec{x}^2$  turns out to be one of the most important model systems in physics with many applications [2].  $SU(n)$  is the symmetry group of the  $n$ -dimensional harmonic oscillator, while  $Sp(2n, R)$  is the corresponding dynamical group. Thus, the  $SU(3)$  symmetry of the three-dimensional harmonic oscillator is a very important approximate symmetry of a system near equilibrium.

Symmetries are very useful in the construction of shell-model structures in nuclear physics as well as in atomic physics. A shell-model structure is based on some exactly solvable limit of an effective interaction potential. An exactly solvable system allows for a well defined set of basis states. In particular, if bound states exist, they can be considered as single-particle levels of the system. Usually, a shell model assumes a mean field with which the particles of the system interact. For example, in atomic physics, the shell structure is mainly due to

the Coulomb field of the nucleus, while in nuclear physics the mean field is often taken to be the Hartree-Fock mean field. In this approach, the particle-particle interaction is assumed to be incorporated as much as possible in the average mean field. In particular, the nuclear spherical shell model is very successful in the description of nuclei [3]. Despite the enormous success of the spherical shell model, it is generally difficult to deal with nuclei in the middle of the shell (mid-shell nuclei) using this model. For such nuclei the collective degrees of freedom are very essential and the shell-model configuration space is very big. Therefore, for these nuclei, a shell model based on the collective degrees of freedom is more appropriate. Elliott's  $SU(3)$  model is useful for understanding the collectivity in light nuclei, up to  $A < 28$  ( $sd$ -shell) [4]. For heavier nuclei with  $A > 80$ , the pseudo- $SU(3)$  version of Elliott's model is very successful in the description of the collective modes [5]. For these nuclei ( $A > 80$ ), the deformed Nilsson model is more accurate in the description of the single-particle levels than the simple spherical shell model [6].

At least in principle, collective phenomena, such as rotational spectra with strong  $B(E2)$  transitions, should be reproduced by the microscopic models. However, to do so using the spherical shell model, one needs sufficiently many particle configurations. Unfortunately, the dimensionality of the space grows combinatorially with the number of particles placed in the allocated levels. This binomial growth is a major computational problem. On the other hand, the  $SU(3)$  model allows for a good understanding of the collective nuclear properties in light and heavy mid-shell nuclei. However, for nuclei near closed shells, the spherical shell model is more favorable due to the dominance of the single-particle phenomena in these nuclei [7]. Therefore, it seems plausible to consider a hybrid-type calculation that uses these two models. In general, the two bases, the spherical shell-model basis and the  $SU(3)$  shell-model basis, will not be orthogonal to each other. Such a calculation can be considered as an “**oblique**” basis shell-model calculation [8].

The oblique-basis calculation for nuclei is the subject of the research presented here. Oblique-basis calculations are expected to be of a practical value in systems with competing degrees of freedom. For example, our study shows the relevance of the oblique calculation in the case of  $^{24}\text{Mg}$ . For this nucleus, the single particle excitations described by the spherical shell model and the collective excitations described by the  $SU(3)$  shell model are important. When we combine the two bases, we obtain a significant gain in the convergence of the low-energy spectra towards the full space result. In particular, the addition of the leading- $SU(3)$  irreducible representations (irreps) yields the right placement of the  $K = 2$  band and the correct order for most of the low-lying levels. Indeed, an even more detailed analysis shows that the structure of the low-lying states is significantly improved through the addition of a few  $SU(3)$  irreps.

The oblique-basis calculation will be an unnecessary numerical complication for systems where one of the excitation modes is dominant. For example, in the lower  $pf$ -shell nuclei  $^{44}\text{Ti}$  and  $^{48}\text{Cr}$ , the spherical shell model gives a significant part of the low-energy wave functions within a few spherical shell-model configurations, while in the  $SU(3)$  shell-model basis one will need more than a few  $SU(3)$  irreps. This fact is mainly due to the strong breaking of the  $SU(3)$  in the lower  $pf$ -shell induced by the spin-orbit interaction [7]. In spite of the results

in the lower  $pf$ -shell, it is expected that in the mid-shell region some sort of  $SU(3)$  collective structure will gain importance <sup>1</sup>. If this is to happen, then the oblique-basis calculation will be an important alternative for calculating the structure of nuclei, such as  $^{56}\text{Fe}$  and  $^{56}\text{Ni}$ .

Results of the shell-model calculations for lower  $pf$ -shell nuclei show that  $SU(3)$  symmetry breaking in this region is driven by the single-particle spin-orbit splitting. However, even though states of the yrast band exhibit  $SU(3)$  symmetry breaking, the results also show that the yrast band  $B(E2)$  values are insensitive to this fragmentation of the  $SU(3)$  symmetry; specifically, the quadrupole collectivity as measured by  $B(E2)$  transition strengths between low-lying members of the yrast band remain high even though  $SU(3)$  appears to be broken. Results for  $^{44,46,48}\text{Ti}$  and  $^{48}\text{Cr}$  using the Kuo-Brown-3 two-body interaction [9] are given to illustrate these observations.

---

<sup>1</sup>It was pointed by Chairul Bahri that the deformed Nilsson diagram for the  $pf$ -shell suggest a pseudo  $SU(3)$  symmetry. Another alternative could be a quasi- $SU(3)$  symmetry.

# Chapter 2

## The Nuclear Shell Model

In some sense, the shell structure of nuclei is more complicated than the shell structure of atoms. The shell structure of atoms is due to the Coulomb force between the nucleus and the electrons. It may be a nice coincidence, but it is a fact that the Coulomb potential problem in quantum mechanics is an exactly solvable problem [2]. In the case of nuclei, the situation is more complicated. The reason is that there is no single source of a central potential. Instead, all nucleons are considered to act together, generating a mean field. Within this mean field, the problem is more tractable [3]. Here, we do not consider the problem of how to obtain the mean-field potential. Instead, we just use some general symmetry properties that a phenomenological potential and a realistic effective interaction should obey. These symmetry properties provide insight about the relevant single-particle basis within which one can consider the problem.

### 2.1 Magic Numbers in Nuclei

Maria G. Mayer's discussion of the magic numbers in nuclei has clearly demonstrated the nuclear shell structure associated with the independent-particle model for nuclei [10]. In this model, each closed-shell configuration provides a convenient first approximation. In this approximation, one can assume that the system under consideration consists of a closed-shell core plus valence particles in a valence shell. This approach very successfully explains the ground state properties of nuclei [11].

In order to understand and obtain qualitatively good results for the structure of the excited states, one has to consider a configuration mixing in the valence space. This usually leads to a very big model space. Therefore, a further truncation scheme is required. In this chapter, we will discuss two main approaches used in the nuclear shell model, namely the spherical shell-model truncation scheme and the  $SU(3)$  shell-model truncation schemes.

## 2.2 The Nuclear Interaction

From a fundamental point of view, the problem of the relevant nucleon-nucleon interaction is very important. However, it is outside the scope of the research presented here. Even when one is provided with a good phenomenological nucleon-nucleon interaction, there is a lot of hard work to be done before one can finally set things up and calculate some experimentally meaningful results. Usually, a Hartree-Fock procedure is employed to reduce the many-particle Schrödinger equation to a single-particle Schrödinger equation with a self-consistent mean field. Once the single-particle states and energies are defined, then the  $n$ -particle configurations are formed using Slater determinants. Finally, a configuration mixing is used to take into account some of the residual interaction. This process may be simplified by using a phenomenological single-particle potential and a realistic interaction with a set of parameters adjusted to fit the experimental data.

In this section, we consider a phenomenological interaction that contains some effective one-body and two-body potentials that are obtained from the original two-body nucleon-nucleon interaction:

$$H = \sum_{i=1}^A T_i + \frac{1}{2} \sum_{i \neq j}^A V(|r_i - r_j|) \rightarrow \sum_{s \in \{\text{valence particles}\}} (t_s + U_s) + V_{res}.$$

$T_i$  is the kinetic energy of the  $i$ -th nucleon,  $V(|r_i - r_j|)$  is the two-body nucleon-nucleon interaction,  $t_s$  is an effective one-body kinetic energy of the valence particles,  $U_s$  is the effective mean-field potential, and  $V_{res}$  is the effective residual two-body interaction between the valence particles [3]. The effective one-body interaction  $H^{1b} = t + U$  provides a set of single-particle states:

$$H^{1b} \phi_i(x) = (t + U) \phi_i(x) = \varepsilon_i \phi_i(x).$$

The many-body wave function for a fermion system has to obey the Pauli principle. Thus, a fully antisymmetric combination, a Slater determinant, has to be constructed:

$$\Psi(\vec{x}_1, \dots, \vec{x}_n) = \det \begin{vmatrix} \phi_1(\vec{x}_1) & \phi_1(\vec{x}_2) & \cdots & \phi_1(\vec{x}_n) \\ \phi_2(\vec{x}_1) & \phi_2(\vec{x}_2) & \cdots & \phi_2(\vec{x}_n) \\ \vdots & \vdots & \ddots & \vdots \\ \phi_n(\vec{x}_1) & \phi_n(\vec{x}_2) & \cdots & \phi_n(\vec{x}_n) \end{vmatrix}.$$

Here, the single-particle wave functions  $\phi_m(\vec{x}_s)$  correspond to the  $s$ -th particle in the  $m$ -th single-particle state with quantum numbers depending on the exact symmetries of the single-particle problem. Usually, these quantum numbers include angular momentum ( $j$ ) and parity ( $\pi$ ).

## 2.3 Hamiltonian in Second Quantized Form

Given the single-particle levels, one can simplify the notation by going from the coordinate representation of the single-particle levels to an occupation representation. This process is

often called a second quantization since the wave functions are constructed from appropriate creation/annihilation tensor operators acting on a vacuum state:

$$\phi^{\alpha jm}(x) \rightarrow |\alpha jm\rangle = a_{\alpha jm}^+ |0\rangle.$$

Here,  $\alpha$  stands for other quantum numbers, such as harmonic-oscillator shell numbers, spin and isospin labels. The vacuum state  $|0\rangle$  is a reference state on which everything else is built. The vacuum state  $|0\rangle$  may have a different meaning depending on the quantum labels of the annihilation operators. The annihilation operators usually define the vacuum as follows:

$$a_{\alpha jm} |0\rangle = 0.$$

For example, if  $a_{\alpha jm}^+$  and  $a_{\alpha jm}$  represent some real particles, such as fermions, then clearly the vacuum state is a state of no particles at all. If  $a_{\alpha jm}^+$  and  $a_{\alpha jm}$  represent the valence nucleons, then the vacuum state  $|0\rangle$  would represent the closed-shell core. In the forthcoming chapters, we consider  $|0\rangle$  to represent closed-shell nuclei. For example,  $^{16}\text{O}$  is the closed-shell nucleus when we study nuclei in the valence  $sd$ -shell;  $^{40}\text{Ca}$  is the closed-shell nucleus when we study nuclei in the valence  $pf$ -shell.

In this second quantized form, the effective Hamiltonian is:

$$H = \sum_i \varepsilon_i a_i^+ a_i + \frac{1}{4} \sum_{i,j,k,l} V_{ij,kl} a_i^+ a_j^+ a_k a_l. \quad (2.1)$$

Here,  $\varepsilon_i$  are single-particle energies derived from excitation spectra of one valence particle system, i.e.  $^{17}\text{O}$  in the case of the  $sd$ -shell. The  $V_{kl,ij}$  are two-body matrix elements derived from an initial approximation, which are improved by a data fitting across the range of nuclei in consideration. For example, in the case of the  $sd$ -shell we would use the 63 two-body matrix elements obtained by Wildenthal [12].

## 2.4 Spherical Shell Model for Nuclei

We have already mentioned the independent-particle model [11]. This model uses the harmonic-oscillator potential as an effective single-particle potential for nucleons [13] plus a spin-orbit interaction that provides for the correct shell closure [14]. In addition, there is a strong pairing part in the two-body interaction. The pairing interaction and the quadrupole-quadrupole interaction [14] are essential parts of the two-body interaction.

### 2.4.1 Single-Particle Basis

In computations based on the independent-particle basis, we use a phenomenological Hamiltonian (2.1) with single-particle levels labeled by the harmonic-oscillator quantum numbers  $nljm$  as follows:

- $n$  is the harmonic-oscillator shell,

- $l$  is the angular momentum quantum number,
- $j = l \pm \frac{1}{2}$  is the total angular momentum of the nucleon with spin  $1/2$ ,
- $m$  is the third projection of the total spin  $\vec{j}$ .

Within the above labeling scheme, the single-particle wave functions in the coordinate representation have the form:

$$\phi_{nlsjm}(x) = \langle x | nlsjm \rangle = \sum_{m=m_l+m_s} \langle lm_l, sm_s | jm \rangle R_{nl}(r) Y_{lm_l}(\theta, \varphi) \chi_{m_s}. \quad (2.2)$$

Here,  $\langle lm_l, sm_s | jm \rangle$  stand for the Clebsch-Gordan coefficients of  $SU(2)$ ,  $R_{nl}(r)$  are the radial wave functions,  $Y_{lm_l}(\theta, \varphi)$  are the spherical harmonics, and  $\chi_{m_s}$  are the internal spin  $\frac{1}{2}$  wave functions for nucleons.

## 2.4.2 Many-Particle Basis

In the occupation number representation, Slater determinant states are constructed from  $n_1 \dots n_k$  nucleons by means of the fermion particle creation operators  $a_i^+$ :

$$|n_1 \dots n_k\rangle = \prod_{s=1}^k (a_s^+)^{n_s} |0\rangle, \quad (2.3)$$

where the operators  $a_i^+$  and  $a_i$  obey a Fermi algebra:

$$\begin{aligned} a_i^+ a_j^+ + a_j^+ a_i^+ &= 0, \\ a_i a_j + a_j a_i &= 0, \\ a_i^+ a_j + a_j a_i^+ &= \delta_{ij}. \end{aligned}$$

Here, the labels of the operators  $a_i^+$  and  $a_i$  correspond to some specific quantum labels  $nlsjm$  of the spherical single-particle wave functions (2.2).

## 2.4.3 Configuration Truncation and the M-scheme Basis

Based on the independent-particle model, one can make an initial approximation to the wave functions of nuclei. This approximation uses the lowest energy configuration  $[n_1, \dots, n_k]$ , where  $n_i$  is the number of identical particles placed in the  $i$ -th orbital subject to the condition  $0 \leq n_i \leq 2j + 1$ . The energy of such a configuration is given by the expression  $E_{[n_1, \dots, n_k]} = \sum_i \varepsilon_i n_i$ . It is immediately clear that in general there would be some degeneracy. Thus, the proper description of the excitation spectrum would need the two-body part of the interaction to lift this degeneracy. However, even then, using only the few lowest energy configurations is not sufficient to describe properly collective excitons in the mid-shell nuclei.

For heavy mid-shell nuclei, one needs to include a significant number of configurations. One way to proceed and include many configurations is to consider many-particle states with good  $J$  and  $M_J$  via  $SU(2)$  coupling within each configuration. Codes based on this approach usually rely heavily on  $3j$ ,  $6j$ , and higher  $SU(2)$  symbols [15, 16]. Since these  $j$ -symbols are calculated repeatedly, an efficient  $SU(2)$  package and a smart way to store often used coefficients are very essential. Recently, an  $SU(3)$  code using the same strategy has been successfully developed [17]. This code relies on a very efficient data storage technique [18].

An alternative computational method is the  $M$ -scheme approach [19]. In this approach, instead of using states with good  $J$  and  $M_J$ , one uses only states with good  $M_J$  and lets the Hamiltonian select the states of good  $J$ . Diagonalizing the Hamiltonian in such a basis results in a few of the lowest energy eigenstates. The  $M$ -scheme set of states is convenient since  $M_J$  is an additive quantum number. In order to provide for good total angular momentum ( $J$ ), one has to include all states of fixed  $M_J$  within a given configuration. This method relies heavily on large matrix diagonalization algorithms. One such algorithm is the Lanczos algorithm which is very fast and efficient [20]. The Lanczos algorithm is a cornerstone of the modern  $M$ -scheme shell-model codes [21].

To illustrate the spherical shell-model truncation scheme, we consider  $^{24}\text{Mg}$ . For this nucleus, the lowest configuration providing the initial approximation to the ground state is  $0s^4 0p^{12} 0d_{5/2}^8 1s_{1/2}^0 0d_{3/2}^0$ . Here,  $0s^4 0p^{12}$  is the core nucleus  $^{16}\text{O}$ ; the valence space is  $0d_{5/2} 1s_{1/2} 0d_{3/2}$  with the lowest configuration of 8 particles, 4 protons + 4 neutrons, in the  $0d_{5/2}$ . If we explicitly write down a  $jj$  coupled state with good  $J$  and  $M_J$  within the  $0d_{5/2}^8$  configuration, then we would see that all the states with a fixed total  $M_J$  within the  $0d_{5/2}^8$  configuration contribute to this state with good  $J$  and  $M_J$ . Since the Hamiltonian ( $H$ ) respects the rotational symmetry, its eigenvectors must have good  $J$  and  $M_J$  values. Therefore, diagonalizing  $H$  in the space of all the states with fixed  $M_J$  within the  $0d_{5/2}^8$  configuration will automatically produce eigenstates with different  $J$  values and same  $M_J$  values.

Usually, one has to include many configurations by using some selection principle. Often, the selection scheme uses the energy of the configurations. In this scheme, one includes only configurations that are within some range  $\Delta E$  relative to the lowest energy configuration. Another selection scheme, which we use for the present study, considers the number of particles excited out of the lowest energy configuration into the full harmonic-oscillator shell. This selection scheme takes into account possible collective pair excitations when applied with two and four particle excitations outside of the lowest energy configuration.<sup>1</sup>

---

<sup>1</sup>Recently, it has been shown that one can successfully extrapolate some observables, such as energy eigenvalues, quadrupole moments, B(E2) transition strengths and Gamow-Teller transition strengths, using successively bigger truncation spaces. For more details see nucl-th/0203012 by Mizusaki and Imada and nucl-th/0112014 by Zelevinsky and Volya.

## 2.5 The $SU(3)$ Shell Model for Nuclei

If one considers a system near equilibrium, then it is possible to approximate its potential with a harmonic-oscillator potential. Since the symmetry group of the three-dimensional harmonic oscillator is  $SU(3)$ , it is plausible to use  $SU(3)$  basis states. In this section we discuss the  $SU(3)$  shell model. We begin with a review of Elliott's  $SU(3)$  model [4]. In particular, we present two single-particle labeling schemes, the spherical and cylindrical labeling scheme. Then, the structure of a general  $SU(3)$  irrep in the cylindrical labeling scheme is given. Next, we describe the  $SU(3)$  truncation scheme which is based on  $SU(3)$  invariant two-body interactions. We conclude the section with a brief discussion of the  $SU(3)$  breaking interactions.

### 2.5.1 Labeling of the States in Elliott's $SU(3)$ Model

In this section we review group theoretical concepts that are important to the development of the theory and introduce  $SU(3)$  conventions adopted in our discussion. We consider the physical reduction,  $SU(3) \supset SO(3)$ , and the canonical group reduction,  $SU(3) \supset U(1) \otimes SU(2)$ , with their respective labels.

First we consider the physical group reduction  $SU(3) \supset SO(3)$ . This reduction yields a convenient labeling scheme for the generators of  $SU(3)$  in terms of  $SO(3)$  tensor operators. The commutation relations for these  $SU(3) \supset SO(3)$  tensor operators are given in terms of ordinary  $SO(3)$  Clebsch-Gordan coefficients (CGC)  $(jm, j'm'|j''m'')$  [4]:

$$\begin{aligned} [L_m, L_{m'}] &= -\sqrt{2}(1m, 1m'|1m+m')L_{m+m'}, \\ [Q_m, L_{m'}] &= -\sqrt{6}(2m, 1m'|2m+m')Q_{m+m'}, \\ [Q_m, Q_{m'}] &= 3\sqrt{10}(2m, 2m'|1m+m')L_{m+m'}. \end{aligned} \tag{2.4}$$

Here,  $L_m$  are generators of the angular momentum and  $Q_m$  is an algebraic quadrupole operator.

Within this reduction scheme, states of an  $SU(3)$  irrep  $(\lambda, \mu)$  have the following labels:

- $(\lambda, \mu)$  –  $SU(3)$  irrep labels,
- $l$  – total orbital angular momentum, which corresponds to the second order Casimir operator of  $SO(3)$ ,
- $m_l$  – projection of the angular momentum along the laboratory  $z$ -axis,
- $k$  – projection of the angular momentum in a body-fixed frame, which is related to multiple occurrences of  $SO(3)$  irreps with angular momentum  $l$  in the  $(\lambda, \mu)$  irrep.

Unfortunately, this scheme has only one additive label, namely  $m_l$ , and in addition, there are technical difficulties associated with handling the  $k$  label.

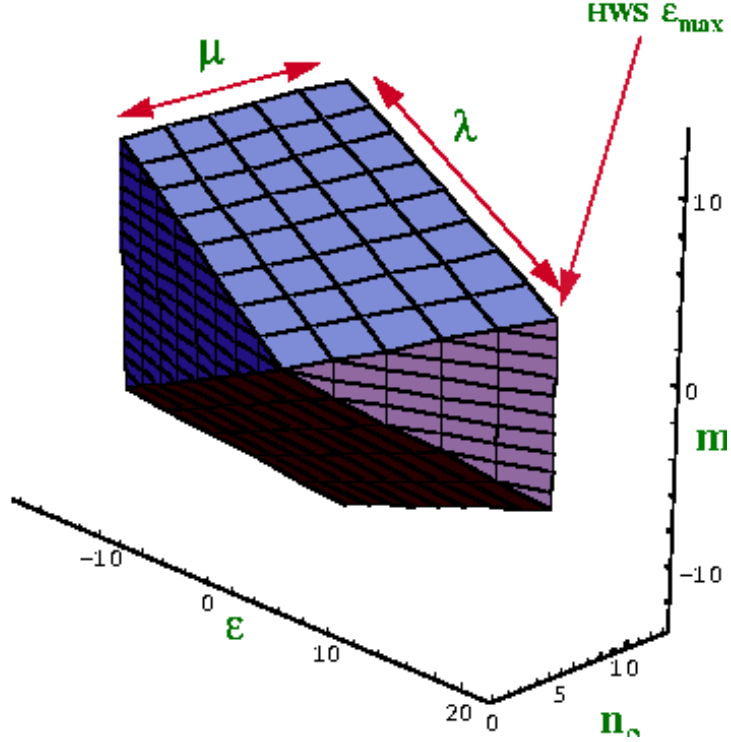


Figure 2.1: Three-dimensional view of the  $(\lambda, \mu)$   $SU(3)$  irrep.

The labeling scheme for our study is the canonical group reduction,  $SU(3) \supset U(1) \otimes SU(2)$  [22]. In this scheme  $Q_0$  is the  $U(1)$  generator and the  $SU(2)$  generators are proportional to  $L_0$ ,  $Q_{+2}$ , and  $Q_{-2}$  [4]. Under the action of the generators of these  $U(1)$  and  $SU(2)$  groups, the remaining four generators of  $SU(3)$  transform like two conjugate spin  $[\frac{1}{2}]$   $SU(2)$  tensors with  $\varepsilon = \pm 3$  values for  $Q_0$ . In this scheme, states of a given  $SU(3)$  irrep  $(\lambda, \mu)$  have the following labels:

- $(\lambda, \mu)$  –  $SU(3)$  irrep labels,
- $\varepsilon$  – eigenvalue of the quadrupole moment ( $Q_0$ ),
- $m_l$  – projection of the orbital angular momentum along the  $z$ -axis ( $L_0$ ),
- $n_\rho$  – related to the second order Casimir operator of  $SU(2)$ , which for symmetric  $(\lambda, 0)$  irreps is simply the number of oscillator quanta in the  $(x, y)$  plane.

This canonical reduction,  $SU(3) \supset U(1) \otimes SU(2)$ , has two additive labels,  $\varepsilon$  ( $Q_0$ ) and  $m_l$  ( $L_0$ ) and the allowed values of these labels for fixed  $SU(3)$  irrep  $(\lambda, \mu)$  are given by [23]:

$$\begin{aligned}\varepsilon &= 2\lambda + \mu - 3(p + q) \\ n_\rho &= \mu + (p - q) \\ m_l &= n_\rho - 2m\end{aligned}\tag{2.5}$$

where  $0 \leq p \leq \lambda$ ,  $0 \leq q \leq \mu$ , and  $0 \leq m \leq n_\rho$ .

### 2.5.2 $SU(3)$ Truncation Scheme

It should be pointed out that the quadrupole operator  $Q$  used in (2.4) is actually an algebraic quadrupole operator

$$Q_{2\mu}^a = \sqrt{\frac{4\pi}{5}} \sum_i \left( \frac{r_i^2}{b^2} Y_{2\mu}(\hat{r}_i) + b^2 p_i^2 Y_{2\mu}(\hat{p}_i) \right),$$

with  $b^2 = \frac{\hbar}{m\omega}$ . However, the matrix elements of  $Q^a$  reduce to the matrix elements of the physical collective quadrupole operator  $Q^c$  within a single harmonic-oscillator shell.

$$Q_{2\mu}^c = \sqrt{\frac{16\pi}{5}} \sum_i \frac{r_i^2}{b^2} Y_{2\mu}(\hat{r}_i).$$

In general, the set of operators  $Q^c$  and  $L$  are part of a  $Sp(6, R)$  Lie algebra. Within the  $Sp(6, R)$  model, the  $Q^c$  operators connect same parity harmonic-oscillator neighbor shells [24].

The algebraic realization of the  $SU(3)$  model has the advantage that one can easily connect the important collective operators with the algebraically significant  $SU(3)$  operators. An example of a significant  $SU(3)$  operator is the second order Casimir operator of  $SU(3)$ :

$$C_2^{SU(3)} = \frac{1}{4}(3L^2 + Q \cdot Q).\tag{2.6}$$

By using the generators of  $SU(3)$  as labeled by the physical reduction  $SU(3) \supset SO(3)$ , we can easily write a general algebraic  $SU(3)$  Hamiltonian:

$$H = H_{osc} + \chi Q \cdot Q + \frac{1}{2\mathcal{J}} L \cdot L + a C_3^{SU(3)} + b L \cdot Q \cdot L + c(L \cdot Q) \cdot (Q \cdot L) + d L \cdot S\tag{2.7}$$

Here,  $H_{osc}$  is the harmonic-oscillator Hamiltonian with single-particle energies  $\varepsilon_n = \hbar\omega \left(n + \frac{3}{2}\right)$ . The strength of the quadrupole-quadrupole interaction is  $\chi$ . The ‘bare’ classical moment of inertia is  $\mathcal{J}$ , when the effective moment of inertia will depend on  $a, b, c$  and  $d$ . The parameter  $a$  is related to the third order Casimir operator  $C_3^{SU(3)}$  of  $SU(3)$ . The strengths of the other

$SO(3)$  invariant interactions, denoted by  $b$  and  $c$ , contain third and fourth order products of the  $SU(3)$  generators relevant to the multiplicity of the  $SO(3)$  irreps within the physical reduction  $SU(3) \supset SO(3)$  [25]. If  $b$  and  $c$  are such that  $bL \cdot Q \cdot L + c(L \cdot Q) \cdot (Q \cdot L) \sim \gamma K^2 + L^2$  where  $\gamma$  is the strength of the  $K$ -band splitting, then the collective states in the  $SU(3) \supset SO(3)$  chain labeled by  $|N[f](\lambda\mu)\kappa LSJM_J\rangle$  would provide a basis in which  $H$  is diagonal.

The main advantage of using an algebraic Hamiltonian, such as (2.7), is its  $SU(3)$  symmetry. Therefore, an  $SU(3)$  invariant Hamiltonian ( $H$ ) does not connect states from different  $SU(3)$  irreps. Since the  $Q \cdot Q$  interaction is proportional to the  $C_2$  of  $SU(3)$ , it can be used as an essential  $SU(3)$  truncation scheme. This scheme prescribes  $C_2$ -ordered importance of the  $SU(3)$  irreps. In this scheme, one selects  $SU(3)$  irreps  $(\lambda, \mu)$  with  $C_2 = \lambda^2 + \mu^2 + \lambda\mu + 3(\lambda + \mu)$  values close to the biggest possible  $C_2$  value. The irrep with the biggest possible  $C_2$  value is called the leading  $SU(3)$  irrep. The leading irrep often corresponds to a total spin  $S = 0$  configuration. This way the leading irrep becomes also the dominant irrep for the low-lying energy states because the strength of the  $L \cdot S$  interaction is usually expected to be small. This is due to the strong spin-pairing which tends to bring  $S = 0$  lower in energy. However, the one-body part of the  $\sum_i l_i \cdot s_i$  interaction can cause significant deviation in the dominance of the leading irrep.

Expressing the  $SU(3)$  Hamiltonian (2.7) in a second quantized form (2.1) gives:

$$H = \hbar\omega \left( n + \frac{3}{2} \right) \sum_i a_i^+ a_i + \frac{1}{4} \sum_{i,j} (\chi \langle ij | Q \cdot Q | kl \rangle + \dots) a_i^+ a_j^+ a_k a_l. \quad (2.8)$$

Here, the labels  $i$  are shorthand notation for the single-particle labels in the  $SU(3)$  shell-model scheme, that is,  $i \rightarrow \tau\tau_0(\eta, 0)\kappa l s j m_j$  in the  $SU(3) \supset SO(3)$  chain or respectively  $i \rightarrow \tau\tau_0(\eta, 0)n_\rho \varepsilon m_l s m_s$  in the  $SU(3) \supset SU(2)$  chain. As usual,  $\tau = 1/2$  is the isospin quantum number with  $\tau_0 = \pm 1/2$  for protons/neutrons respectively, and  $(\eta, 0)$  is the  $SU(3)$  irrep corresponding to a given harmonic-oscillator shell  $n$  ( $\eta = n$ ). The remaining labels were discussed in the previous section on the  $SU(3)$  shell model.

### 2.5.3 Interactions that Break the $SU(3)$ Symmetry

Degenerate single-particle energies are an essential ingredient for good  $SU(3)$  symmetry; this is clear from our discussion on the general algebraic  $SU(3)$  Hamiltonian (2.7) and its second quantized form (2.8). However, we already discussed that the breaking of the single-particle degeneracy by the spin-orbit interaction is essential for the description of the correct nuclear shell closures in terms of the independent-particle model. Therefore, in case of a significant single-particle splitting, which is due to the orbit-orbit interaction  $\sum_i l_i^2$  and the spin-orbit interaction  $\sum_i l_i \cdot s_i$ , there would be a significant disturbance in the  $SU(3)$  truncation scheme. In this case, the spherical shell model described earlier would work and its truncation scheme could be used.

Another  $SU(3)$  breaking factor is the pairing interaction. This interaction is a very essential short-range two-body nuclear interaction that can have significant impact on any  $SU(3)$ -based calculations as well as on the spherical shell-model type calculations. Although

we have studied some effects of the pairing interaction in the  $sd$ -shell as well as in the  $pf$ -shell, we would rather not engage in this matter. We only mention that effects of the pairing in the context of the pseudo- $SU(3)$  model have been studied before by C. Bahri [26], and currently we are considering incorporating the pairing effects within an oblique-basis type calculation via the broken pair model [3].

# Chapter 3

## Toy Model of a Two-Mode System

The study of  $^{24}\text{Mg}$ , which will be discussed later in more detail, has successfully demonstrated the oblique-basis concept [8]. The quality of the results for  $^{24}\text{Mg}$  are due to the near equal importance of the two basis sets used. On the one hand, the spherical shell-model basis is well-suited for description of the single-particle excitations; on the other hand, the  $SU(3)$  shell model puts an emphasis on the collective excitations in nuclei. These two modes are crucial for the  $^{24}\text{Mg}$  example.

In general, determining the relevant excitations is a cornerstone in the study of any system; in some sense this is the art of physics. Usually one basis works well for one system, but fails for another system. The reason is that in any general method, such as the variational method, perturbation theory, or fixed-basis matrix diagonalization, one needs to start with a good guess about the Hamiltonian and the states that describe the relevant excitation modes [27].

When applying perturbation theory, one is often concerned with a small perturbation of an exactly solvable limit of the full Hamiltonian [29, 30]. However, there are many examples when the relevant Hamiltonian has more than one exactly solvable limit [31, 32]. This is a common situation when a dynamical symmetry group is used in the construction of the Hamiltonian [33], [34], [35]. *What shall we do if the system described by such a Hamiltonian is nowhere near any of the exact limits?* In these situations, the problem may be better approached by using states associated with both limits. This set of states will form an oblique-mixed-mode-basis for the calculation.

Taking into account the importance of the relevant energy scale of a problem and the wave function localization with respect to the range of the potential, the oblique-basis method can be taken beyond the idea of using two orthonormal basis sets. Specifically, one can consider a variationally-improved basis set starting with some initially guessed basis states. In the occupation number representation for the nuclear shell model, this variationally-improved basis method seems inapplicable.<sup>1</sup> However, the method seems interesting because

---

<sup>1</sup>In the occupation-number representation one assumes a fixed single-particle structure and then expands the states in the Slater determinants provided by this basis. From this point of view, there is no room for variationally-improved basis states since each Slater determinant is a single-integer machine word.

of its possible relevance to multi-shell *ab-initio* nuclear and atomic physics calculations. The method may also be related to some renormalization-type techniques. Therefore, a brief discussion of the variationally-improved basis and its possible applications is given in the Appendix.

In this chapter some relevant mathematical notation and concepts used in the oblique-basis method are introduced. Specifically, we demonstrate the concept of the oblique basis on a simple two-mode system, the one-dimensional harmonic oscillator in a box. First, we discuss the concept and then the two exactly solvable limits of our toy model are briefly summarized. A qualitative discussion of the expected spectrum of the one-dimensional harmonic oscillator in a box is given. This is followed by an example spectrum and quantitative estimates. Some specific problems related to the structure of the Hilbert space will be addressed. Finally, the main results will be discussed, especially a quasi-perturbative behavior and a coherent structure within the strong mixing region.

### 3.1 Harmonic Oscillator in a One-Dimensional Box

Let us start with an abstract two-mode system. For simplicity, we assume that the Hamiltonian for the system under investigation has two exactly solvable limits, for example:

$$H = (1 - \lambda)H_0 + \lambda H_1 + \lambda(1 - \lambda)H_2. \quad (3.1)$$

Here,  $H_0$  and  $H_1$  are two exactly solvable Hamiltonians. This way, we have  $H \rightarrow H_0$  in the limit  $\lambda \rightarrow 0$  and  $H \rightarrow H_1$  when  $\lambda \rightarrow 1$ . In the vicinity of these two limits we can approach the problem using standard perturbation theory. However, for  $\lambda \approx \frac{1}{2}$  we have a very mixed system with unclear behavior which could be complicated further by an interaction  $H_2$  between the natural modes of  $H_0$  and  $H_1$ .

In the expression (3.1),  $\lambda$  is introduced to simplify the discussion. In general, we have more than one parameter in the Hamiltonian. Often the exactly solvable limits are described as hypersurfaces in the full parameter space. It could even be that there are three or more exactly solvable limits. For example, the Interacting Boson Model (IBM) has three exactly solvable limits [2]. Another example with three exactly solvable limits is the commonly used nuclear schematic interaction. It has nondegenerate single-particle energies ( $\varepsilon_i$ ), pairing ( $P^+P$ ) two-body interaction, and quadrupole-quadrupole ( $Q \cdot Q$ ) two-body interaction:

$$H = \varepsilon_i N_i + GP^+P - \chi Q \cdot Q.$$

Here, we consider the simplest two-mode system that is sufficiently close to the problem we have to solve for nuclei. The system under consideration consists of a one-dimensional harmonic oscillator in a one-dimensional box of size  $2L$  [36]:

$$H = \frac{1}{2m}p^2 + V_L(q) + \frac{m\omega^2}{2}q^2. \quad (3.2)$$

where  $V_L(q)$  is the confining potential which is zero for  $|q| < L$  and  $\infty$  for  $|q| \geq L$ . This system has two exactly solvable limits. A more realistic model might consist of a three-dimensional harmonic oscillator and a square-well potential since these two potentials are known to be good starting points in the nuclear shell model [37].

The one-dimensional harmonic oscillator in a one-dimensional box model has been used as an example by Barton, Bray, and Mackane in their discussion on the effects of the distant boundaries on the energy levels of a one-dimensional quantum system [38]. Also, some studies have already been done for the cylindrical symmetric system of a three-dimensional harmonic oscillator between two impenetrable walls [39]. However, the bi-modal structure of the problems has not been discussed in these studies. The essential two-mode regime of such problems has been studied in the context of a two-dimensional confinement of a particle in an external magnetic field by Rosas *et al.* [40]. Some authors have generalized the one-dimensional harmonic oscillator by introducing time dependent parameters in the Hamiltonian [41] and have recognized the two limiting cases of a free particle and harmonic oscillator. The infinite square well and the harmonic oscillator have been considered as the two limiting cases of a power-law potential within the context of wave packet collapses and revivals [43, 42]. Here, we focus our study on the bi-modal structure of the one-dimensional harmonic oscillator in a one-dimensional box.

The first limit of the toy model (3.2) is  $\omega = 0$ . This is a free particle in a one-dimensional box with size  $2L$  :

$$H_0 = \frac{1}{2m}p^2 + V_L(q). \quad (3.3)$$

The eigenvectors and energies are labeled by  $n = 0, 1, \dots$  and are given by the expressions:

$$\begin{aligned} \Phi_n(q) &= \begin{cases} \sqrt{\frac{1}{L}} \cos\left((n+1)\frac{\pi q}{2L}\right) & \text{if } n \text{ is even} \\ \sqrt{\frac{1}{L}} \sin\left((n+1)\frac{\pi q}{2L}\right) & \text{if } n \text{ is odd} \end{cases}, \\ E_n &= \frac{1}{2m} \left((n+1)\frac{\pi}{2}\right)^2 \left(\frac{\hbar}{L}\right)^2. \end{aligned} \quad (3.4)$$

This limit corresponds to extreme nuclear matter when the short range nuclear force produces an effective interaction well represented by a square-well potential [37]. We can think of this limit as a one-dimensional equivalent of a three-dimensional model where nucleons are confined within a finite volume of space representing the nucleus.

The other exactly solvable limit of the toy model (3.2) is the harmonic oscillator in one dimension:

$$H_1 = \frac{1}{2m}p^2 + \frac{m\omega^2}{2}q^2. \quad (3.5)$$

In dimensionless coordinates

$$q \rightarrow \tilde{q} \sqrt{\frac{\hbar}{m\omega}}, \quad p \rightarrow \tilde{p} \sqrt{m\hbar\omega},$$

we have:

$$H_1 = \hbar\omega \frac{1}{2} (\tilde{p}^2 + \tilde{q}^2).$$

Thus the eigenvectors and energies are labeled by  $n = 0, 1, \dots$  and are given by the expressions:

$$\begin{aligned} \Psi_n(q) &= \sqrt{\frac{1}{bn!2^n\sqrt{\pi}}} H_n\left(\frac{q}{b}\right) \exp\left(-\frac{1}{2}\frac{q^2}{b^2}\right), \quad b = \sqrt{\frac{\hbar}{m\omega}} \\ E_n &= \hbar\omega \left(n + \frac{1}{2}\right). \end{aligned} \quad (3.6)$$

Where  $H_n$  are the Hermite polynomials. This limit corresponds to the three-dimensional harmonic oscillator model for nuclei.

In a one-dimensional toy model, the anharmonic oscillator with a quartic anharmonicity would be the appropriate counterpart of the  $Sp(6, R)$  shell model since the quadrupole-quadrupole interaction  $Q \cdot Q$  goes as  $\sim r^4$  and  $Q$  connects same parity harmonic oscillator shells. If we restrict the model space to only one harmonic oscillator shell, then we can use the algebraic quadrupole moment  $\tilde{Q}$  of Elliott [4] because within a single shell  $\tilde{Q}$  is the same as  $Q$  [2]. Thus for our study it is appropriate to consider the one-dimensional harmonic oscillator to correspond to the  $SU(3)$  shell model for nuclei.

## 3.2 Spectral Structure at Different Energy Scales

Often in physics the spectrum of a system is different for different energy scales. This usually reflects the existence of different excitation modes of the system. For the toy model Hamiltonian (3.2) we can clearly define three spectral types:

- Spectrum of a particle in a one-dimensional box (3.4) with quadratic dependence on  $n$  ( $E_n \sim n^2$ ),
- Spectrum of the one-dimensional harmonic oscillator (3.6) with linear dependence on  $n$  ( $E_n \sim n$ ),
- Intermediate spectrum that is neither of the above two types.

From Fig. 3.1 we expect that the particle in a box spectrum should be operative at high energies. These energies are energies where the box boundaries dominate over the harmonic oscillator potential. In this regime one can use standard perturbation theory to calculate the energy for a particle in a box perturbed by a harmonic oscillator potential. It can be shown that perturbation theory will give better results for higher energy levels. For  $n \rightarrow \infty$  the first correction ( $\delta E_n^1$ ) approaches the constant value of  $m\omega^2 L^2/6$ . An estimate on when the perturbation calculations are feasible using  $E_{n+1}^0 - E_n^0 \gg \langle n | V | n \rangle$  gives:

$$n \gg 2m^2\omega^2 L^4 / (3\hbar^2\pi^2). \quad (3.7)$$

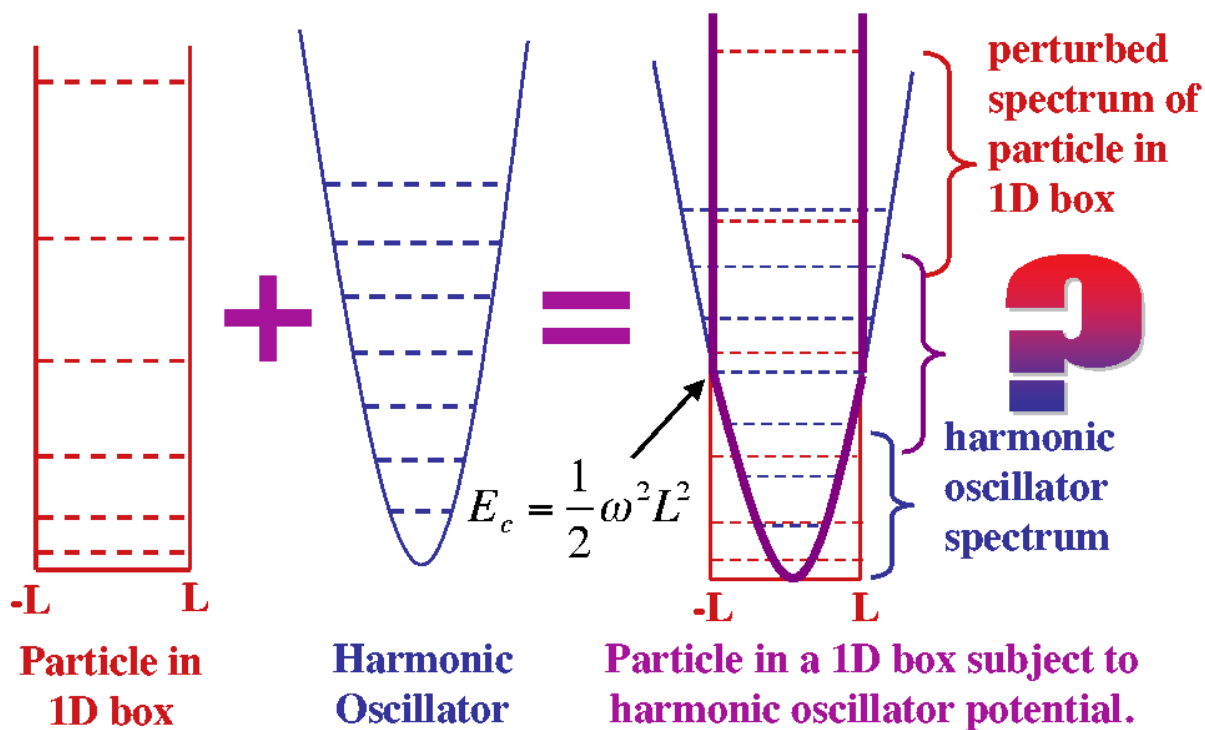


Figure 3.1: Two-mode toy system. The structure of the interaction potential of a particle in a one-dimensional box subject to a harmonic oscillator restoring force towards the center of the box.

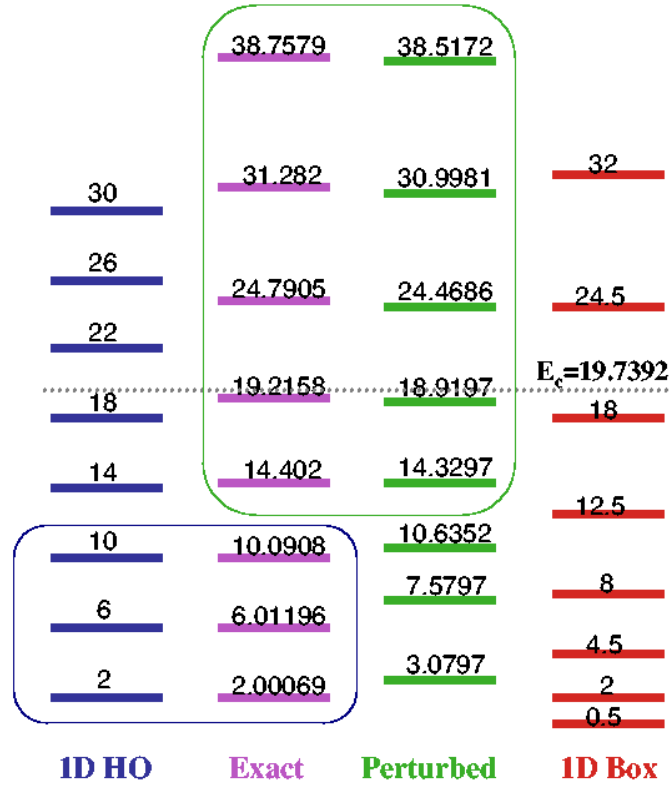


Figure 3.2: Spectral structure of the two-mode system for  $m = \hbar = 2L/\pi = 1$  and  $\omega = 4$ .

This analysis is confirmed by the numerical calculations shown in Fig. 3.2 where the perturbed particle in a box spectrum is really operative at  $n > 3$  for the case of  $m = \hbar = 2L/\pi = 1$  and  $\omega = 4$ .

The intermediate spectrum should be observed when the harmonic oscillator turning points coincide with the walls of the box. Therefore, the critical energy scale that separates the two extreme spectral structures is given by:

$$E_c = \frac{m\omega^2}{2}L^2 \quad (3.8)$$

Notice that the constant energy shift  $m\omega^2 L^2/6$  in the energy of the high energy levels  $\delta E_{n \gg 1}^1$  is one-third of the critical energy ( $E_c/3$ ).

At low energies, where the one-dimensional harmonic oscillator determines the classical turning points to be far from the boundaries, we expect to see the harmonic oscillator spectrum as shown in Fig. 3.2. The number of harmonic oscillator states that will be

observed is easily estimated using:

$$E_c > E_n^{ho} \Rightarrow n_{\max}^{ho} = \frac{1}{2} \frac{m\omega L^2}{\hbar} - \frac{1}{2} \quad (3.9)$$

It should be pointed out that there is a compatible number of levels, usually bigger than  $n_{\max}^{ho}$ , below the  $E_c$  corresponding to a free particle in a box:

$$E_c > E_n^{1D} \Rightarrow n_{\max}^{1D} = \frac{2}{\pi} \frac{m\omega L^2}{\hbar} - 1. \quad (3.10)$$

However, these states are mixed by the harmonic oscillator potential toward the corresponding harmonic oscillator wave functions.

Using the ratio of the ground state energies,  $E_{g.s.}^{HO}/E_{g.s.}^{1D} = 4m\omega L^2/(\hbar\pi^2)$ , together with (3.9) and (3.10), the following spectral situations apply:

- For  $\frac{m\omega L^2}{\hbar} > \left(\frac{\pi}{2}\right)^2$  there are levels below  $E_c$  corresponding to the harmonic oscillator and the free particle in a box such that  $E_{g.s.}^{HO} > E_{g.s.}^{1D}$ . However, only the harmonic oscillator levels are seen in the low energy spectrum.
- For  $\left(\frac{\pi}{2}\right)^2 > \frac{m\omega L^2}{\hbar} > \frac{\pi}{2}$  there are only the ground states  $E_{g.s.}^{1D}$  and  $E_{g.s.}^{HO}$  below  $E_c$  and  $E_{g.s.}^{1D} > E_{g.s.}^{HO}$ .
- For  $\frac{\pi}{2} > \frac{m\omega L^2}{\hbar} > 1$  there is only the ground state of the harmonic oscillator  $E_{g.s.}^{HO}$  below  $E_c$ .

Therefore, the smallest number of states<sup>2</sup> to illustrate the two mode spectra is the case of  $m = \hbar = 1$ ,  $L = \pi/2$  and  $\omega = 4$ . With these parameters, formula (3.9) gives  $n_{\max}^{HO} = 4.5348$ . Thus one should see no more than 4 equidistant states as shown in Fig. 3.2. In Fig. 3.2 there are three clear equidistant energy levels that correspond to a harmonic oscillator spectrum.

With respect to the critical energy  $E_c$ , there is a more explicit classification of the spectral structure:

- Perturbed particle in a one-dimensional box spectrum for energies  $E \gg E_c$  such that (3.7) holds,
- One-dimensional harmonic oscillator spectrum (3.6) for energies  $E_c \gg E$  such that (3.9) holds,
- Intermediate spectrum for energies  $E \approx E_c$ .

---

<sup>2</sup>For simplicity we usually fix the parameters as follows:  $m = \hbar = 1$ ,  $L = \pi/2$ .

### 3.3 Toy Model Calculations and Results

Despite the simplicity of the toy model (3.2), the harmonic oscillator in a box exhibits some of the essential characteristics of a more complex system. Our main interest is in problems associated with the use of fixed-basis calculations. In particular, one such problem is the slow convergence of the calculations [36]. If one can implement an exact arithmetic, one may not worry too much about the slow convergence when enough time, storage, and other resources are provided. However, numerical calculations are plagued with numerical errors that may grow significantly and render the results meaningless. From this point of view, a calculation that converges slowly may be compromised by accumulated numerical error.

#### 3.3.1 On the Hilbert Space of the Basis Wave Functions

Before discussing the toy model using an oblique basis, it is instructive to discuss briefly the harmonic oscillator problem (3.5) using the wave functions for a free particle in a one-dimensional box (3.4); and vice versa, solving the problem of a free particle in a one-dimensional box (3.3) using the wave functions for a particle in the harmonic oscillator potential (3.6).

Due to the structure of the wave functions, there are some specific problems that need to be addressed. For example, using wave functions for a free particle in a one-dimensional box to solve the harmonic oscillator problem may not be appropriate especially for high energy states  $E \gg E_c$ . The problem is that any linear combination of wave functions with the same localized support, in our case the wave functions are localized within the box, will still be a function with the same localized support (see Fig. 3.3). That is, any linear combination of wave functions that are zero outside of the box is a function that is zero outside of the box too. Because the harmonic oscillator potential gets wider for higher and higher energies, any higher energy wave function must spread more than the previous one. Similarly, the spreading of the harmonic oscillator wave functions is responsible for the troubles that arise in solving the problem of a free particle in a one-dimensional box using the harmonic oscillator wave functions. The essence of these problems is in the structure of the corresponding Hilbert spaces.

The influence of the boundary conditions on the properties of a quantum mechanical system has been recognized from the dawn of quantum mechanics. It is well known that some separable problems may re-couple due to the boundary conditions [45]. Some recent studies on the problem of confined one-dimensional systems using equations for relevant cut-off functions have been pioneered by Barton, Bray, and Mackane [38]. Their method has been further developed in a more general setting by Berman [44]. Other authors aim at variational procedures using simple cut-off functions [47, 46] or derive asymptotic estimates for multi-particle systems using the Kirkwood-Buckingham variational method [48]. Somewhat different approaches focus on shape-invariant potentials and use supersymmetric partner potentials to derive energy shifts and wave function approximations [49], as well

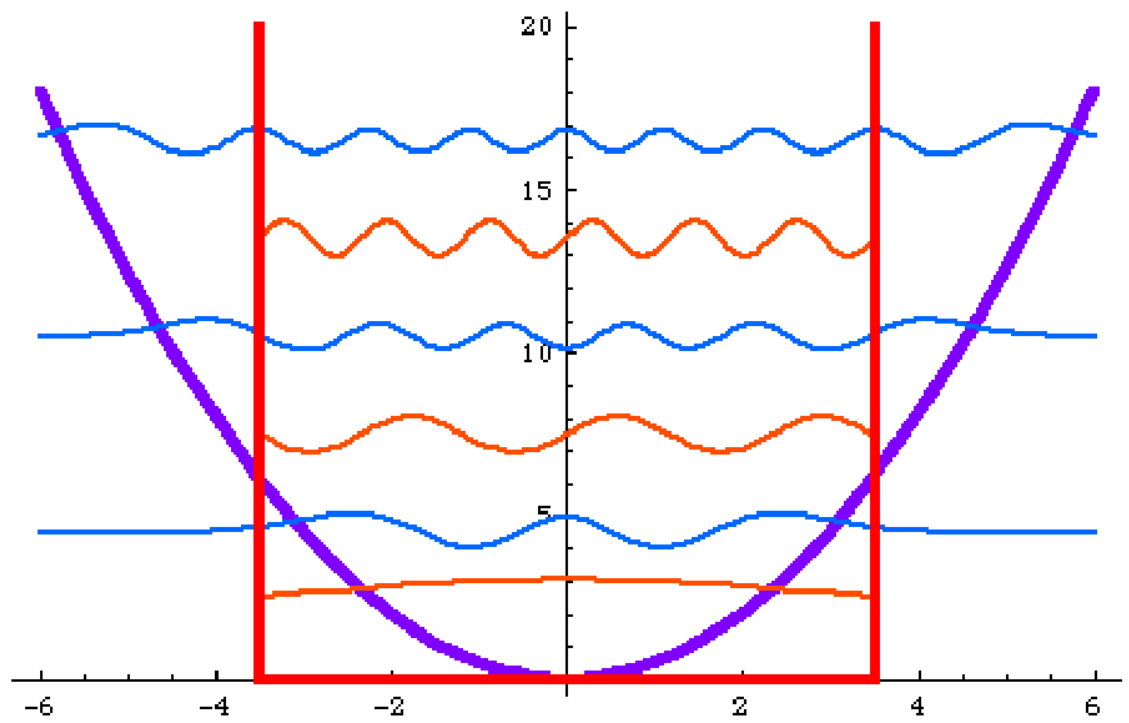


Figure 3.3: Spreading of the wave functions for the harmonic oscillator (blue) and particle in a box (red).

as sample-size dependence of the ground-state energy [50]. In the next few paragraphs we discuss the structure of the relevant Hilbert spaces when confinement is present.

### • Harmonic Oscillator in the One-Dimensional Box Basis

Now we consider the harmonic oscillator problem (3.5) using the wave functions for a free particle in a one-dimensional box (3.4). There are no difficulties for energies  $E \ll E_c$  (3.8) where the harmonic oscillator potential is still within the box. However, for energies  $E \gg E_c$  the basis wave functions are localized only on the interval  $[-L, L]$ . Thus they cannot provide the necessary spread over the potential width (Fig. 3.3). This situation would be appropriate for the toy model (3.2) but not for the pure harmonic oscillator problem (3.5).

One simple solution of the spreading problem is to continue the basis wave functions by periodicity. This way the necessary spread of the basis wave functions can be achieved and the new basis will stay orthogonal but must be re-normalized.<sup>3</sup> However, these basis wave functions do not decay to zero in the classically forbidden zone. This means that some significant number of basis wave functions will be needed to account for the necessary behavior within the classically forbidden zone.

Another alternative is to change the support domain corresponding to non-zero values of the function by stretching or squeezing it through a scaling of the argument of the basis wave functions,  $x \rightarrow x\alpha_n/L$ . This way the support becomes  $[-L, L] \rightarrow [-\alpha_n, \alpha_n]$ . Here,  $\alpha_n$  is a scale factor for the  $n$ -th basis wave function (3.4) estimated either from the width of the harmonic oscillator potential<sup>4</sup>, or determined by variational minimization. Either way, the new set of basis functions will be non-orthogonal. In general, there may be even a linear dependence. However, for the basis functions discussed here, linear dependence may not appear due to the different number of nodes for each wave function. The number of nodes (zeros) is not changed under the re-scaling procedure. While the potential width scaling is simpler, its applicability is more limited than the variationally-determined one. In general, the variational approach can be extended for much more general situations as discussed in the Appendix.

### • Particle in a Box in the Harmonic-Oscillator Basis

Next, suppose we want to solve the problem of a free particle in a one-dimensional box  $[-L, L]$  (3.3) using the harmonic oscillator wave functions (3.6). The first thing to do is to change the inner product of the wave functions:  $(f, g) = \int_{-\infty}^{\infty} f^*(x)g(x)dx \rightarrow \int_{-L}^L f^*(x)g(x)dx$ . Then, it is immediately clear that the set of orthonormal harmonic oscillator wave functions  $\Psi_n(q)$  (3.6) will lose its orthonormality and even its linear indepen-

---

<sup>3</sup>If one continues the wave functions to infinity, then there is a normalization problem. However, if the continuation is on a finite interval, then the functions can still be normalized.

<sup>4</sup>The initial idea is to use basis states that have a spread compatible with the width of the potential in the energy region of interest, thus resolving the spectra only within that energy scale without calculating the lower energy states. Unfortunately, it does not seem to work since interference causes reduction of the wave spread and therefore drives the solutions towards the lowest eigenstate.

dence.<sup>5</sup> However, this is not the actual trouble in such an approach.<sup>6</sup> Neither the variational nor the potential-width wave function scaling will help to cure the loss of hermiticity of the physically significant differential operators, such as the momentum operator ( $p = -i\hbar\frac{\partial}{\partial x}$ ) and the Hamiltonian operator ( $H = \frac{1}{2m}p^2$ ). This non-hermiticity is due to the behavior of the basis states at the boundary, mainly the non-vanishing of the wave functions at  $-L$  and  $L$ . For detailed analysis on the loss of hermiticity, we refer the reader to the Appendix. In order to recover the hermiticity of the differential operator  $i\frac{\partial}{\partial x}$ , it is sufficient<sup>7</sup> to make sure that our basis wave functions vanish at the boundary points  $-L$  and  $L$ . For this purpose one can look at the nodes of each basis wave function and scale it so that its outer nodes are at the boundary points.<sup>8</sup> Since the physical requirement that the wave functions have to be zero at the boundary is the cornerstone in quantizing the free particle in a one-dimensional box (3.4), it is not surprising that the nodally adjusted harmonic oscillator wave functions are very close to the exact wave functions for the free particle in a one-dimensional box as shown in Fig. 3.4.

In general, calculating the nodes of a function may become very complicated. To avoid problems with finding the roots, one can use the following technique<sup>9</sup>: the idea is to evaluate the value of the wave function at the boundary points, then shift the wave function by a constant to get zeros at the boundary,  $\Psi(q) \rightarrow \Psi(q) - \Psi(L)$ . This idea works well for even wave functions, but has to be generalized for odd wave functions by adding a linear term,  $\Psi(q) \rightarrow \Psi(q) - (\Psi(L)/L)q$ . Thus for a general function we can have:  $\Psi(q) \rightarrow \Psi(q) - (1 + q/L)\Psi(L)/2 - (1 - q/L)\Psi(-L)/2$ . In Fig. 3.4 we have shown some of the resulting wave functions. Notice that this procedure gives a new wave function  $\Psi$  that is well behaved inside the interval  $[-L, L]$  and grows linearly with  $q$  outside the interval  $[-L, L]$ . This is in contrast to the behavior of the cut-off function  $f(q)$  obtained by Barton et al [38]. The function  $f(q)$  has  $L/q$  singularity at the origin ( $q = 0$ ). The use of a cut-off function to enforce boundary conditions has been developed by Barton et al [38] and Berman [44] and provides an interesting integral equation for the cut-off function. On the other hand, a simple cut-off function supplemented by a variational method seems to be very effective [47, 46, 48].

It should be pointed out that by using the above process one can set up and successfully run a modification of the usual Lanczos algorithm, to be discussed later, to solve for the few lowest eigenvectors of the free particle in a one-dimensional box through an arbitrarily chosen initial wave function. The major modification is to project every new function,  $\Psi_{n+1} = H\Psi_n$ ,

---

<sup>5</sup>The set of functions  $\Psi_n(q)$  with support domain restricted to  $[-L, L]$  and denoted by  $\Psi_n(q; [-L, L])$  may become linearly dependent if  $L$  is so small that there are more than one  $\Psi_n(q; [-L, L])$  with the same number of nodes within  $[-L, L]$ .

<sup>6</sup>The oblique basis type calculations described later can successfully remove the linearly dependent basis states in the process of handling the non-orthogonality of the basis.

<sup>7</sup>Wave functions with the same value at  $\pm L$  is the necessary condition; the wave functions should be zero only for an infinite potential at  $\pm L$ .

<sup>8</sup>From the nodal structure of the harmonic oscillator wave functions, given by the Hermite polynomials, it is clear that the first two wave functions ( $\Psi_0$  and  $\Psi_1$ ) cannot be used since they have less than two nodes.

<sup>9</sup> This technique has been suggested by Professor A. R. P. Rau (private communications).

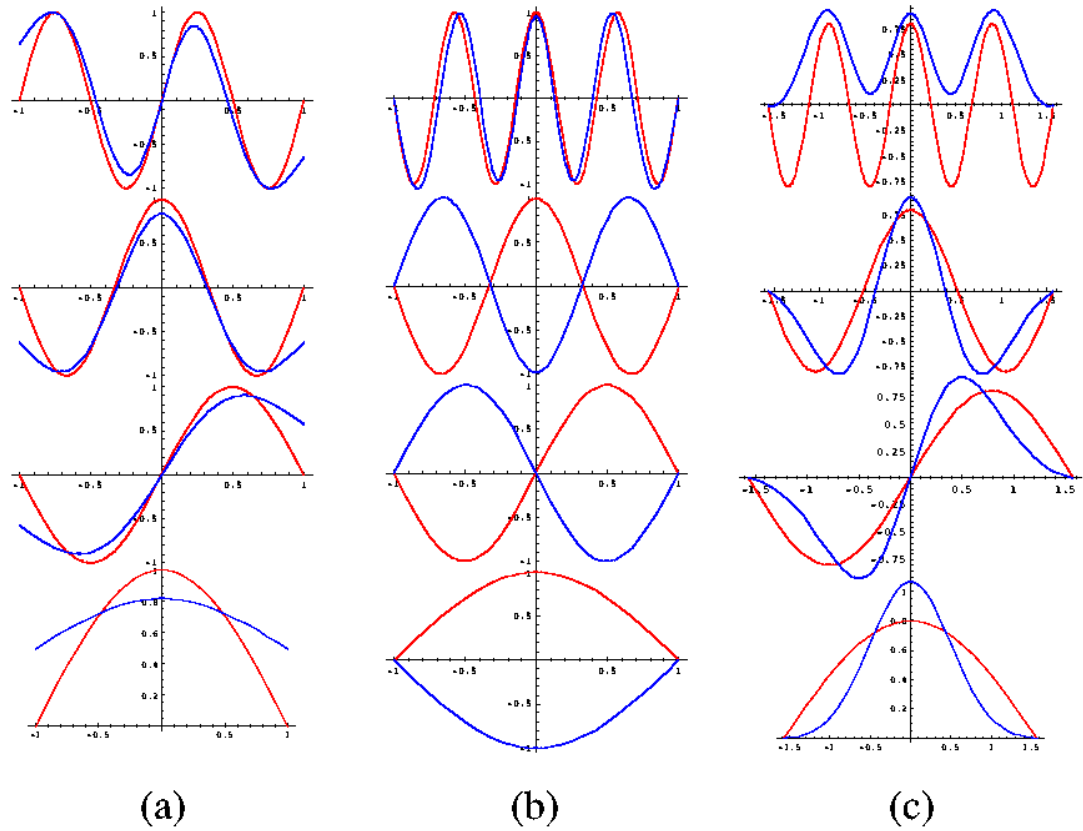


Figure 3.4: Harmonic-oscillator trial wave functions adjusted with respect to the one-dimensional box problem: (a) adjusted according to the potential width  $E_n^{1Dbox} = \omega_n^2 L^2 / 2 \Rightarrow \omega_n = \frac{\hbar}{L^2} (1 + 2n)$ , (b) nodally adjusted, (c) boundary adjusted using  $\Psi(q) \rightarrow \Psi(q) - \Psi(L)(1 + q/L)/2 - \Psi(-L)(1 - q/L)/2$

into the appropriate Hilbert space and subtract the components along any previous basis vectors. Only then should one attempt to evaluate the matrix elements of  $H$  related to the new basis vector that is clearly within the correct Hilbert space. This way, one has to double the number of scalar product operations compared to the usual algorithm where the matrix elements of  $H$  are calculated along with the complete re-orthogonalization of the basis vectors.

### 3.3.2 Discussion of the Toy Model Results

Having considered the main problems one may face in studying the simple toy model (3.2),

$$H = \frac{1}{2m}p^2 + V_L(q) + \frac{m\omega^2}{2}q^2,$$

we close the discussion with a sample spectrum for the case of  $m = \hbar = 2L/\pi = 1$  and  $\omega = 4$ .

As one can see in Fig. 3.2, the first three energy levels are really equally distant from one another and coincide with the harmonic oscillator levels as expected from (3.9). For these states, the wave functions are also the harmonic oscillator wave functions. The intermediate spectrum is almost missing. After the  $E_c$ , the spectrum is that of a free particle in a 1D box perturbed by the harmonic oscillator potential. The oblique-basis type calculation reproduces the first eight low energy states within a 14-dimensional calculation, seven nodally adjusted harmonic oscillator states and seven states of a free particle in a box, while the fixed-basis calculation, using only the wave functions of a free particle in a one-dimensional box, requires 18 basis states.

Due to the simplicity of the toy model, one does not find any big numerical advantage of the oblique-basis calculation compared to the calculations using the fixed basis of the 1D box wave functions. There are two main reasons for this: (1) there is a sharp energy scale  $E_c$  that separates the two modes, (2) the spectrum above the energy  $E_c$  has a nice regular structure.

The nice regular structure above the energy  $E_c$  results in a very favorable situation for the usual fixed-basis calculations since the dimension of the space needed to obtain the  $n$ -th eigenvalue grows as  $n + \alpha$ . The parameter  $\alpha$  is relatively small and does not change much in a particular region of interest. For example, the  $\omega = 16$  calculations need only  $\alpha = 15$  extra basis vectors when calculating any of the eigenvectors up to the hundredth vector. The relatively constant value of  $\alpha$  can be understood by considering the harmonic oscillator potential as an interaction that creates excitations out of the  $n$ -th unperturbed 1D box state. Therefore,  $\alpha$  is the number of 1D box states with energies in the interval  $E_n^0$  and  $E_n^0 + \omega^2/2 \langle \Phi_n | x^2 | \Phi_n \rangle$  where  $E_n^0$  is the  $n$ -th unperturbed 1D box state energy. There is a fast de-coupling of the higher energy states from any finite excitation process that starts out of the  $n$ -th state. The fast de-coupling is due to the increasing energy spacing of the 1D box spectrum. This results in a finite number of states mixed by the presence of the harmonic oscillator potential. Using the upper limit  $E_c/3$  on  $\delta E_n^1$ , one can easily estimate  $\alpha$ :

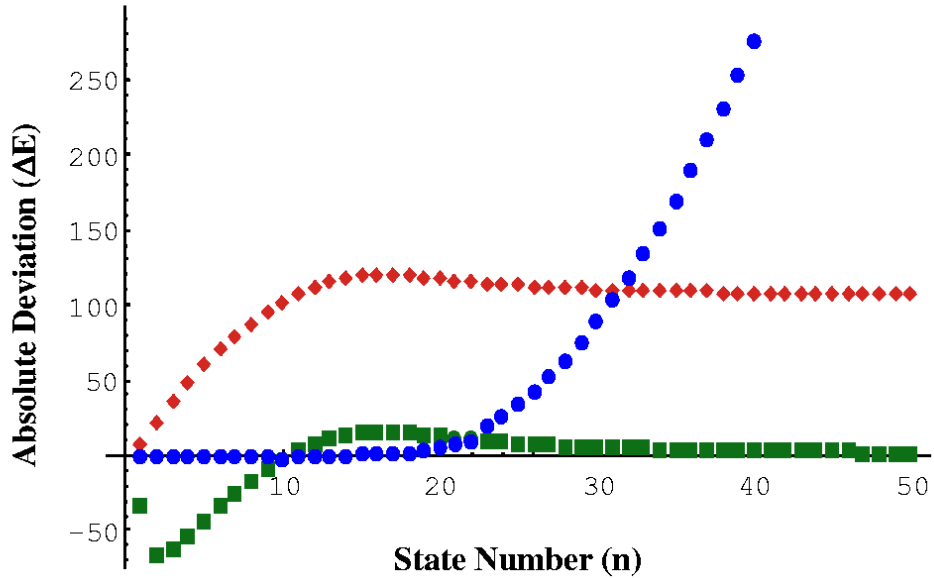


Figure 3.5: Absolute deviations from the exact energy eigenvalues for  $\omega = 16$ ,  $L = \pi/2$ ,  $\hbar = m = 1$  as a function of  $n$ . Blue circles represent deviation of the exact energy eigenvalue from the corresponding harmonic oscillator eigenvalue ( $\Delta E = E_n^{exact} - E_n^{HO}$ ), the red diamonds are the corresponding deviation from the energy spectrum of a particle in a 1D box ( $\Delta E = E_n^{exact} - E_n^{1D}$ ), and the green squares are the first-order perturbation theory results.

$$\alpha \approx \frac{1}{3}n_{\max}^{1D}.$$

The sharp separation of the two modes allows for a safe use of the harmonic oscillator states without any rescaling. This is especially true when  $\omega$  is very big since then the low energy states are naturally localized within the box. Therefore, there is a clear shortcut: instead of diagonalizing the Hamiltonian in some 1D box wave-function basis, one can just use the harmonic oscillator wave functions.

Fig. 3.5 shows the absolute deviation ( $\Delta E = E_n^{exact} - E_n^{estimate}$ ) of the exact energy spectrum for the case of  $\omega = 16$ ,  $L = \pi/2$ ,  $\hbar = m = 1$ . Here,  $E_n^{estimate}$  refers to the three energy estimates one can make: the harmonic oscillator  $E_n^{HO}$ , particle in a 1D box  $E_n^{1D}$ , and the first order perturbation theory estimate considering the harmonic oscillator potential as a perturbation ( $E_n^{1D} + \omega^2/2 \langle \Phi_n | x^2 | \Phi_n \rangle$ ). There are about 19 states that match a harmonic oscillator spectrum which is consistent with the expected value from (3.9). After the  $n = 20$

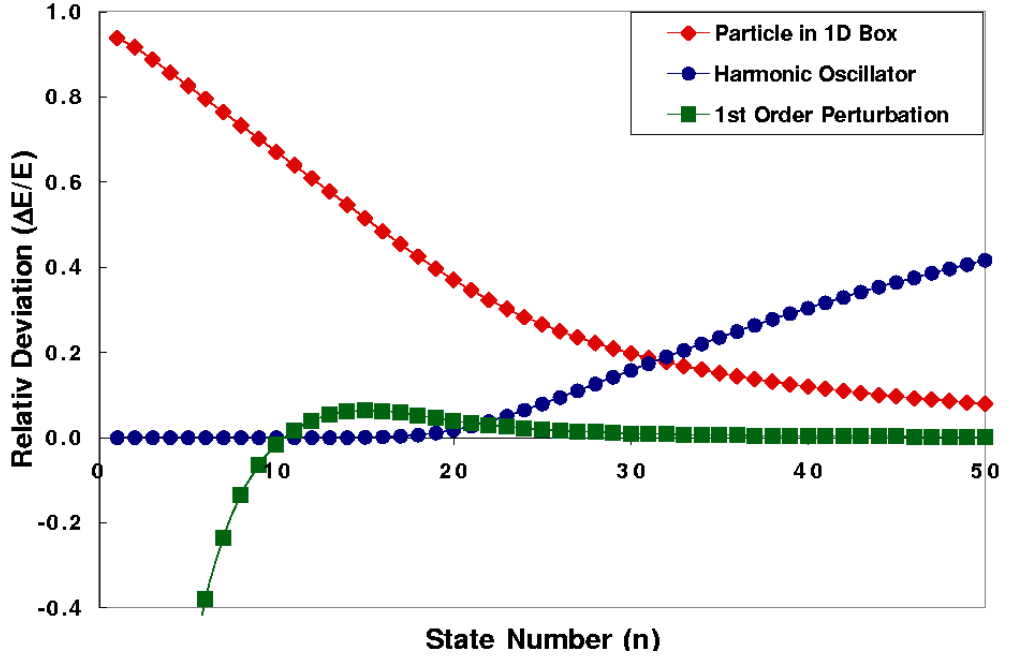


Figure 3.6: Relative deviations from the exact energy eigenvalues for  $\omega = 16$ ,  $L = \pi/2$ ,  $\hbar = m = 1$  as a function of  $n$ . The blue circles represent deviation of the exact energy eigenvalue from the corresponding harmonic oscillator eigenvalue ( $\Delta E/E = 1 - E_n^{HO}/E_n^{exact}$ ), the red diamonds are the corresponding relative deviation from the energy spectrum of a particle in a 1D box ( $\Delta E/E = 1 - E_n^{1D}/E_n^{exact}$ ), and the green squares are the first-order perturbation theory results.

level, the perturbation theory gives increasingly better results for the energy eigenvalues. Fig. 3.6 shows the relative deviation ( $1 - E_n^{estimate}/E_n^{exact}$ ) of the exact energy spectrum for the case of  $\omega = 16$ ,  $L = \pi/2$ ,  $\hbar = m = 1$ .

From these graphs, it seems that the transition region is somewhat absent since the first-order perturbation theory takes on immediately after the breakdown of the harmonic oscillator spectrum. Even though the first-order perturbation theory gives good estimates for the energy levels in this transition region, this is not a manifestation of a proper perturbation theory. Rather, it is a manifestation of a coherent behavior [51]. What actually happens in this region is a coherent mixing of 1D box states by the harmonic oscillator potential in the sense of a quasi-symmetry discussed in the Appendix.

Notice that perturbation theory is valid, as expected, for high energy states determined by the expression (3.7). For the high energy spectrum the harmonic oscillator potential acts as a small perturbation. Thus the first-order corrections in the energy and the wave function are small. Fig. 3.7 shows that the main component of the 105th exact wave function comes from the 105th 1D box wave function, as it should for small perturbations.

For low energy states, perturbation theory around the 1D box states is not appropriate

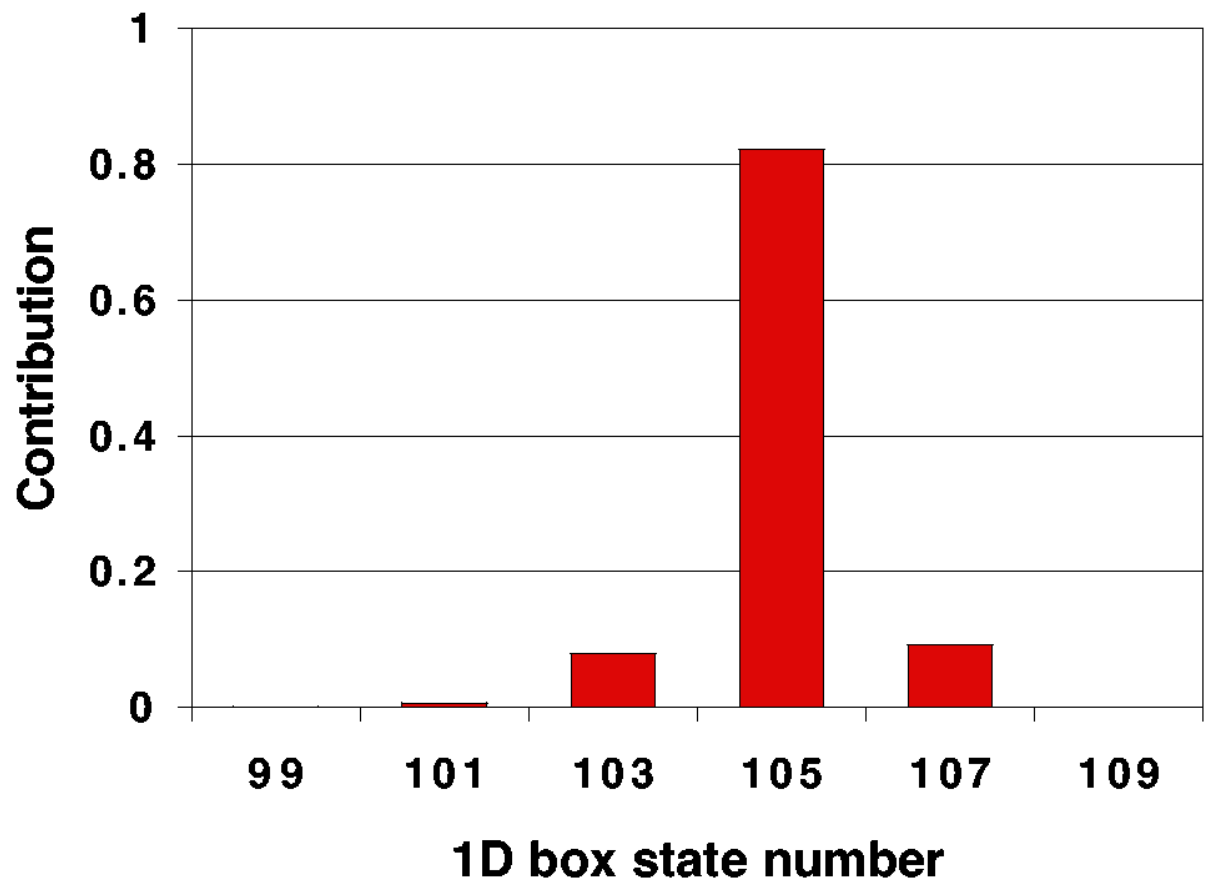


Figure 3.7: Non-zero components of the 105th exact eigenvector in the basis of a free particle in a one-dimensional box. Parameters of the Hamiltonian are  $\omega = 16$ ,  $L = \pi/2$ ,  $\hbar = m = 1$ .

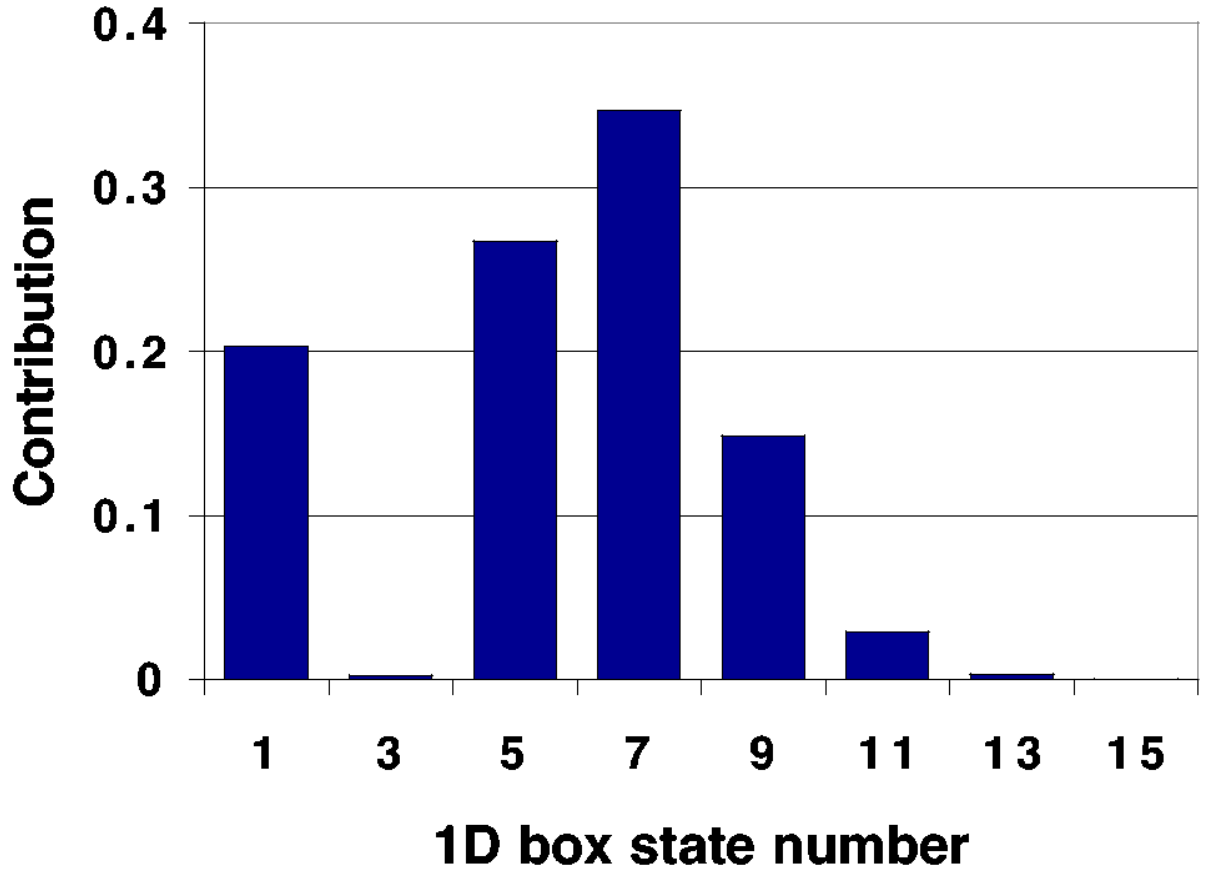


Figure 3.8: Non-zero components of the third harmonic oscillator eigenvector as expanded in the basis of a free particle in a one-dimensional box. Parameters of the Hamiltonian are  $\omega = 16$ ,  $L = \pi/2$ ,  $\hbar = m = 1$ .

since the harmonic oscillator states are the true states in this region. Specifically, for  $m = \hbar = 2L/\pi = 1$  and  $\omega = 16$ , the first ten states are exactly the harmonic oscillator states with a very high accuracy. The next ten states have high overlaps with the corresponding harmonic oscillator wave functions. For example, starting from 0.999999 at the tenth state, the overlaps go down to 0.880755 at the twentieth state; after that the overlaps get small very quickly. Fig. 3.8 shows the structure of the third exact eigenvector when expanded in the 1D box basis. Notice that the third 1D box wave function is almost missing from the structure of the third harmonic oscillator wave function. Such small overlap can happen at particular values of the parameter  $\omega L^2$  relevant for the problem at hand.

This pattern of having a small component of the exact wave function along the corresponding 1D box wave function continues to persist into the transition region. This is an

unexpected behavior considering the fact that the first order estimates of the energy levels are relatively good. Thus we are confronted with a situation where perturbation theory is not appropriate since level spacing is smaller than the magnitude of the “perturbing potential” but the expectation values of the full Hamiltonian are relatively close to the exact eigenvalues<sup>10</sup>, even though the corresponding 1D box wave functions are not at all present in the exact wave function as shown in Fig. 3.9.

In conclusion, there is a clear shortcut when using the oblique-basis idea. This allows one to use the correct wave functions in the relevant low and high energy regimes relative to  $E_c$ . There is a clear coherent mixing in the transition region. Such a phenomenon has been also observed in the lower  $pf$ -shell nuclei  $^{44-48}\text{Ti}$  and  $^{48}\text{Cr}$  which will be discussed in the next chapters. Due to the simplicity of the model, there is a small numerical gain in using oblique-basis calculations. However, there could be other cases with a significant gain in using the oblique-basis type calculations. Nuclear physics provides one such example as demonstrated in our study of  $^{24}\text{Mg}$  [8]. Another two-mode system of interest is a particle confined in two dimensions by an external magnetic field. This system is interesting because there is a lifting of the infinite degeneracy of Landau like states due to the confinement [40].

---

<sup>10</sup>A simple explanation of this effect is that the unperturbed energies  $E_n^0$  are such that  $E_n^0 > \delta E_n^1$ .

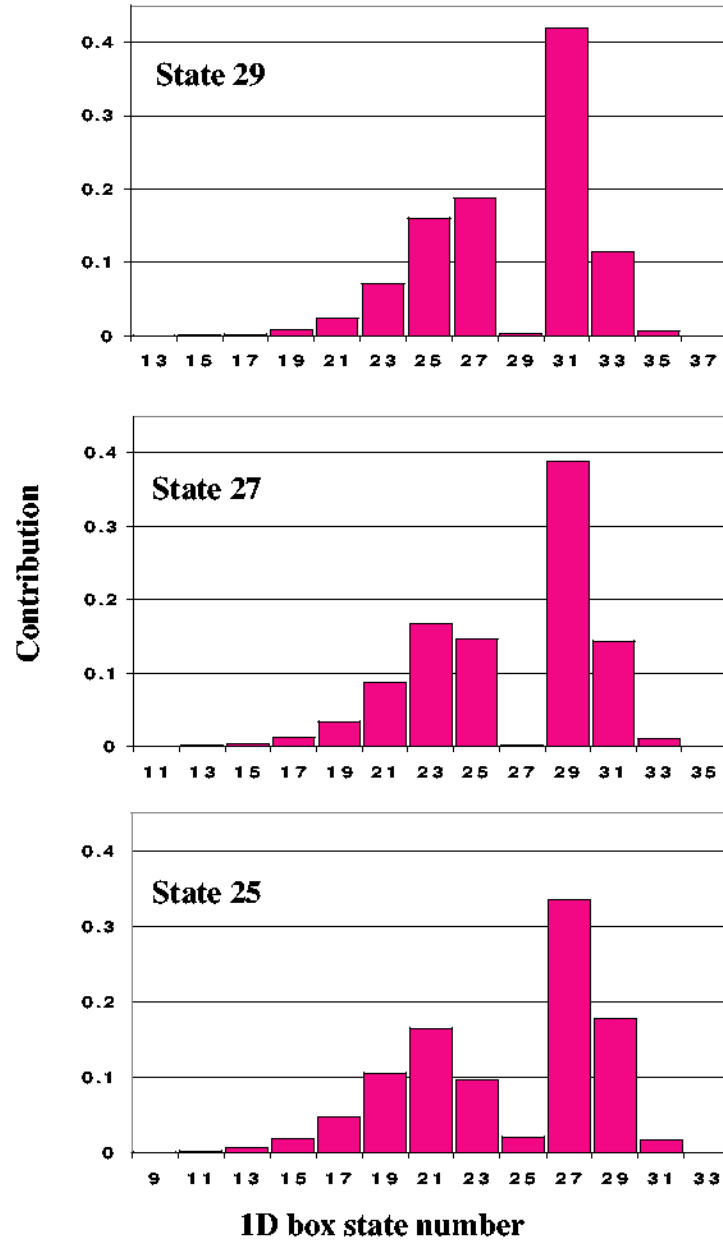


Figure 3.9: Coherent structure with respect to the non-zero components of the 25th, 27th and 29th exact eigenvector in the basis of a free particle in a one-dimensional box. Parameters of the Hamiltonian are  $\omega = 16$ ,  $L = \pi/2$ ,  $\hbar = m = 1$ .

# Chapter 4

## Oblique Shell-Model Basics

Some modern shell-model codes are based on the so-called  $m$ -scheme logic, namely, the model space is spanned by many-particle configurations (Slater determinants) with **good third component of the total angular momentum** ( $M_J$ ) [52, 53]. A good total angular momentum  $J$ , which is a conserved symmetry due to the isotropy of the space, is obtained either by angular momentum projection before, after, or as a consequence of the diagonalization of the Hamiltonian. Codes of this type normally achieve a good description of nuclear phenomena dominated by the single-particle effects. In these codes the basis consists of single machine words representing the many-particle configurations  $|n_1 \dots n_k\rangle = \prod_{s=1}^k (a_s^+)^{n_s} |0\rangle$ .

Unfortunately, an equally good description of collective phenomena within the framework of this approach is difficult to obtain due to the computational problems associated with the size of the needed model space. On the other hand, the  $SU(3)$ -based shell-model scheme is designed to give a simple interpretation of the collective nuclear phenomena. An ideal scenario would incorporate both the single-particle degree of freedom and the collective degree of freedom, allowing the Hamiltonian of the system to “choose” the admixture that is most appropriate. In this chapter, we discuss some of the computational methods and techniques used in our calculations.

### 4.1 Generalized Eigenvalue Problem

The usual procedure for solving an eigenvalue problem  $\hat{H}\vec{v} = \lambda\vec{v}$  is to cast it into a matrix equation. In a non-orthogonal basis [54], this matrix equation includes an overlap matrix ( $\Theta_{ij} = \langle i|j\rangle$ ) and has the form

$$\sum_j (H_{ij}v_j - \lambda\Theta_{ij}v_j) = 0. \quad (4.1)$$

For an orthonormal basis the overlap matrix becomes the identity matrix ( $\Theta_{ij} \rightarrow \delta_{ij}$ ), and the matrix form of the eigenvalue problem is

$$\sum_j H_{ij} v_j = \lambda v_i. \quad (4.2)$$

When the overlap matrix  $\Theta$  is positive-definite, the Cholesky algorithm [55], which decomposes  $\Theta$  into the product of an upper diagonal matrix ( $U$ ) and its transposed ( $U^T$ ),  $\Theta \rightarrow UU^T$ , can be used to cast the generalized eigenvalue problem (4.1) back into the standard matrix equation (4.2):

$$H' \vec{v}' = \lambda \vec{v}', \quad H' = U^{-1} H (U^{-1})^T, \quad \vec{v}' = U^T \vec{v}. \quad (4.3)$$

The use of the Cholesky algorithm is essential for identifying the linearly dependent vectors within the oblique basis. For large spaces, the effective eigenvalue problem (4.3) can be solved efficiently by using an appropriately modified Lanczos algorithm which we will discuss in a later section.

For the calculations that will be discussed later, we use two basis sets. The first set consists of spherical shell-model states (ssm-states) expressed in spherical single-particle coordinates ( $nlj$ ). The second set has a good SU(3) structure (su3-states) which track nuclear deformation [56]; this basis set is given in cylindrical single-particle coordinates. By construction, both sets have the third projection  $M_J$  of the total angular momentum  $J$  as a good quantum number [22, 19]. Schematically, these basis vectors and their overlap matrix can be represented in the following way:

$$\text{basis vectors} : \quad \begin{pmatrix} e_\alpha : \text{ssm} - \text{basis} \\ E_i : \text{su3} - \text{basis} \end{pmatrix}, \quad (4.4)$$

$$\text{overlap matrix} : \quad \Theta = \begin{pmatrix} \mathbf{1} & \Omega \\ \Omega^+ & \mathbf{1} \end{pmatrix}, \quad \Omega_{\alpha i} = e_\alpha \cdot E_i, \quad (4.5)$$

$$\text{Hamiltonian matrix} : \quad H = \begin{pmatrix} H_{ssm \times ssm} & H_{ssm \times su3} \\ H_{su3 \times ssm} & H_{su3 \times su3} \end{pmatrix} = \begin{pmatrix} H_{\alpha\beta} & H_{\alpha j} \\ H_{i\beta} & H_{ij} \end{pmatrix}. \quad (4.6)$$

In the above,  $\alpha$  and  $i$  span the following ranges:  $\alpha = 1, \dots, \dim(\text{ssm-basis})$  and  $i = 1, \dots, \dim(\text{su3-basis})$ .

Calculations in a nonorthogonal oblique basis require an evaluation of the matrix elements of physical operators plus a knowledge of the scalar product ( $e_\alpha \cdot E_i$ ) related to the overlap matrix. While it may be desirable to have an analytical expression for the overlap matrix, as we have for the single-particle overlap matrix [57], for practical purposes it suffices either to know the representation of each basis state in a common set that spans the full space, which is counter to the overall objective of reducing the number of basis states to a manageable subset, or to expand one set in terms of the other. For the present work, the  $e_\alpha$ , which can be represented by a single machine word in a spherical single-particle scheme, were expanded

in a cylindrical basis, which is the representation for our collective SU(3) basis vectors. This transformation is handled by an efficient routine that exploits two computational aids: bit manipulation via logical operations and a weighted search tree for fast data storage and retrieval [18]. Transformation of this type has to be done at least once per ssm basis state ( $e_\alpha$ ). We transform the ssm-basis states since the result is usually a vector with fewer components than a typical SU(3) basis state. There is a simple way to calculate the overlap between states in different single-particle bases [58]. However, for the calculation of matrix elements of the Hamiltonian, it is better to transform each  $e_\alpha$  vector in the basis used by the SU(3) states.

Matrix elements of the one-body and two-body Hamiltonian

$$H = \sum_i \varepsilon_i a_i^\dagger a_i + \frac{1}{4} \sum_{i,j} V_{kl,ij} a_i^\dagger a_j^\dagger a_k a_l$$

have to be evaluated in each subspace ( $H_{\alpha\beta}$  and  $H_{ji}$ ), as well as between the two spaces ( $H_{\alpha i}$  and  $H_{j\beta}$ ), see (4.6). The  $H_{\alpha\beta}$  part is normally given and evaluated in a spherical single-particle basis. By transforming the Hamiltonian to a cylindrical single-particle basis one can obtain the  $H_{ji}$  part of  $H$ . In order to compute the off-diagonal blocks ( $H_{\alpha i}$ ,  $H_{j\beta}$ , and overlap matrix elements between SU(3) and ssm-basis states), both basis sets are expanded in a basis of Slater determinants using cylindrical single-particle states. For example, any vector within the two irreps (8,4) and (9,2) of  $^{24}\text{Mg}$  has at most 2120 cylindrical Slater determinants; each ssm state, which itself is a single spherical Slater determinant, typically expands into less than 1296 cylindrical Slater determinants. We do not expand the SU(3) states into spherical-basis Slater determinants because that would require a significant fraction of the entire spherical shell-model space, defeating the rationale of our approach. Taking into account the significant number of Hamiltonian matrix elements ( $H_{ij}$  and  $H_{i\beta}$ ) between multi-component states, it should be clear that this is the most time consuming part of the calculation. The extra labels associated with the intrinsic quadrupole moment  $\varepsilon$  of each basis state is used to produce well-structured band-like matrices and to speed up the calculation. Specifically, basis states are pre-ordered according to their deformation as reflected by  $\varepsilon$ , and during the evaluation of  $H$  a  $\Delta\varepsilon$  selection rule is applied.

It is important to point out that knowledge of the overlap matrix  $\Theta$  and the matrix elements of  $H$  in the two spaces ( $H_{\alpha\beta}$ ,  $H_{ij}$ ) is not enough to obtain the correct off-diagonal block  $H_{\alpha i}$ . This is clear from the following explicit expression for  $H_{\alpha i}$  which contains a summation along ( $\bar{\beta}$ ) that lies outside of the oblique model space ( $\beta, i$ ):

$$H_{\alpha i} = \sum_{\beta} H_{\alpha\beta} \Theta_{\beta i} + \sum_{\bar{\beta}} H_{\alpha\bar{\beta}} \Theta_{\bar{\beta} i}.$$

Thus a direct evaluation of  $H_{\alpha i}$  is required.

## 4.2 Geometrical Visualization of the Oblique Basis

It is instructive to consider a geometrical visualization of the oblique-basis concept. Since a set of vectors defines a hyperplane, it is natural to ask the question: “What is the angle between hyperplanes defined by the bases under consideration?” To answer this question, first consider the angle  $\theta$  between a normalized SU(3) basis vector  $\vec{v}$  and the subspace  $V$  spanned by the spherical shell-model basis vectors. The length of the projected vector  $\vec{v}_V \in V$  is given by  $\cos(\vec{v}, V) = \cos \theta = |\vec{v}_V|$ . The space  $V$  of the spherical shell-model basis vectors induces a natural basis  $\vec{n}_\varepsilon$  in the SU(3) space ( $\vec{n}_\varepsilon = n_\varepsilon^i \vec{E}_i$ ). The angle between each new basis vector  $\vec{n}_\varepsilon$  and the space  $V$  will again be the length of its projection into the space  $V$ , but it has the nice property that this set of orthogonal basis vectors stays orthogonal after the projection into the space  $V$ :

$$\begin{aligned} \cos \theta_\varepsilon &= \cos(\vec{n}_\varepsilon, V) = |\vec{n}_{\varepsilon V}|, \\ \vec{n}_{\varepsilon V} &= \sum_{i,\alpha} n_\varepsilon^i (\vec{E}_i \cdot \vec{e}_\alpha) \vec{e}_\alpha = \sum_{i,\alpha} n_\varepsilon^i \Theta_{i\alpha} \vec{e}_\alpha, \\ |\vec{n}_{\varepsilon V}|^2 &= \sum_\alpha \left( \sum_i n_\varepsilon^i \Theta_{i\alpha} \right)^2 = \sum_{\alpha,i,j} n_\varepsilon^i \Theta_{i\alpha} n_\varepsilon^j \Theta_{j\alpha}. \end{aligned}$$

In matrix notation this reads

$$|\vec{n}_{\varepsilon V}|^2 = \vec{n}_\varepsilon \cdot \hat{\Theta} \cdot \hat{\Theta}^T \cdot \vec{n}_\varepsilon,$$

where the natural basis vectors  $\vec{n}_\varepsilon$  are eigenvectors of the symmetric matrix  $\hat{\Theta} \cdot \hat{\Theta}^T$

$$\hat{\Theta} \cdot \hat{\Theta}^T \cdot \vec{n}_\varepsilon = \varepsilon^2 \vec{n}_\varepsilon. \quad (4.7)$$

It follows that  $|\vec{n}_{\varepsilon V}|^2 = \vec{n}_\varepsilon \cdot \hat{\Theta} \cdot \hat{\Theta}^T \cdot \vec{n}_\varepsilon = \varepsilon^2 \vec{n}_\varepsilon \cdot \vec{n}_\varepsilon = \varepsilon^2$ , and thus the matrix  $\hat{\Theta} \cdot \hat{\Theta}^T$  is positive definite ( $|\vec{n}_{\varepsilon V}|^2 = \varepsilon^2 \geq 0$ ) with eigenvalues determined by the  $\cos \theta$ . This construction allows for a simple visualization of the space spanned by the oblique basis: Choose the  $x$ -axis to correspond to the space  $V$  of all the spherical shell-model basis vectors and represent the SU(3) space as a collection of unit vectors each at an angle  $\cos \theta = \varepsilon$  with respect to the  $x$ -axis. This construction will be applied later to the geometry of oblique-basis space calculations to demonstrate the relative orthogonality of the two vector sets,  $e_\alpha$  and  $E_i$ .

## 4.3 The Lanczos Algorithm

The Lanczos algorithm is an essential scheme for obtaining a small number of eigenvectors corresponding to the lowest or highest eigenvalues [20, 28]. It has been applied successfully to spatial dimensions on the order of  $10^6$  and even pushed up to  $10^8$  [59]. This algorithm is a simple and very efficient method to build a basis of the Hilbert space associated with an eigenvalue problem for an operator  $H$ . In its simplest form, one starts with a trial state and applies  $H$  over and over to generate new states; the process can be applied as many times as desired. This way one generates an orthonormal basis in which the corresponding matrix

of the operator  $H$  is tri-diagonal. The method is recursive and could be used in numerical, as well as in analytic calculations [60]. For our toy model described earlier, we have used analytic realization (coordinate representation) of the algorithm while for the calculations in nuclei a numerical matrix realization has been more suitable due to the Fock representation of the states.

In brief, the algorithm starts with the choice of a first normalized vector  $\vec{v}_1$  ( $\langle \vec{v}_1 | \vec{v}_1 \rangle = 1$ ). In matrix calculations this vector is often chosen randomly. Then  $H$  is applied on  $\vec{v}_1$  and a new vector orthogonal to  $\vec{v}_1$  is constructed,  $\vec{v}_2 = H\vec{v}_1 - \langle \vec{v}_1 | H\vec{v}_1 \rangle \vec{v}_1$ . Next  $\vec{v}_2$  is normalized and used to generate a new vector and so on. It can be shown that the basis  $\{\vec{v}_n\}$  generated this way is orthonormal, and  $H$  is tri-diagonal in this basis. However, numerical noise destroys the orthogonality and requires one to do full reorthogonalization of each newly generated vector with all previous vectors. One important feature of the Lanczos algorithm is that at each new iteration it provides the vector that has the next most important contribution within the model space. However, this is true only if our first vector is a good trial guess to an exact state. A trial vector with some bad components can cause problems.

Another feature of the Lanczos algorithm is that it preserves the symmetry of the initial vector when this symmetry is a symmetry of the Hamiltonian as well.<sup>1</sup> For example, if  $H$  is invariant under parity transformation, then the algorithm will produce only even parity states. Similarly, if we start with a state with good  $J$  and  $M_J$ , then applications of  $H$  will only produce states of the same symmetry. While this can be viewed as an advantage, sometimes it can be a problem especially when the symmetry has a finite irreducible sub-space. For example, if we start with a vector from a finite irreducible sub-space, then after a finite number of iterations the algorithm will exhaust the sub-space and any new vector will be linearly dependent on the previously generated vectors. This breakdown of the algorithm is generally overcome by introducing a new guess vector. In large matrix diagonalizations, the new vector could be a random Gaussian vector, or it could be “the next vector” from a prior given set. In our toy model, we carried out Lanczos type calculations using the harmonic-oscillator basis as a prior given set.

An interesting variation to the Lanczos algorithm aiming at a particular  $k$ -th eigenvector has been suggested by Davidson [61]. In the Davidson algorithm, one tries to increase the speed of convergence by modifying the way a new vector is generated. For example, the Lanczos algorithm uses  $\vec{w}_n = H\vec{v}_n$  as a seed for a new vector  $\vec{v}_{n+1}$  while the Davidson algorithm uses the vector  $\vec{w}_n = (\lambda_k I - \text{diag}(H))^{-1} (He_k - \lambda_k e_k)$  with enhanced components along the  $k$ -th eigenvector. In the Davidson expression for  $\vec{w}_n$ ,  $e_k$  and  $\lambda_k$  are the approximate  $k$ -th eigenvector and eigenvalue after the  $n$ -th iteration, and  $\text{diag}(H)$  is the diagonal part of  $H$ .

To solve the generalized eigenvalue problem (4.3), we have to modify the Lanczos algorithm. In doing so, it is more efficient to perform consecutive action of the matrices  $U$  and  $H$  on the resulting vectors. The computational time in this case grows like the dimensionality

---

<sup>1</sup>The Lanczos algorithm should in principle conserve symmetries; however, machine round-off error often mixes in different states. The round-off error is also the reason for performing a complete re-orthogonalization for each newly generated state.

of the space to the second power ( $n^2$ ). This is to be compared to the case when one would first fully multiply these three matrices:  $(U^{-1})^T$ ,  $H$ , and  $U^{-1}$ , which grows as the third power of  $n$  ( $n^3$ ), and then act on vectors.

In closing this section, we would like to point out some possible future applications of the Lanczos algorithm and its modifications. Although recently the algorithm is mostly used in huge matrix diagonalizations [20, 62], it can also have some applications to constrained problems as mentioned in our toy model discussion of a particle in a box in the harmonic-oscillator basis. For such problems, one would have to project  $\vec{w}_n = H\vec{v}_n$  in the space determined by the constraints, and only after that proceed with the calculation. Another interesting application is related to the long standing problem of doing *ab-initio* calculations in nuclear physics with effective interactions derived from a NN-interaction. Some current advances in this field which takes advantage of the Lanczos algorithm has been reported by Haxton *et al.* [63, 64]. A link between the Lanczos method and space projection techniques, such as Brueckner, Feshbach, and Bloch-Horowitz projection treatments [36, 65, 66] also seems intriguing [63].

## 4.4 Mixed-Symmetry Basis for the Nuclear Shell Model

Even though the purpose of this work has been reiterated several times in different contexts, we feel strong motivation to state it again, but this time in the context of a pure practical curiosity. Specifically, can we do calculations using two or more important basis sets as usually employed in different shell models? In particular, can we use spherical shell-model states, which are related to the single-particle  $j$ -shell symmetry ( $\otimes^{2j+1}U(1) = U(1) \otimes \dots \otimes U(1) \otimes U(1)$ ), together with  $SU(3)$  shell-model states, which are related to the  $Q \cdot Q$  interaction? With these questions in mind, which will be answered in the positive sense in the next chapter, we continue our examination of the oblique basis concept by focusing on the structure of the two basis sets used in our mixed-symmetry shell-model calculations. In the rest of the chapter, we briefly go over the spherical single-particle basis, which is then followed by a discussion of the  $SU(3)$  symmetry-adapted basis.

### 4.4.1 Spherical Basis for Single-Particle Excitations

We have already introduced the main concepts and notations in a previous chapter, as well as the basic idea for configuration truncation in the  $m$ -scheme basis. Here, we would like to touch upon some details related to the specifics of our calculations. First of all the spherical basis states are taken from an old  $m$ -scheme code *NUCK (GLASGOW)* [21]. This code has been used as a benchmark and a testing ground of our oblique code results. The output from *NUCK* containing the spherical shell-model states (ssm-states) is used as input for *GlsqwBasis2Redstick* which gives a binary form of the proton-neutron basis states for use by the oblique code *su3pn*. In order to speed the calculations when  $SU(3)$  states are also included, there is an option to use  $\varepsilon$ -sorted ssm-states (sorting is provided by *EpsSorting*).

## 4.4.2 SU(3) Basis for Collective Excitations

We have already reviewed Elliott's  $SU(3)$  shell model [4] and some of the single-particle labeling schemes in a previous chapter. In this section, we briefly discuss the  $SU(3)$  package used to generate  $SU(3)$  symmetry-adapted states with good third component of the total angular momentum. Next the  $SU(3)$  single-particle shell-model basis states are discussed, and the action of the  $SU(3)$  generators is explained. It is then followed by a discussion of the structure of the *Extreme Weight State(s)* (EWS) of an  $SU(3)$  irrep for protons (neutrons), and especially the *Highest Weight State(s)* (HWS) of the so-called leading  $SU(3)$  irreps. Once a HWS is known, then all states of the corresponding irrep can be constructed using  $SU(3)$  step operators [23]. Proton (neutron) states with good third component of the angular momentum ( $M_J$ ) are obtained by considering the direct product  $SU(3) \otimes SU_S(2)$  using spin highest weight states, as well as spin *Lowest Weight States(s)* (LWS) [22]. Once the proton and neutron highest weight states are constructed, then they can be coupled to different possible proton-neutron highest weight states:

$$(SU(3) \otimes SU_S(2))_p \otimes (SU(3) \otimes SU_S(2))_n \rightarrow (SU(3) \otimes SU_S(2))_{pn}.$$

This is the so-called strong coupling scheme. This scheme is used to couple the proton and neutron irreps to some final proton-neutron irreps. Each extreme weight state can be used for the generation of all states of good  $M_J$  within a given  $SU(3)$  irrep. Another possible coupling scheme extends  $SU_S(2)$  to  $SU(4) \supset SU_S(2) \otimes SU_T(2)$ . This is the supermultiplet scheme which is a good symmetry for light nuclei. Since the goodness of the supermultiplet scheme does not extend to heavy nuclei, we will not consider it further in this study.

### • The SU(3) Basis Generator

The package for generation of  $SU(3)$  symmetry-adapted states with good third component of the total angular momentum consists of two major codes: (1)  $SU(3)$  proton-neutron HWS generator (*SU3\_HWS\_GEN*) and (2) proton-neutron generator of good  $M_J$  (*PNGGMJ*). The *SU3\_HWS\_GEN* routine provides the input for *PNGGMJ* which generates the basis states needed for our oblique calculations.

The overall algorithm has four basic components: 1) definition of the single-particle levels and matrix elements of the  $SU(3)$  generators for a given proton (neutron) shell; 2) generation of the HWS of  $SU(3) \otimes SU_S(2)$  for a given spin  $S$  and number of protons (neutrons)  $N$ ; 3) coupling of the proton HWS and neutron HWS to the desirable proton-neutron  $SU(3)$  HWS and  $SU_S(2)$  LWS; 4) generation of all proton-neutron  $SU(3) \otimes SU_S(2)$  states with good third component of the total angular,  $M_J$ .

The *PNGGMJ* code accepts any pn-HWS and generates all the states with a given  $M_J$  value. However, the *SU3\_HWS\_GEN* code does not generate all possible pn-HWS since one purpose of the current project is to include a few essential  $SU(3)$  basis states in an  $m$ -scheme type calculation. Thus the *SU3\_HWS\_GEN* code is set to generate only the leading proton and neutron configurations and their possible couplings. Therefore, an additional code (*SU3Lister*) is needed to allow for a quick look at all the proton-neutron  $SU(3)$  irreps

that can be generated by the current version of the *SU3\_HWS\_GEN* code. As a reference to a complete list of proton-neutron  $SU(3)$  irreps, one can use the  $SU(3)$  reduced matrix elements package [17]. If other HWS are desired, then the *SU3\_HWS\_GEN* code can be modified to generate non-leading HWS. This could be done either by using Bahri’s method [17] or perhaps by using another more direct approach tailored to the particular application at hand. The generation of non-leading HWS is important when one wishes to include states that are not maximally deformed in their intrinsic configuration. For example, non-leading HWS will be important if the non- $Q \cdot Q$  parts of the interaction play a significant role.

• **Single-Particle Levels and the  $SU(3)$  Matrix Elements**

The foundation of a microscopic type symmetry-adapted shell-model calculation is the structure of the single-particle levels (SPL). The single-particle levels should be related to a representation of the symmetry group which is  $SU(3)$  in our case. Therefore, a discussion focused on the  $SU(3)$  single-particle levels and matrix elements of the  $SU(3)$  generators is desirable and will be given in the following few paragraphs.

**Single-particle Levels - Ordering Scheme:** Single-particle levels of the  $\eta = 0, 1, 2, \dots$  ( $s, p, sd, \dots$ ) harmonic oscillator shell belong to the symmetric  $(\eta, 0)$  irrep of  $SU(3)$ . Because  $\mu = 0$ , a typical three-dimensional representation of  $SU(3)$  basis states, Fig. 4.1, reduces to a special two-dimensional triangular shape ( $\varepsilon$  and  $n_\rho$  become linearly dependent), Fig. 4.2. Also, because  $SU(3)$  is a compact group, its irreps are finite dimensional, and many-particle (fermion) configurations can be conveniently represented as binary strings with a 1 or 0 symbolizing the presence or absence of a particle in the corresponding single-particle level. (The latter, together with a “sign rule” to accommodate fermion statistics, is a convenient computer implementation of a Slater determinant representation of the basis states.)

Recall that the canonical reduction,  $SU(3) \supset U(1) \otimes SU(2)$ , has two additive labels  $\varepsilon$  ( $Q_0$ ) and  $m_l$  ( $L_0$ ), and the allowed values of these labels for fixed  $SU(3)$  irrep  $(\lambda, \mu)$  are given by [23]:

$$\varepsilon = 2\lambda + \mu - 3(p + q), \quad n_\rho = \mu + (p - q), \quad m_l = n_\rho - 2m \quad (4.8)$$

where  $0 \leq p \leq \lambda$ ,  $0 \leq q \leq \mu$ , and  $0 \leq m \leq n_\rho$ .

A convenient ordering scheme (which tracks the arrows in Fig. 4.2) is set by requiring a simple representation of many-particle configurations with maximum quadrupole deformation. This objective can be achieved if the states are ordered by  $\varepsilon$  (quadrupole moment) first and then by  $m_l$  (third component of the angular momentum).

**Action of  $SU(3)$  Generators on Single-Particle States:** To be able to apply the  $SU(3)$  generators on many-particle configurations, it suffices to know the action of these generators on the single-particle states. The eight generators of  $SU(3)$  belong to the self-adjoint  $(1, 1)$  irrep of  $SU(3)$ . The operator structure should be chosen in the most convenient form for the application under consideration. For the present application, this choice is the same as used

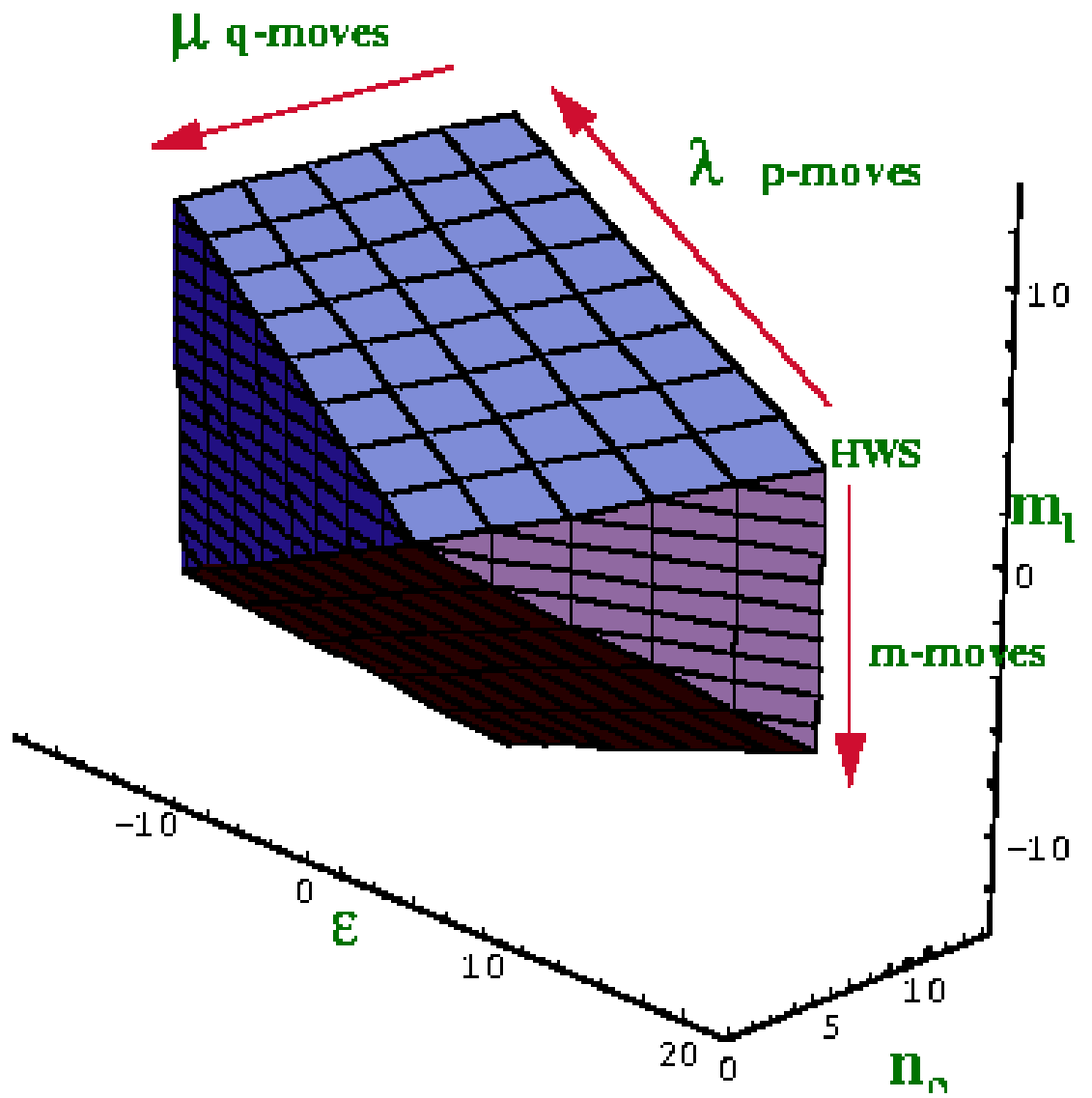


Figure 4.1: Three-dimensional view of the  $(\lambda, \mu)$   $SU(3)$  irrep together with the action of the  $SU(3)$  step operators.

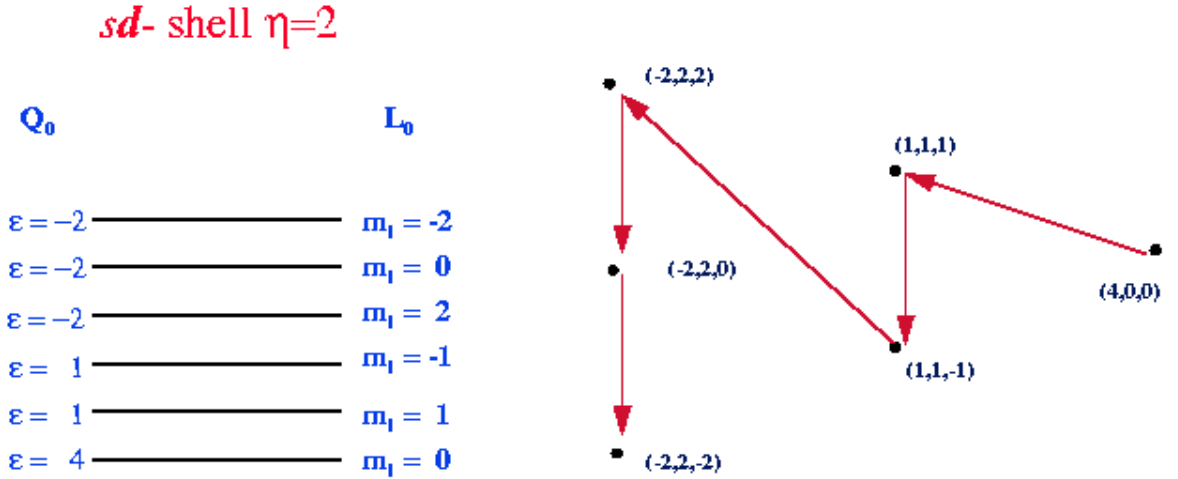


Figure 4.2: Ordering scheme of the single-particle levels.

for the basis states, namely, the  $SU(3) \supset SU(2) \otimes U(1)$  reduction. The matrix elements of the  $SU(3)$  generators can be obtained either by using an application of the appropriate Wigner-Eckart theorem or by using explicit expressions [23] for determining the action of the operators on the basis states. For computational purposes, it is better to adopt a direct solution. We use the fact that the action of the operators is on a product of single-particle levels each of which belongs to a symmetric  $(\eta, 0)$  irrep of  $SU(3)$ . This allows the matrix elements of the  $SU(3)$  generators to be calculated using properties of the  $SU(2)$  only (Fig. 4.3).

A key feature is the fact that the six non-diagonal generators of  $SU(3)$  (recall that  $L_0$  and  $Q_0$  are diagonal) are rising or lowering generators of  $SU(2)$  subgroups of  $SU(3)$ . The three  $SU(2)$  subgroups and their respective actions are shown in Fig. 4.3. States that are collinear with one of the sides of the triangular shape shown on the right in the figure form an irrep of the corresponding  $SU(2)$  subgroup.

- **Action of  $SU(3)$  Generators on Many-Particle States**

Having been supplied with the single-particle levels and the action of the  $SU(3)$  generators on them, we can construct many-particle states and extend the action of the  $SU(3)$  generators to these many-particle states as well. Since one goal of the oblique-basis project is to include essential  $SU(3)$  basis states in an  $m$ -scheme type calculation, we would briefly discuss the maximally deformed HWS for protons (neutrons). These HWS are the leading proton (neutron) irreps and can be coupled easily to the leading and other proton-neutron

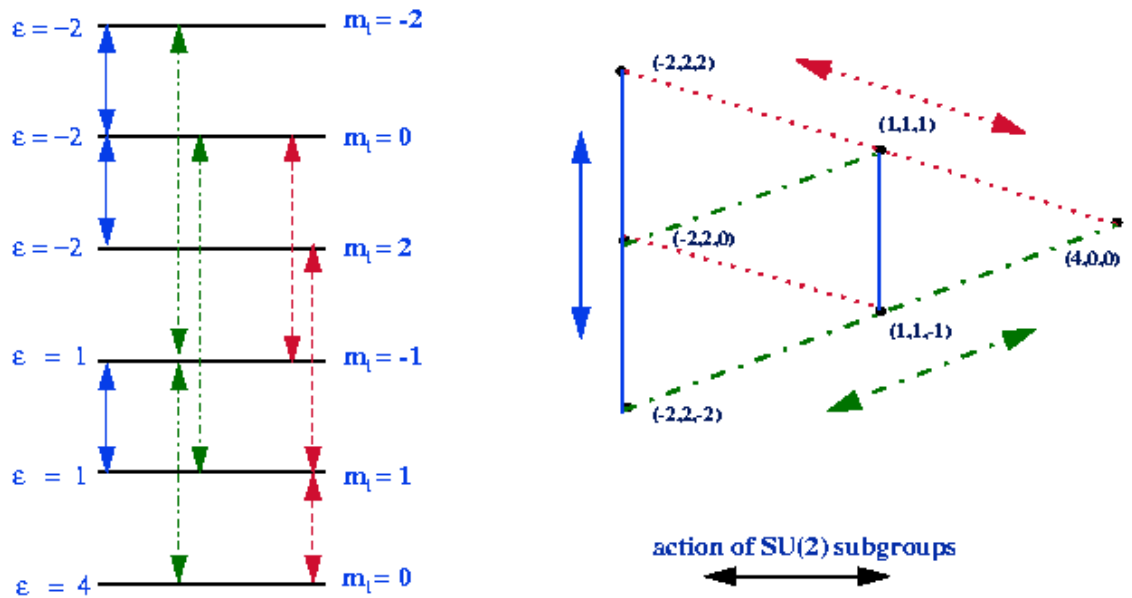


Figure 4.3: Action of the  $SU(3)$  generators on the single particle levels. The diagram on the left shows that applying an  $SU(3)$  generator to a single-particle state results in another single-particle state. The diagram on the right shows the action of the six non-diagonal generators of  $SU(3)$ . The vertical solid lines represent the action of the  $SU(2)$  subgroup that enters the  $SU(3) \supset SU(2) \otimes U(1)$  chain.

irreps for a given nucleus. Once we have an  $SU(3)$  HWS  $\otimes SU_S(2)$  LWS state, we can easily generate all the states with good  $M_J$  within this  $SU(3) \otimes SU_S(2)$  irrep.

**Highest Weight States of  $SU(3) \otimes SU_S(2)$  for Leading Irreps:** So far we have constructed single-particle states and evaluated matrix elements of the generators of  $SU(3)$  when they act on these states. The next step is to construct many-particle HWS of  $SU(3) \otimes SU_S(2)$ . In the chosen  $SU(3)$  labelling scheme, there are seven extreme states which correspond to the vertex points of the three-dimensional diagram (Fig. 4.1) of a general  $(\lambda, \mu)$  irrep. We are particularly interested in the vertex that has the maximum value for the quadrupole moment of the system (Fig. 4.1). Our HWS is the state with  $\varepsilon = 2\lambda + \mu$ ,  $n_\rho = \mu$ , and  $m_l = \mu$ . This HWS (maximum value of  $m_l$  for maximum  $\varepsilon$ ) can be easily constructed by ensuring that the action of the  $SU(3)$  rising generators annihilates it. Indeed, for such a HWS, the values of  $\lambda$  and  $\mu$  can be determined from its  $\varepsilon$  and  $m_l$  labels.

Selecting the leading  $(\lambda, \mu)$  irrep (HWS with maximum overall value of  $\varepsilon$ ) out of all possible irreps of an  $N$  fermion system with total system spin  $S$  is very simple within the chosen scheme. This is because the number of particles with spin up  $n_\uparrow$  and spin down  $n_\downarrow$  is uniquely determined by the solution of two linear equations:

$$N = n_\uparrow + n_\downarrow, \quad 2S = n_\uparrow - n_\downarrow.$$

The second of these two equations expresses the fact that we also require the state to be highest weight with respect to  $SU_S(2)$ . Further, maximizing the value of  $Q_0$  is achieved by filling the single-particle states of the  $(\eta, 0)$  irrep (Fig. 4.2) from bottom to top. The chosen scheme ensures that this simple procedure gives maximum values for  $\varepsilon$  and  $m_l$ . The  $SU(3)$  irrep labels  $(\lambda, \mu)$  are obtained by evaluating the quadrupole moment ( $Q_0$ ) and angular momentum projection ( $L_0$ ) which are additive quantum numbers.

For example, in the  $sd$ -shell, there are six single-particle levels corresponding to the  $(2, 0)$  irrep of  $SU(3)$ . The HWS of the leading irrep for  $N = 6$  particles and total system spin  $S = 1$  is  $(3, 3)$  (Fig. 4.4), whereas for  $S = 0$  the leading  $SU(3)$  irrep is  $(6, 0)$  (Fig. 4.5). These many-particle configurations are HWS with respect to  $SU(3)$  and  $SU_S(2)$ .

**Generating  $SU(3)$  States with Step Operators:** Once we have the HWS of  $SU(3) \otimes SU_S(2)$ , we can generate any other state of the  $SU(3)$  irrep  $(\lambda, \mu)$  by applying step operators similar to those given by Hecht. This process is needed when we produce proton-neutron coupled  $SU(3)$  irreps. By using the parameterization (4.8) [23], we can identify the corresponding step operators, Fig. 4.1.

It is important to note that applying  $p$ -move or  $q$ -move step operators to states on the top surface yields other states (or zero) on that same surface. Since the states on the top surface are HWS with respect to  $SU(2)$  in the  $SU(3) \supset SU(2) \otimes U(1)$  reduction, the  $m$ -move step operator is an  $SU(2)$  lowering operator which changes the third component of the angular momentum ( $m_l$ ). The  $p$ -move and  $q$ -move step operators can be obtained by imposing the restriction that they generate only transformations within the  $SU(2)$  HWS space. From an algebraic perspective, the  $p$ -move and the  $m$ -move operators are linear in  $SU(3)$  generators

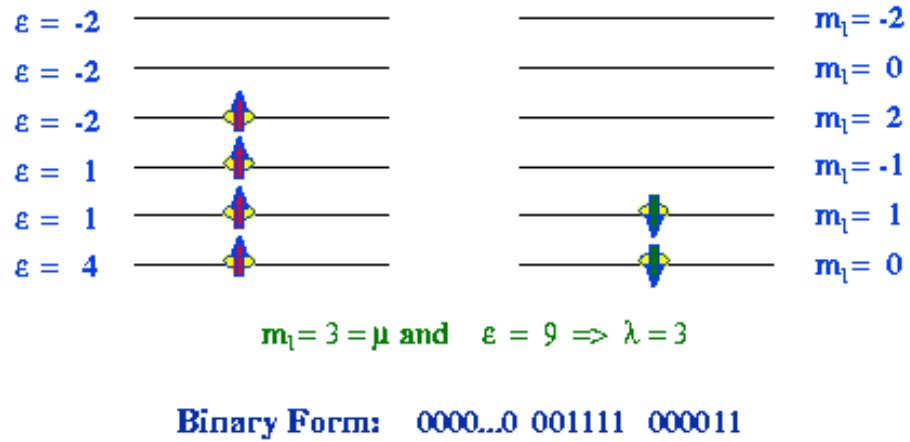


Figure 4.4: Highest weight state of the leading (3,3) irrep for  $N = 6$  and  $S = 1$  in the  $sd$ -shell.

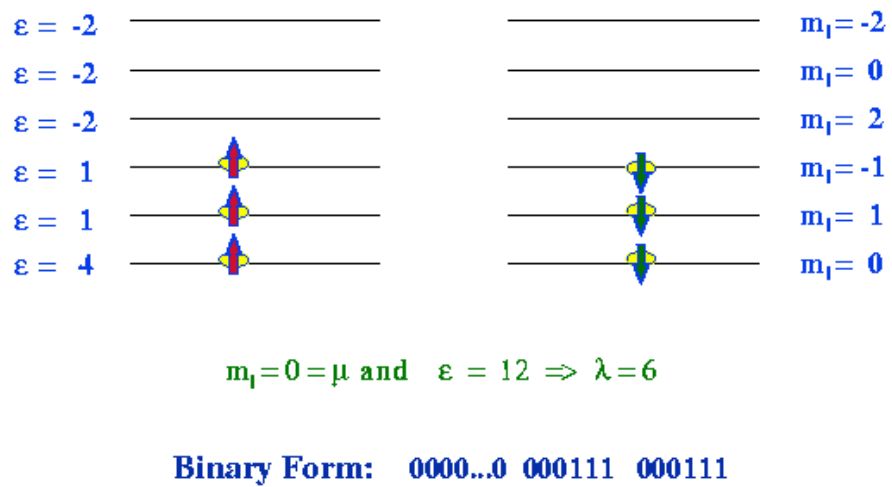


Figure 4.5: Highest weight state of the leading (6,0) irrep for  $N = 6$  and  $S = 0$  in the  $sd$ -shell.

while the  $q$ -move operator is quadratic. Nevertheless, the state generation process can be written in such a way that the  $q$ -move operator effectively reduces to a linear action. These step operators can also be obtained by a projection operator technique [67].

**Generating Proton-Neutron  $SU(3)$  Highest Weight States:** In brief, the generation of the proton-neutron  $SU(3)$  HWS is just a matter of  $SU(3)$  and  $SU_S(2)$  couplings. However, the actual algorithm for the generation process is somewhat backwards to the structure of the sentences that we would use to describe it. What we mean by this is that when the number of protons and the number of neutrons are given together with their harmonic oscillator shells, then the algorithm does a loop over all possible total proton-neutron spins ( $S_{pn}$ ). For each total spin ( $S_{pn}$ ), loops are made over the possible proton spin ( $S_p$ ) and neutron spin ( $S_n$ ) that can couple to the total spin ( $S_{pn}$ ). This way the proton HWS can be constructed, as described in the previous sections, by using the proton number ( $N_p$ ) and spin ( $S_p$ ) to get the  $(SU(3) \otimes SU_S(2))_p$  HWS state. The same is done for the neutron HWS. This way all the major labels,  $|N(\lambda, \mu)\varepsilon, n_\rho, m_l\rangle_p \otimes |SM_S\rangle_p$  for protons and  $|N(\lambda, \mu)\varepsilon, n_\rho, m_l\rangle_p \otimes |SM_S\rangle_p$  for neutrons, have been determined and one can proceed with the details of the coupling to  $|N(\lambda, \mu)\varepsilon, n_\rho, m_l\rangle_{pn} \otimes |SM_S\rangle_{pn}$ .

$$(SU(3) \otimes SU_S(2))_p \otimes (SU(3) \otimes SU_S(2))_n \rightarrow (SU(3) \otimes SU_S(2))_{pn}.$$

One final detail on the generation process is that the proton HWS state is actually an  $SU(3)$  HWS but a spin LWS while for the neutrons it is an  $SU(3)$  and a spin HWS. Then they are coupled to a proton-neutron  $SU(3)$  HWS with a spin LWS structure. The reason behind this is that in the  $SU(2)$  type coupling one does a loop such that  $m_p + m_n = m_{pn}$ . Hence, if  $m_p$  is the minimal  $m$ -value of the proton spin such that  $m_p + m_n = m_{pn}$  for a fixed  $m_{pn}$ , then the  $m_n$  should be the maximal  $m$ -value of the neutron spin. Therefore, the loop which satisfies  $m_p + m_n = m_{pn}$  will have an increase of  $m_p$  and simultaneous decrease of  $m_n$  so that  $m_{pn}$  stays fixed. This is also the reason why the total proton-neutron state is a LWS ( $M_S = -S_{pn}$ ) so that the coupling to the good  $M_J = M_l + M_S$  is done in the same way since  $M_l$  is at maximum in the proton-neutron  $SU(3)$  HWS.

**Generating States of Good  $M_J$ :** Since the action of the  $SU(3)$  commutes with that of the spin group ( $SU_S(2)$ ), it is not difficult to achieve the final goal of states with good third component of the total angular momentum ( $M_J$ ). Recall that we have just generated proton-neutron EWS ( $SU(3)^{HWS} \otimes SU_S(2)_{LWS}$ ). We also introduced the procedure to generate other states of an  $SU(3)$  irrep by applying step operators. Each of these states remains a LWS of  $SU_S(2)$ . Hence, after each move on the top surface (see Fig. 4.1), using  $p$ -move or  $q$ -move step operators, we can apply spin rising and angular momentum lowering to the corresponding state toward  $M_J = M_l + M_s$ . This way, we can generate all proton-neutron states with labels:  $N, S, (\lambda, \mu), \varepsilon, n_\rho, M_l$ , and  $M_J$ .

# Chapter 5

## $^{24}\text{Mg}$ Mixed-Symmetry Calculations

The success and applicability of the oblique-basis approach to  $^{24}\text{Mg}$ , which will be demonstrated in the following sections, can be related to the fact that the spherical shell-model states are eigenstates of the one-body Hamiltonian ( $\sum \varepsilon_i a_i^+ a_i$ ) while the two-body part of the Hamiltonian ( $\sum_{i,j} V_{kl,ij} a_i^+ a_j^+ a_k a_l$ ) is strongly correlated with the quadrupole-quadrupole interaction ( $Q \cdot Q$ ) which is diagonal in the SU(3) basis [68]. By combining spherical shell-model states and SU(3) states, one accommodates, from the onset, the dominant modes of the system.

In this chapter we discuss the oblique-basis technique as applied to  $^{24}\text{Mg}$  [8]. This is a strongly deformed nucleus with well-known collective properties and is one of the best manifestations of the Elliott's SU(3) symmetry [4]. In terms of dimensionality of the model space, adding a few leading SU(3) irreps to a highly truncated spherical shell-model basis results in significant gains in the convergence of the low-energy spectra towards the full space result. In particular, the addition of leading SU(3) irreps yields the right placement of the K=2 band and the correct order for most of the low-lying levels. Indeed, an even more detailed analysis shows that the structure of the low-lying states is significantly improved through the addition of a few SU(3) irreps. The Hamiltonian used in our analysis is the Wildenthal interaction [12].

In the following sections we summarize some of the important features of the spherical, SU(3), and mixed-symmetry type shell-model calculations. First we discuss the dimensions of each model space. Then we consider the ground-state energy as a function of the model space used. Next we focus on the structure of the low-energy spectrum, and finally we discuss the structure of the states as compared to the exact *sd*-shell results.

### 5.1 Structure of the Model Spaces

One important question in any computational study is the dimensions of the matrices involved, as well as the structure of the model space used. In this section, we address this question by briefly summarizing the space structure and dimensions for the spherical, SU(3), and oblique shell-model calculations.

Table 5.1: Labels and  $M_J = 0$  dimensions for various  $^{24}\text{Mg}$  calculations. The leading SU(3) irrep is denoted by (8,4) while (8,4)&(9,2) implies that (9,2) irreps have also been included. The SM( $n$ ) spaces correspond to spherical shell-model partitions with  $n$  valence particles excited out of the  $d_{5/2}$  shell into the  $s_{1/2}$  and  $d_{3/2}$  levels.

Model space	(8, 4)	(8, 4)&(9, 2)	SM(0)	SM(1)	SM(2)	SM(4)	FULL
space dimension	23	128	29	449	2829	18290	28503
% of the full space	0.08	0.45	0.10	1.57	9.92	64.17	100

### 5.1.1 Model Space Dimensions

Our model space for  $^{24}\text{Mg}$  consists of 4 valence protons and 4 valence neutrons in the  $0\hbar\omega$   $sd$ -shell. The  $m$ -scheme dimensionality ( $M_J = 0$ ) of this space is 28503. This space is denoted as FULL in the figures that follow. To test the effects of truncations, calculations were also carried out permitting  $n$  particles to be excited out of the lowest  $d_{5/2}$  orbit, i.e.  $d_{5/2}^{8-n}(d_{3/2}s_{1/2})^n$ , and are denoted as SM( $n$ ). The SM(2) approximation is of particular interest since it allows one to take into account the effect of pairing correlations (one pair maximum) in the ‘secondary levels’ ( $s_{1/2}$  and  $d_{3/2}$  for the  $^{24}\text{Mg}$ ) with a minimum expansion of the model space. The SU(3) part of the basis includes two scenarios: one with only the leading representation of SU(3), which for  $^{24}\text{Mg}$  is the (8,4) irrep, with dimensionality 23 for the  $M_J = 0$  space and denoted in what follows by (8,4); and another with the (8,4) irrep plus the next most important representation of SU(3), namely the (9,2). The (9,2) irrep occurs three times, once with  $S = 0$  ( $M_J = 0$  dimensionality 15) and twice with  $S = 1$  ( $M_J = 0$  dimensionality  $2 \times 45 = 90$ ). All three (9,2) irreps have total  $M_J = 0$  dimensionality of  $15+90=105$ . The (8,4)&(9,2) case has total  $M_J = 0$  dimensionality of  $23+105=128$  and is denoted by (8,4)&(9,2). In Table 5.1 we summarize the dimensionalities involved.

### 5.1.2 Visualizing the Oblique Basis for $^{24}\text{Mg}$

After obtaining an idea of the space dimensions involved, we now try to visualize the oblique basis. The method described in the previous chapter can be used to visualize the structure of the oblique basis. First, consider the SM(2) space enhanced by the SU(3) irreps (8,4)&(9,2). Since the SM(2) and (8,4)&(9,2) spaces are both relatively small (see Table 5.1), we expect the basis vectors of these spaces to be nearly orthogonal. This orthogonality is clearly seen from inset (a) in Fig. 5.1. Inset (b) in Fig. 5.1 shows a loss of orthogonality between the SM(4) and the (8,4)&(9,2) basis vectors. This is due to the fact that SM(4) space is about 64% of the full  $sd$ -space. Therefore, there is a relatively high probability that some linear combinations of SU(3) basis vectors lie in the SM(4) space. Indeed, it can be shown that there are five vectors from (8,4)&(9,2) that lie within the SM(4) space. Such redundant vectors are identified and excluded from the calculation within the Cholesky

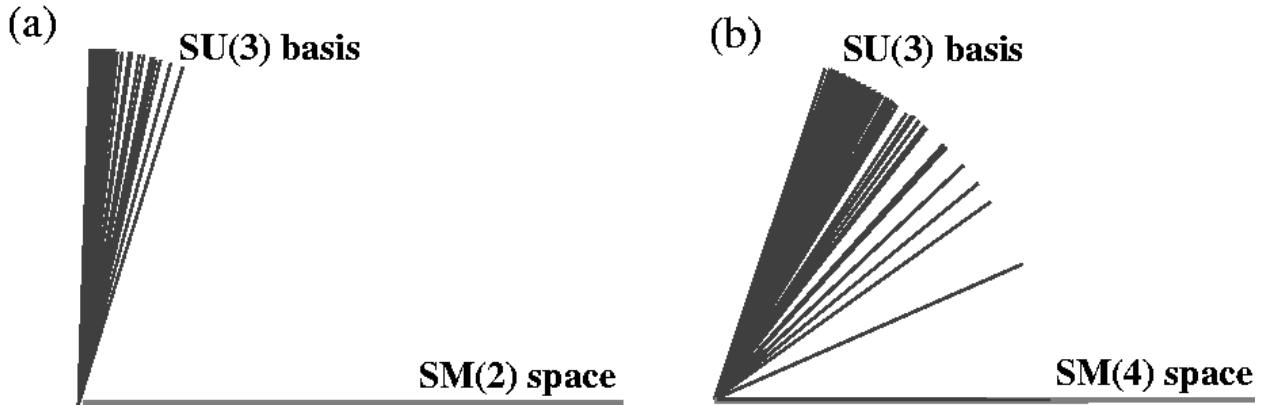


Figure 5.1: Orthogonality of the basis vectors in the oblique geometry. The SU(3) space consists of (8,4)&(9,2) basis vectors with the shell-model spaces (SM(n) with n=2 and 4) indicated by a horizontal line. (a) SM(2) and the natural SU(3) basis vectors and (b) SM(4) and the natural SU(3) basis vectors. In the latter case (b), there are five SU(3) vectors that lie in the SM(4) space.

algorithm when it is applied to the overlap matrix ( $\Theta \rightarrow UU^T$ ).

## 5.2 Spectral Characteristics

Reproducing the correct energy spectra of a nucleus is one of the goals of any nuclear-structure study. Since we are trying to develop a new concept for nuclear structure studies, the mixed-symmetry approach, we are currently comparing our results only with full shell-model calculations. Therefore, a computation-to-computation comparison is our reality check. In the next sub-sections we compare the ground-state energy and energy spectrum for  $^{24}\text{Mg}$  as calculated with the Wildenthal interaction [12] using spherical, SU(3), and mixed-symmetry shell-model bases.

### 5.2.1 Ground-State Energy

We now turn to the consideration of the main results of the oblique-basis calculation, starting with ground-state convergence issues. The results shown in Fig. 5.2 illustrate that the oblique-basis calculation gives good dimensional convergence in the sense that the calculated ground-state energy for the SM(2)+(8,4)&(9,2) calculation is 3.3 MeV below the calculated energy for the SM(2) space alone. Adding the SU(3) irreps only increases the size of the space from 9.9% to 10.4% of the full space. Compare this 0.5% increase in the size of the space with the huge (54%) increase in going from SM(2) to an SM(4) calculation. For the latter, the ground-state energy is 4.2 MeV lower than the SM(2) result, somewhat

better than for the SM(2)+(8,4)&(9,2) calculation but in 64.2% rather than 10.4% of the full model space.

The exponential fall-off of the ground-state energy in Fig. 5.2 is striking. It has been observed many times, and has been recently suggested as a possible extrapolation procedure for obtaining the ground-state energy [69]. An even more rigorous extrapolation procedure has been suggested by Mizusaki and Imada [70]. Within this procedure, one can also estimate the error of a given calculation. Their procedure is also applicable to other observables, as well.

## 5.2.2 Energy and Angular Momentum of the Low Lying States

Fig. 5.3 and Fig. 5.4 show that the oblique-basis calculation positions the K=2 band head correctly. Furthermore, most of the other low-energy levels are also positioned correctly. The results for pure spherical and pure SU(3) calculations are shown in Fig. 5.3. As can be seen from the results in Fig. 5.3, an SM(4) calculation (64% of the full model space) is needed to get the ordering of the lowest angular momentum states correctly. Also, notice that in this case the third and fourth energy levels are practically degenerate. On the other hand, it only takes 0.5% of the full space to achieve comparable success with SU(3). In particular, Fig. 5.3 shows that an SU(3) calculation using only the (8,4) and (9,2) irreps gives the right ordering of the lowest levels. Note that the first few low-energy levels for SM(2) are close in energy to the corresponding low-energy levels for the (8,4)&(9,2) result. Since these two spaces are nearly orthogonal (see Fig. 5.1), these two sets of levels mix strongly in an oblique calculation and yield excellent results. The comparable ground-state energies of the SM(2) and (8,4)&(9,2) configurations can also be seen in Fig. 5.2.

Compare the spectra shown in Fig. 5.3 with the results from the oblique-basis calculations shown in Fig. 5.4. From this comparison one can see that the correct level structure can be achieved by using 1.6% (SM(1)+(8,4)) of the full *sd*-space. However, one should also notice that for the SM(0)+(8,4) space, which is only 0.2% of the full space and the minimum oblique-basis calculation, the results are quite close to the correct level structure. Despite the fact that the ground-state energy of the oblique-basis calculation is higher than the ground-state energy for the SM(4)-type calculation, the oblique calculations are favorable in terms of dimensionality considerations and correctness of the level structure.

## 5.3 Overlaps with the Full *sd*-shell Calculation

Figs. 5.5–5.8 focus on the actual structure of the states by showing overlaps of eigenstates calculated in the SM(n), SU(3), and oblique bases with the corresponding states of the full space calculation. Specifically, in Fig. 5.5, overlaps of states for pure SM(n) and pure SU(3)-type calculations are given. Note that the SM(4) states have big overlap (90%) for the first few eigenstates. This should not be too surprising since SM(4) covers 64% of the full space.

The results in Fig. 5.5 show that in general SU(3)-based calculations give much better results than the low-dimensional SM(n)-type calculations. The SM(n)-based calculations

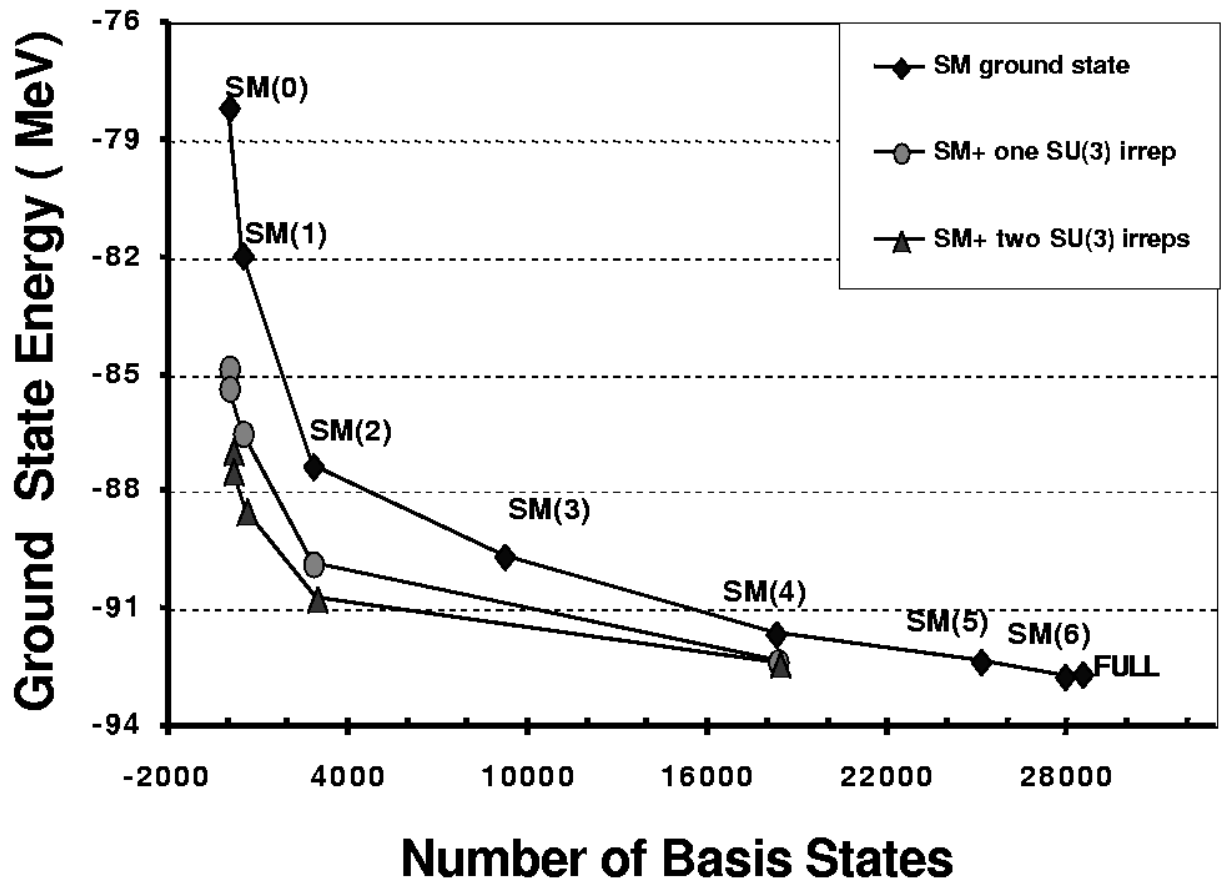


Figure 5.2: Calculated ground-state energy for  $^{24}\text{Mg}$ . Ground-state energy as a function of the various model spaces. Note the dramatic increase in binding (3.3 MeV) in going from SM(2) to SM(2)+two SU(3) irreps, (8,4)&(9,2), (a 0.5% increase in the dimensionality of the model space). Enlarging the space from SM(2) to SM(4) (a 54% increase in the dimensionality of the model space) adds 4.2 MeV in binding energy.

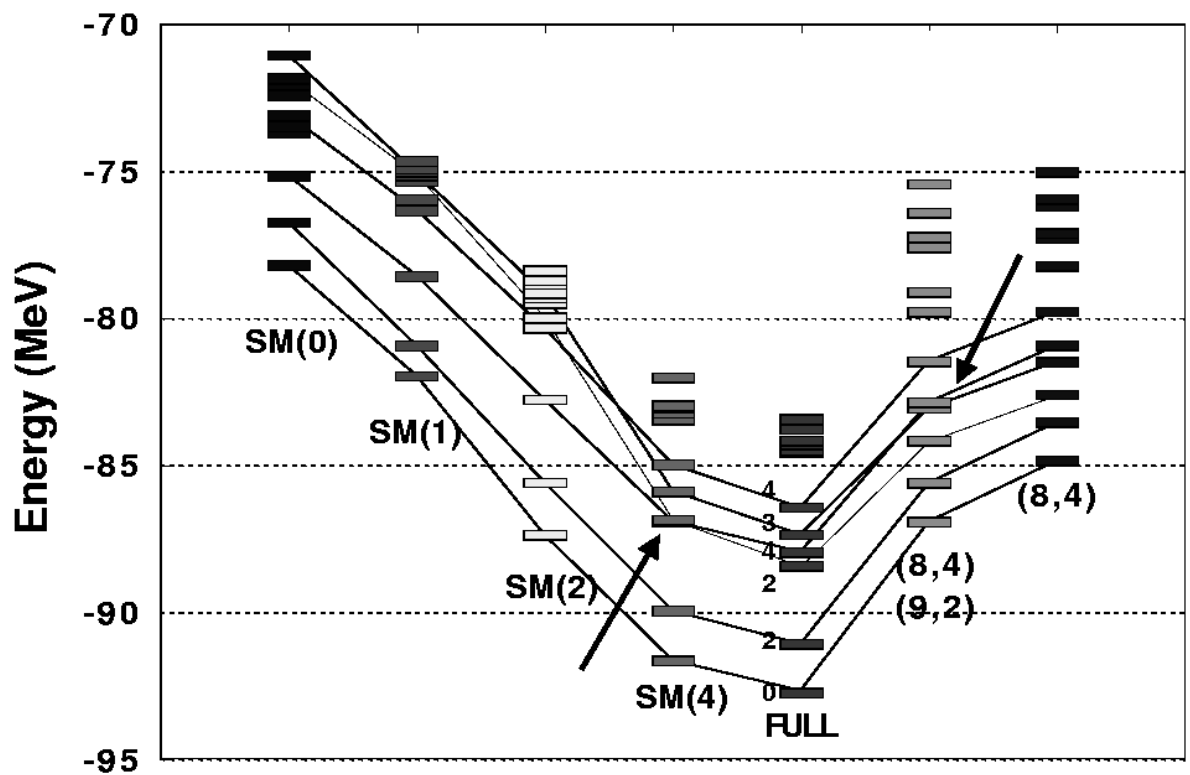


Figure 5.3: Structure of the energy levels for  $^{24}\text{Mg}$  for different calculations. Pure  $m$ -scheme spherical basis calculations are on the left-hand side of the graph; pure  $\text{SU}(3)$  basis calculations are on the right-hand side; the spectrum from the FULL space calculation is in the center.

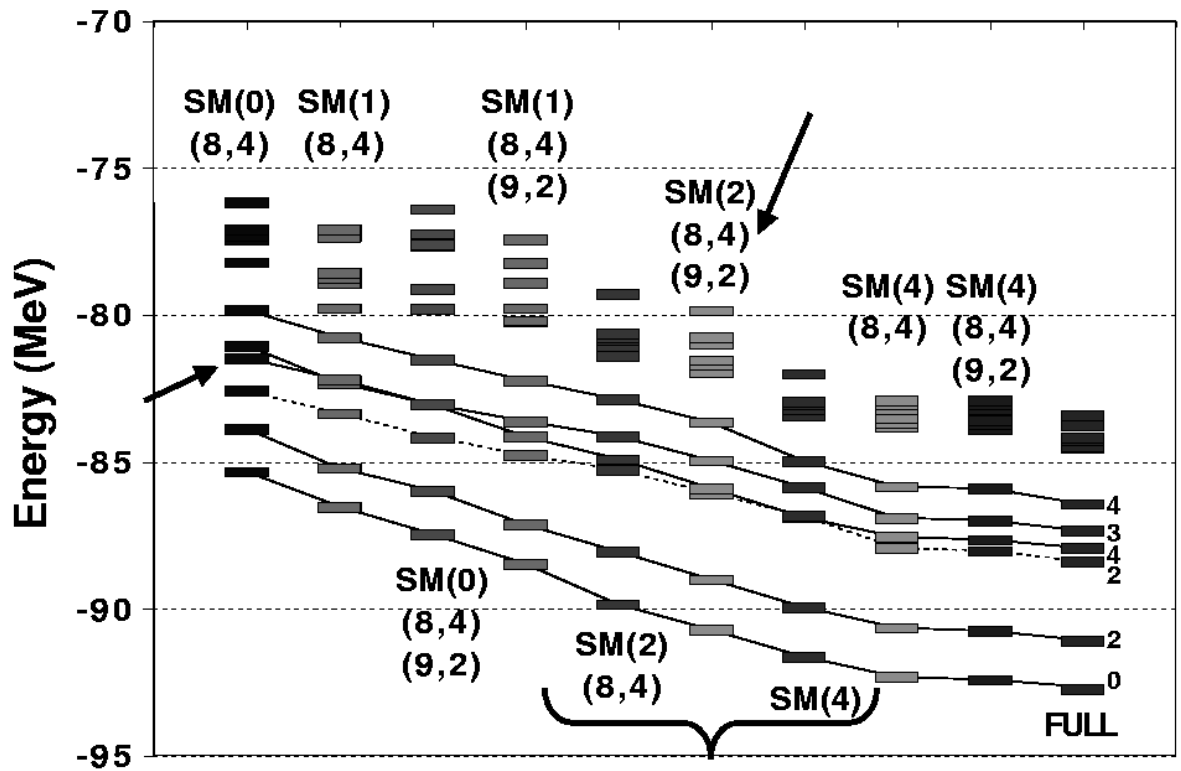


Figure 5.4: Energy levels for  $^{24}\text{Mg}$  as calculated for different oblique bases. The SM(4) basis calculation is included for comparison.

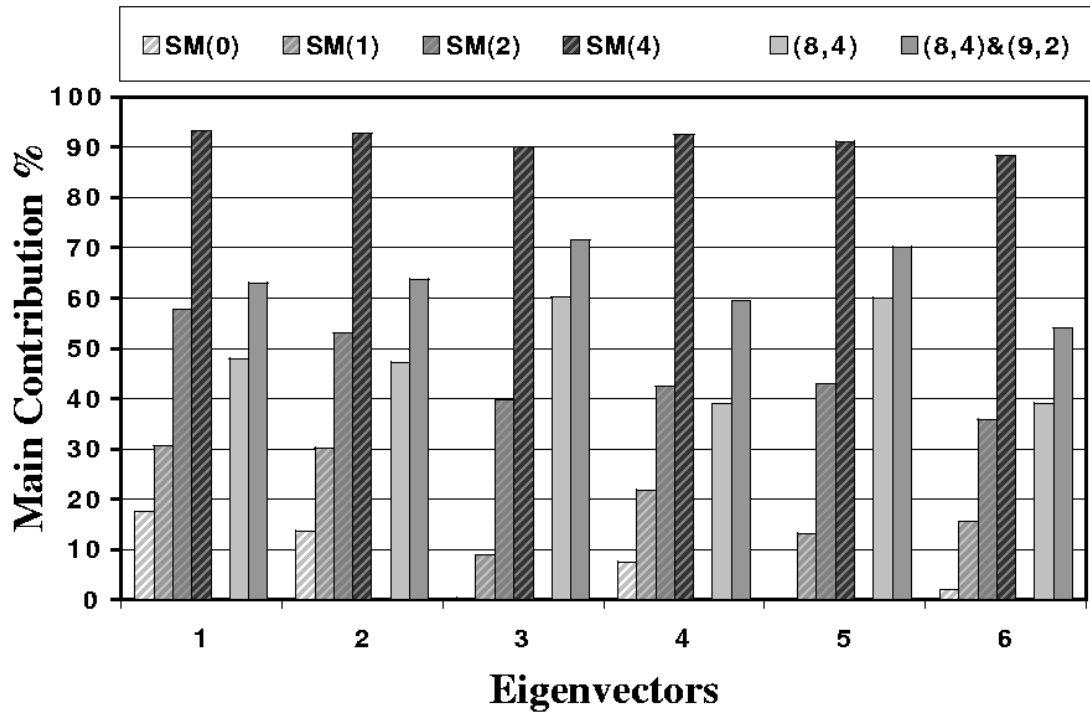


Figure 5.5: Overlaps of the pure spherical and SU(3) with the FULL states. The first four bars represent the SM(0), SM(1), SM(2), and SM(4) calculations, the next two bars represent SU(3) calculations, etc.

have irregular overlaps along the low-lying states and require SM(4), which is 64% of the full space, to get relatively well behaved overlaps. This can be seen most clearly from the inset labeled SM in Fig. 5.6. Note that the SM(0) contributions to the third, fifth, and sixth states are very low while SM(1) and SM(2) have varying contributions. The structure of the SU(3)-type states leads to a stable picture for the oblique calculations as shown in the inset SM(n)+(8,4) and SM(n)+(8,4)&(9,2) in Fig. 5.6.

In Fig. 5.7, the improvement in the structure of the calculated states is followed as the SU(3) states are added to the SM(n) basis. From this graph, one can see that the improvement to the SM(0)- and SM(1)-type calculation is due mainly to the goodness of SU(3) itself. The improvement obtained in the oblique calculation is due to the SU(3) enhancement of the SM(2) space. From this graph, one can also conclude that there is only a small gain in going to the SM(4)-based oblique calculation. However, this improvement can not be achieved by any other means with such a small increase in the model space. This is clear from a careful examination of Fig. 5.2 where one can see that the SM(5) result, which has 25142 basis vectors (88% of the full  $sd$ -space), gives the same ground-state energy as the SM(4)+(8,4)&(9,2) result (64.6% of the full  $sd$ -space).

Finally, to compare the three schemes – SU(3), SM(n), and the various oblique-basis combinations – representative overlaps are shown in Fig. 5.8. From these results, it is very clear that SU(3)-type basis states yield the right structure in a very low order. In particular, in Fig. 5.8, it can be seen that a 90% overlap with the exact eigenvectors can be achieved by using only 10% of the total space, SM(2)+(8,4)&(9,2). Furthermore, Fig. 5.8 also shows that SU(3) enhances the SM(4) results yielding eigenstates with overlaps that are very close ( $\approx 98\%$ ) to the exact results.

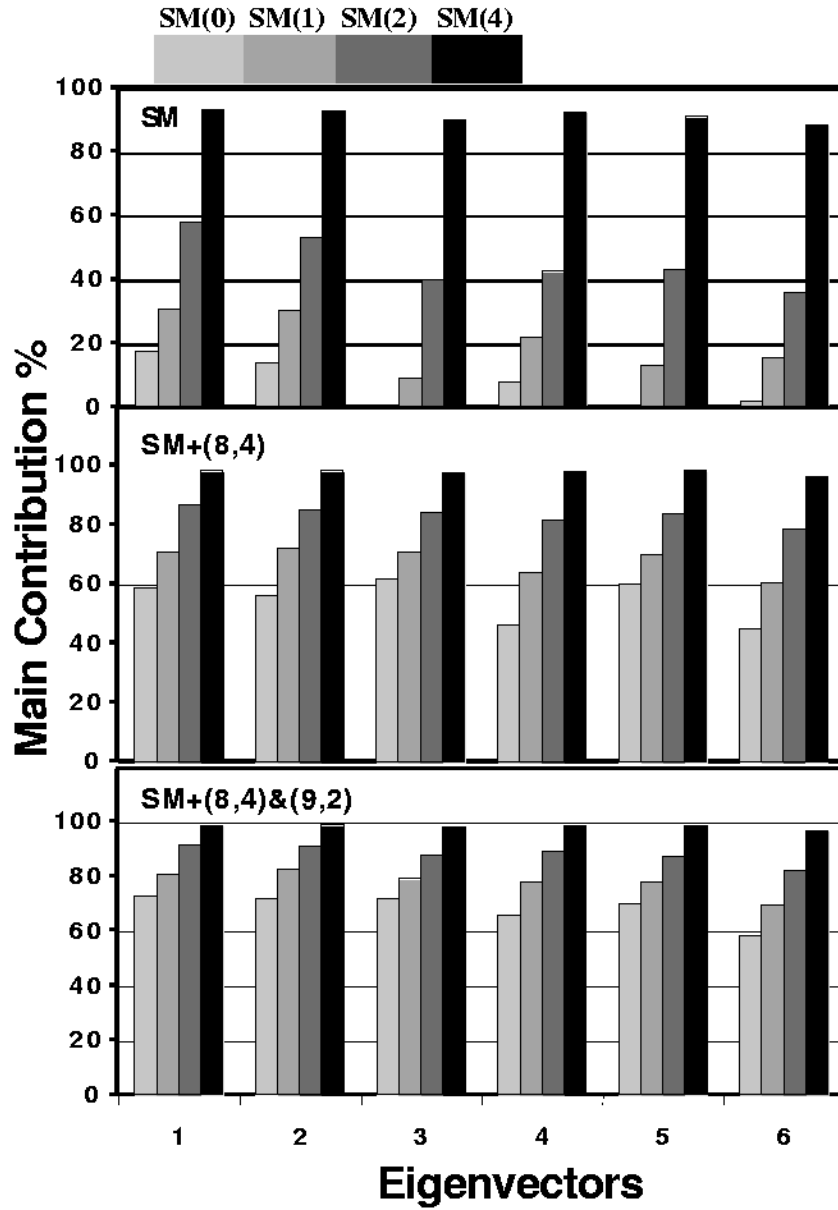


Figure 5.6: Overlaps of the oblique-basis states with the exact states (set I). Inset SM contains the overlaps for the pure spherical shell-model basis states only. Inset SM+(8,4) contains the overlaps of the SM basis enhanced by the leading SU(3) irrep (8,4). Inset SM+(8,4)&(9,2) has the (9,2) irreps included as well.

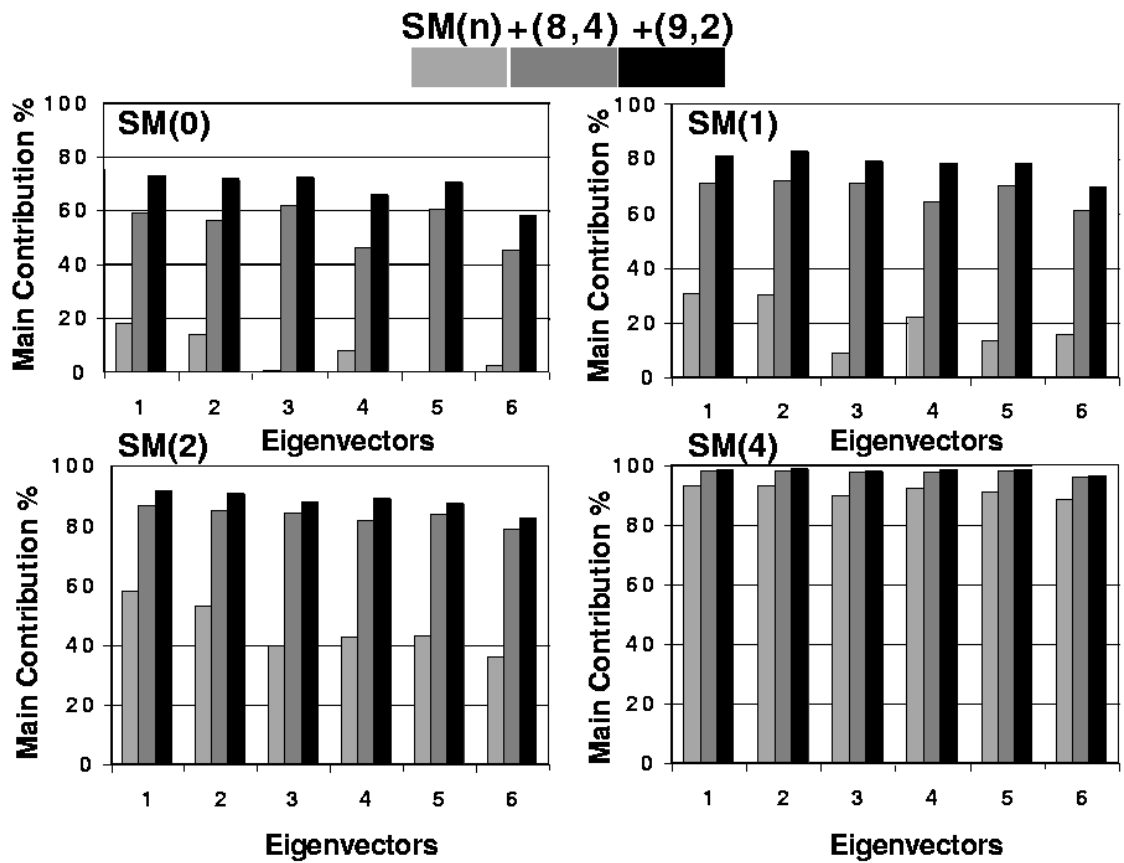


Figure 5.7: Overlaps of the oblique-basis states with the exact states (set II). Each inset represents a particular SM(n)-type calculation, showing how the overlaps change along the corresponding oblique-basis calculation.

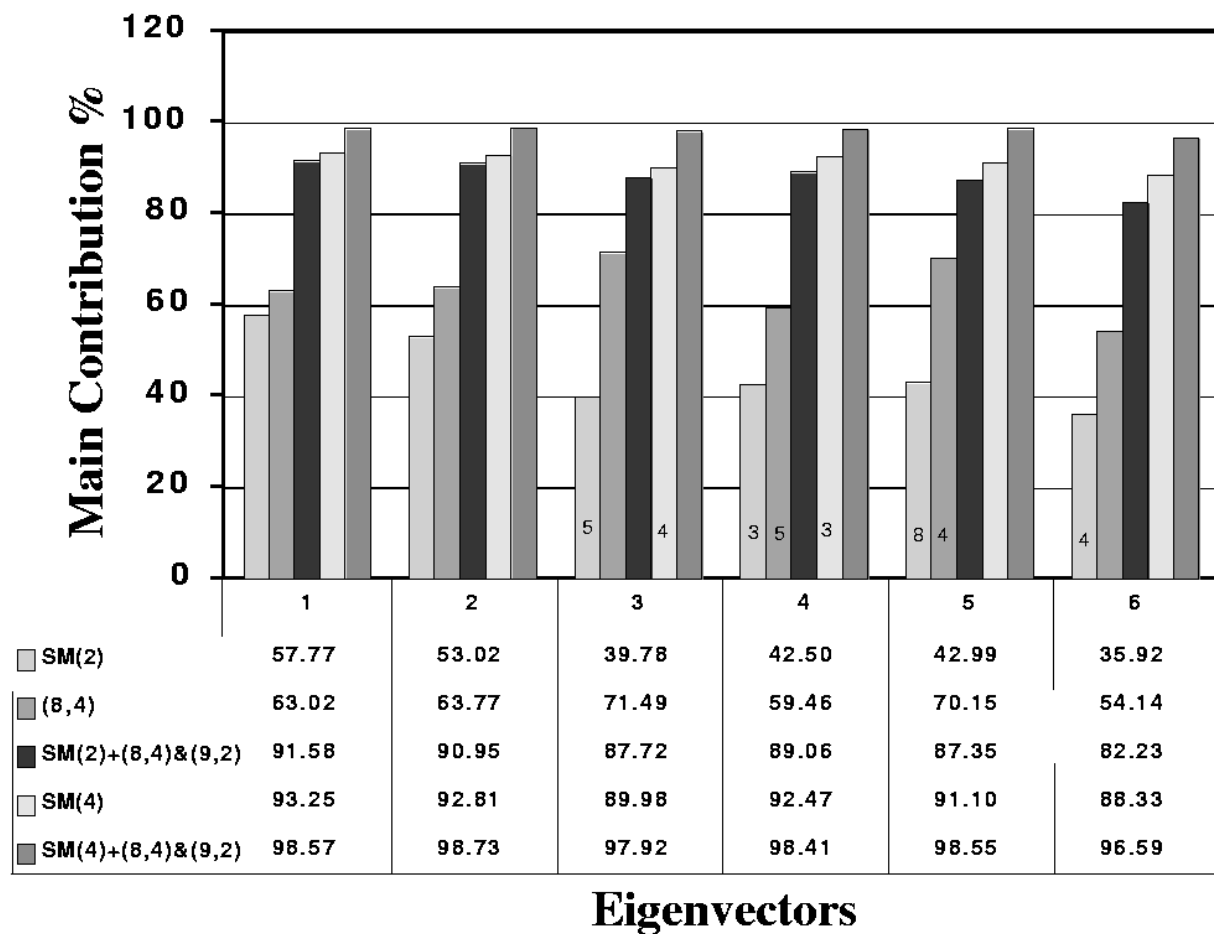


Figure 5.8: Representative overlaps of pure SM(n), pure SU(3), and oblique-basis results with the exact full *sd*-shell eigenstates. A number within a bar denotes the state with the overlap shown by the bar if it is different from the number for the exact full-space calculation shown on the abscissa. For example, for SM(2) the third eigenvector overlaps the most with the fourth exact eigenstate, not the third, while the fifth SM(2) eigenvector has the overlap shown with the third exact eigenstate.

# Chapter 6

## Study of Lower $pf$ -shell Nuclei

For  $^{24}\text{Mg}$ , the single-particle excitations, described by the spherical shell model, and the collective excitations, described by the  $SU(3)$  shell model, are of comparable importance. In the previous chapter, we have shown the relevance of the oblique-basis calculation for  $^{24}\text{Mg}$ . It is, therefore, natural to seek other nuclear systems to apply the mixed-symmetry method to. The even-even nuclei in the  $sd$ -shell are one place to start. For the  $sd$ -shell nuclei, however, one can perform full  $sd$ -shell calculations with modern computer codes.

The  $pf$ -shell nuclei are another option. For these nuclei, full  $pf$ -shell calculations have just recently been achieved [59, 72]. However, adding only the leading and next to the leading irreps, as it has been done for  $^{24}\text{Mg}$ , is not sufficient for the lower  $pf$ -shell nuclei, Ti and Cr, to obtain results as good as those for  $^{24}\text{Mg}$ . This is because the spherical shell model provides a significant part of the low-energy wave functions of these nuclei within a few spherical shell-model configurations, while in the  $SU(3)$  shell-model basis one needs more than a few  $SU(3)$  irreps. This is due mainly to the strong breaking of  $SU(3)$  in the lower  $pf$ -shell induced by the spin-orbit interaction [7]. When the spin-orbit splitting is removed, the importance of the  $SU(3)$  basis is restored. Although the usual  $SU(3)$  structure of the states is lost, there is an adiabatic  $SU(3)$  mixing which gives rise to the coherent structure of the yrast states. We have already seen this coherent mixing phenomenon in our toy model. In nuclei, however, this coherent mixing can be interpreted as an illustration of the intrinsic state idea where all the states within a given band can be projected out from a particular intrinsic state [4]. Even more, in nuclei this coherent structure is assumed to be a result of an adiabatic  $SU(3)$  mixing which means that some observables stay close to the  $SU(3)$  limit, that is, as if there was a pure  $SU(3)$  symmetry. Specifically, the  $B(E2)$  values remain strongly enhanced with values close to the  $SU(3)$  symmetry limit. It is important to point out that there is a coherent mixing of the spherical shell-model states as well.

In this chapter, we will discuss our study of the even-even lower  $pf$ -shell nuclei  $^{44-48}\text{Ti}$  and  $^{48}\text{Cr}$ . First, we show what a few  $SU(3)$  irreps can do for us within a mixed-symmetry calculations for  $^{44}\text{Ti}$  nucleus. Then, we focus on the spin-orbit interaction that strongly breaks the  $SU(3)$  symmetry. We conclude this chapter by discussing the coherent structure of the states and the adiabatic  $SU(3)$  mixing which produces enhanced  $B(E2)$  values.

Table 6.1: Labels and  $M_J = 0$  dimensions for various  $^{44}\text{Ti}$  oblique calculations.

Model space	(12, 0)	(12, 0)&(10, 1)	SM(0)	SM(1)	SM(2)	SM(4)	FULL
space dimension	7	84	72	580	1908	3360	4000
% of the full space	0.18	2.1	1.8	14.5	47.7	84	100

## 6.1 $^{44}\text{Ti}$ Oblique-Basis Results

The simplest even-even nucleus in the  $pf$ -shell, from a computational point of view, is  $^{44}\text{Ti}$ . In this section we discuss our oblique-basis calculations for  $^{44}\text{Ti}$ . If one compares the spherical shell-model with the  $SU(3)$  shell-model results within the framework of a realistic interaction, such as KB3 interaction [9], then  $SU(3)$  seems to be badly broken. Specifically, the ground-state energy and wave function are poorly reproduced. This seems to be a common trend in the even-even  $sd$ -shell nuclei as well [71]. Even the ground-state energies within the oblique-basis calculations do not look prominent. However, at a closer examination one finds that the oblique-basis idea still works. The results may be not as good as in  $^{24}\text{Mg}$ , but there are some close analogies. For example, the SM(1) space in  $^{44}\text{Ti}$  seems to be what SM(2) is for  $^{24}\text{Mg}$ , while the SM(2) space in  $^{44}\text{Ti}$  seems to be what SM(4) is for  $^{24}\text{Mg}$ . By that we mean that the  $SU(3)$  enhanced SM(1) basis in  $^{44}\text{Ti}$  gives overlaps that are compatible with the overlaps of the pure SM(2) calculation. In the next few sub-sections we briefly illustrate these findings.

### 6.1.1 Model Space Dimensions

The model space for  $^{44}\text{Ti}$  consists of 2 valence protons and 2 valence neutrons in the  $pf$ -shell. We use the same notation for the  $m$ -scheme spherical bases as in 5.1. The  $SU(3)$  part of the basis includes the leading irrep of  $SU(3)$ , which for  $^{44}\text{Ti}$  is (12,0) with  $M_J = 0$  dimensionality 7, and the next to the leading irrep, namely the (10,1). The (10,1) irrep occurs three times, once with  $S = 0$  ( $M_J = 0$  dimensionality 11) and twice with  $S = 1$  ( $M_J = 0$  dimensionality  $2 \times 33 = 66$ ). All three (10,1) irreps have total  $M_J = 0$  dimensionality of  $11+66=77$ . The (12,0)&(10,1) case has total  $M_J = 0$  dimensionality of  $7+77=84$  and is denoted by (12,0)&(10,1). In Table 6.1 we summarize the dimensionalities involved.

As in the case of  $^{24}\text{Mg}$ , there are linearly dependent vectors within some of the  $^{44}\text{Ti}$  calculations. For example, there is one such vector in the SM(2)+(12,0) space, two in the SM(3)+(12,0), two in the SM(1)+(12,0)&(10,1), twelve in the SM(2)+(12,0)&(10,1), and thirty-three in the SM(3)+(12,0)&(10,1). Each linearly dependent vector is handled as discussed in the chapter devoted to  $^{24}\text{Mg}$ .

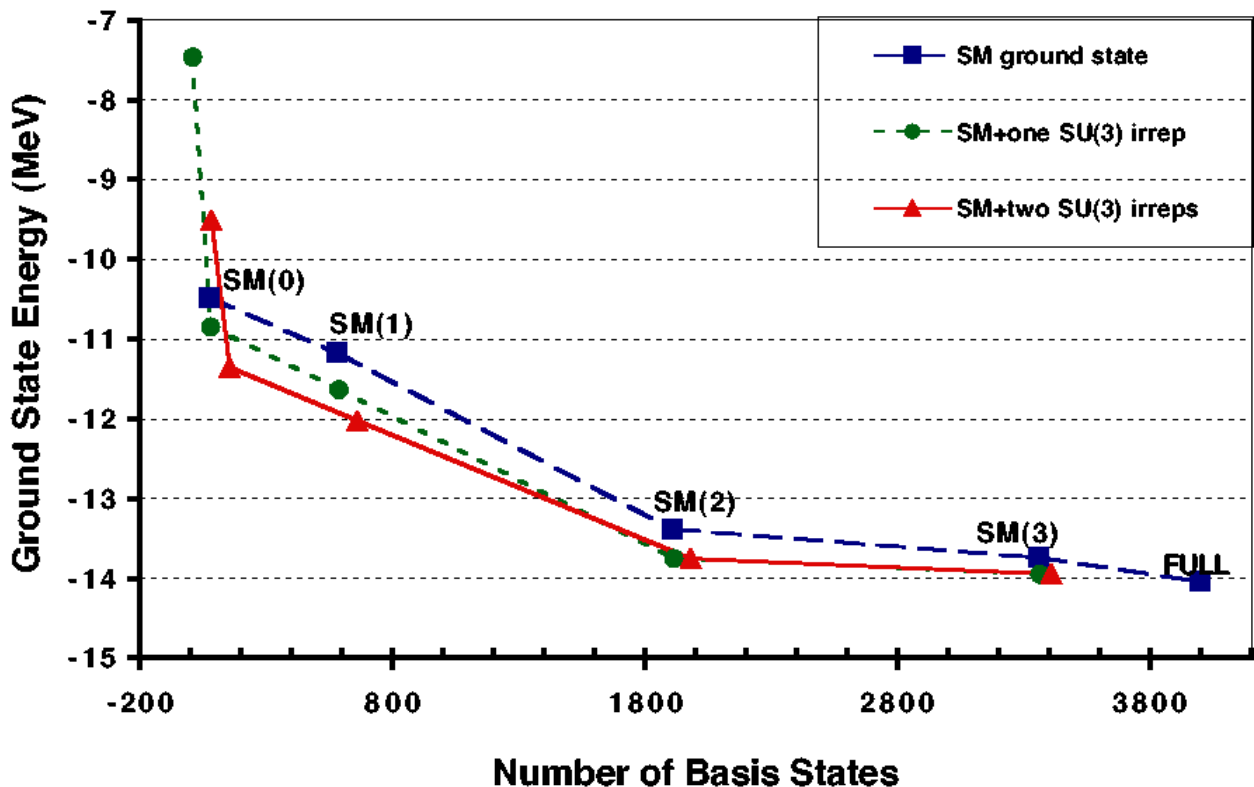


Figure 6.1: Ground-state energy for  $^{44}\text{Ti}$  as a function of the various model spaces. The SU(3) irreps used are (12,0) and (10,1).

### 6.1.2 Ground-State Energy

Fig. 6.1 shows that the oblique-basis calculation of the ground-state energy for  $^{44}\text{Ti}$  does not give results as good as for  $^{24}\text{Mg}$ . The calculated ground-state energy for the SM(1)+(12,0)&(10,1) calculation is 0.85 MeV below the calculated energy for the SM(1) space alone. Adding the two SU(3) irreps to the SM(1) space increases the size of the space from 14.5% to 16.6% of the full space. This is a 2.1% increase, while going from the SM(1) to SM(2) involves an increase of 33.2% in the model space. For the latter, the ground-state energy is 2.2 MeV lower than the SM(1) result.

### 6.1.3 Energy Spectrum of the Low Lying States

We have seen that the position of the K=2 band head for  $^{24}\text{Mg}$  is correct for the SU(3)-type calculations but not for the low-dimensional SM(n) calculations. In  $^{44}\text{Ti}$  this seems to be the opposite, the SM(n)-type calculations reproduce the position of the K=2 band head while the SU(3) do not, as shown in the upper graph in Fig. 6.2. Furthermore, most of the low-energy levels are much higher for the pure SU(3) limit than for the pure SM(n) case.

Thus, one may expect that these two sets of levels (the SM( $n$ ) and the SU(3)) may not mix as strongly in an oblique calculation as for the  $^{24}\text{Mg}$  case. Surprisingly, the oblique-basis calculations seem to produce a good spectral structure as shown in the lower graph in Fig. 6.2. Notice that the SM(2)+(12,0)&(10,1) spectrum is very good and compatible with the SM(3) spectrum. This is 50% compared to 84% of the model space.

### 6.1.4 Overlaps with the Exact Calculation

The top graph in Fig. 6.3 shows overlaps of states for pure SM( $n$ ) and pure SU(3)-type calculations while the lower part shows some selected overlaps from the oblique calculations. Notice that the overlaps of the pure SU(3)-type calculations are very small, often less than 40%, while the SM( $n$ ) results are far better with the SM(2)-type calculations having about 80% overlap with the exact states. Note that the SM(3) states have big overlap (>97%) for the first few eigenstates. This is not surprising since SM(3) covers 84% of the full space. What is surprisingly good is that the SM(2)+(12,0)&(10,1)-type calculation is as good as the SM(3). Even more, the SM(1)+(12,0)&(10,1) overlaps seem to be often bigger than the SM(2) overlaps.

## 6.2 Set Up for the Study of the $SU(3)$ Breaking

To understand better the results of the mixed-mode calculations described in the previous section, we need to recall that the oblique-basis method is expected to work well if we are dealing with two or more competing and compatible modes. Therefore, if the Hamiltonian of the system is dominated by its one-body term, then the effect of the two-body part will be suppressed. However, if the single-particle energies are degenerate, the importance of  $SU(3)$  should reappear. In the next subsections, we discuss the structure of the Hamiltonian, as well as some of the computational methods used in our calculations.

### 6.2.1 Interaction Hamiltonian

To retain clarity of the discussion, we recall the structure and notations of the one- plus two-body Hamiltonian:

$$H = \sum_i \varepsilon_i a_i^\dagger a_i + \frac{1}{4} \sum_{i,j,k,l} V_{kl,ij} a_i^\dagger a_j^\dagger a_k a_l.$$

The summation indexes range over the single-particle levels included in the model space. We only consider levels of the  $pf$ -shell which have the following radial ( $n$ ), orbital ( $l$ ) and total angular momentum ( $j$ ) quantum numbers:  $nl_j = \{0f_{7/2}, 0f_{5/2}, 1p_{3/2}, 1p_{1/2}\}$ . In what follows, the radial quantum number ( $n$ ) is dropped since the  $l_j$  labels provide a unique labelling scheme for single-shell applications. It is common practice to replace the four single-particle energies  $\varepsilon_i$  by the  $l^2$  and  $l \cdot s$  interactions:  $\sum_i \varepsilon_i a_i^\dagger a_i \rightarrow \epsilon(n_i - \alpha_i l_i \cdot s_i - \beta_i l_i^2)$ ,

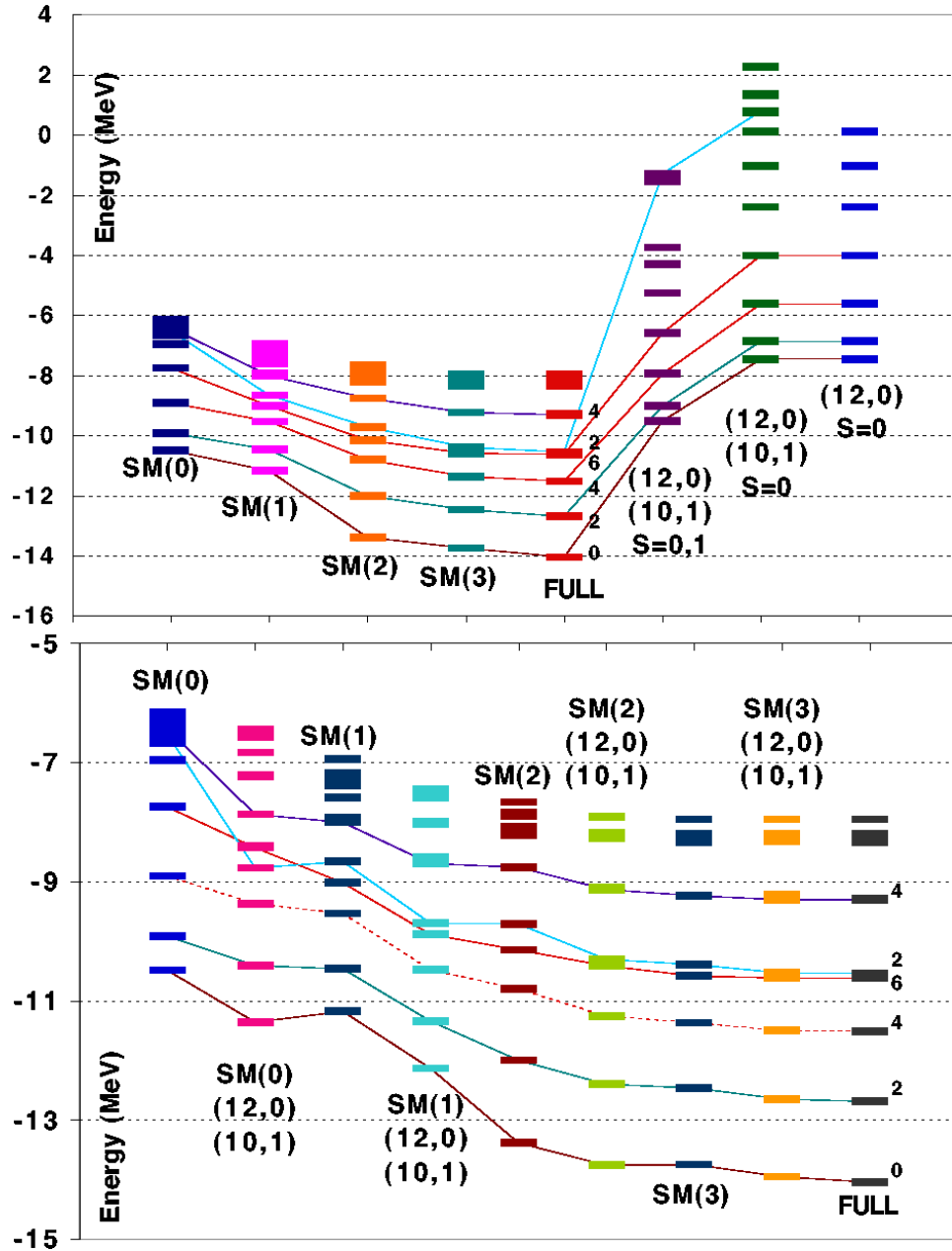


Figure 6.2: Structure of the energy levels for  $^{44}\text{Ti}$  for different calculations. Pure  $m$ -scheme spherical-basis calculations are on the left-hand side of the upper graph; pure SU(3)-basis calculations are on the right-hand side; the spectrum from the FULL space calculation is in the center. The spectra from oblique-basis calculations are in the lower graph.

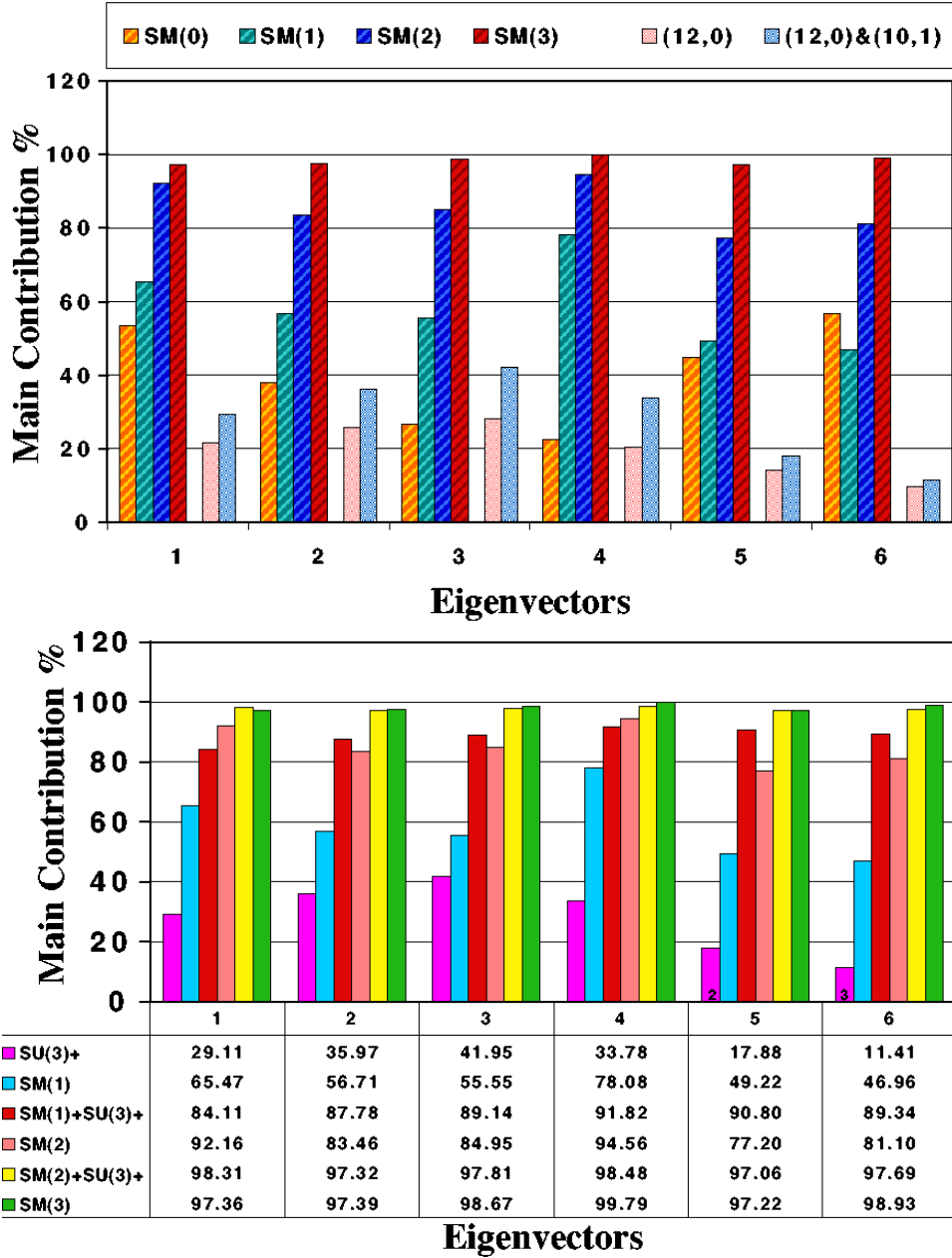


Figure 6.3:  $^{44}\text{Ti}$  wave function overlaps of pure spherical,  $\text{SU}(3)$ , and oblique states with the FULL states. The first four bars in the upper graph represent the  $\text{SM}(0)$ ,  $\text{SM}(1)$ ,  $\text{SM}(2)$ , and  $\text{SM}(3)$  calculations, the next two bars represent the  $\text{SU}(3)$  calculations, etc. Representative overlaps of pure  $\text{SM}(n)$ , pure  $\text{SU}(3)$ , and oblique-basis results with the exact full  $pf$ -shell eigenstates are shown in the lower graph.

where  $\epsilon$  is the average binding energy per valence particle,  $n_i$  counts the total number of valence particles, and  $\alpha$  and  $\beta$  are dimensionless parameters giving the interaction strength of the  $l^2$  and  $l \cdot s$  terms. For realistic single-particle energies used in the KB3 interaction (6.1), these parameters are  $\epsilon = 2.6 \text{ MeV}$ ,  $\beta = 0.0096$ ,  $\alpha_p = 1.3333$ , and  $\alpha_f = 1.7143$ . The small value of  $\beta$  signals small  $l^2$  splitting (6.2) while the values of  $\alpha$  demonstrate the presence of a strong spin-orbit splitting.

A significant part of the two-body interaction,  $V_{kl,ij}$ , maps onto the quadrupole-quadrupole ( $Q \cdot Q$ ) and the pairing ( $P$ ) interactions. Since  $Q \cdot Q$  can be written in terms of  $SU(3)$  generators, it induces no  $SU(3)$  breaking, as has been discussed in the first chapters. Hence  $Q \cdot Q$  serves to re-enforce the importance of the Elliott model [4]. However, the pairing interaction mixes different  $SU(3)$  irreps, but in our study it does not seem to cause any strong  $SU(3)$  breaking. In this analysis the two-body part of the Hamiltonian ( $V_{kl,ij}$ ) is fixed by the Kuo-Brown-3 (KB3) interaction matrix elements, and the single-particle energies,  $\epsilon_i$ , are changed as described below.

The following single-particle energies are normally used with the KB3 interaction [9]:

$$\text{KB3 [MeV]} : \epsilon_{p_{\frac{1}{2}}} = 4, \quad \epsilon_{p_{\frac{3}{2}}} = 2, \quad \epsilon_{f_{\frac{5}{2}}} = 6, \quad \epsilon_{f_{\frac{7}{2}}} = 0. \quad (6.1)$$

For the purposes of the current study, it is important to know the centroids of the  $p$ - and  $f$ -shells. For example, the energy centroid of the  $p$ -shell is given by:

$$\epsilon_p = \frac{\epsilon_{p_{\frac{1}{2}}} \dim(p_{\frac{1}{2}}) + \epsilon_{p_{\frac{3}{2}}} \dim(p_{\frac{3}{2}})}{\dim(p_{\frac{1}{2}}) + \dim(p_{\frac{3}{2}})}.$$

In what follows, we label by  $KB3p-f$  that Hamiltonian which uses the KB3 two-body interaction with single-particle  $p$ - and  $f$ -shell energies set to their centroid values:

$$\text{KB3}p-f \text{ [MeV]} : \epsilon_{p_{\frac{1}{2}}} = \epsilon_{p_{\frac{3}{2}}} = 2.6670, \quad \epsilon_{f_{\frac{5}{2}}} = \epsilon_{f_{\frac{7}{2}}} = 2.5710. \quad (6.2)$$

We use  $KB3pf$  for the case when the single-particle energies are set to their overall average:

$$\text{KB3}pf \text{ [MeV]} : \quad \epsilon_p = \epsilon_f = 2.6 \quad (6.3)$$

Due to the near degeneracy of the single-particle energies of the  $KB3p-f$  interaction (6.2), the results for the  $KB3pf$  case are very similar to those for  $KB3p-f$ .

## 6.2.2 Computational Procedures

In our study, we have focused on  $^{44}\text{Ti}$ ,  $^{46}\text{Ti}$ ,  $^{48}\text{Ti}$ , and  $^{48}\text{Cr}$  because these are  $pf$ -shell equivalents of  $^{20}\text{Ne}$ ,  $^{22}\text{Ne}$ ,  $^{24}\text{Ne}$ , and  $^{24}\text{Mg}$ , respectively, which are known to be good  $SU(3)$   $sd$ -shell nuclei. Furthermore, data on these nuclei are readily available from the National Nuclear Data Center (NNDC) [73] and full  $pf$ -shell calculations are feasible [72]. The model

Table 6.2: Space dimensions for the  $m$ -scheme calculations in the full  $pf$ -shell model space. We have used even parity and even isospin basis states with no restrictions on the total angular momentum  $J$  except for the  $M_J = 0$  case where only states with even  $J$  values have been selected.

Nucleus	$M_J = 0$	$M_J = 6$	$M_J = 10$	$M_J = 14$
$^{44}\text{Ti}$	1080	514	30	—
$^{46}\text{Ti}$	43630	32297	4693	134
$^{48}\text{Ti}$	317972	278610	57876	3846
$^{48}\text{Cr}$	492724	451857	104658	8997

dimensionalities for full-space calculations increase very rapidly when approaching the mid-shell region; those for the cases considered here are given in Table 6.2.

The computational procedures and tools used in the analysis of the  $SU(3)$  symmetry breaking are described in this section. In brief, the Hamiltonian and other matrices are calculated using an  $m$ -scheme shell-model code [19] while the eigenvectors and eigenvalues are obtained by means of the Lanczos algorithm [21]. All the calculations are done in the full  $pf$ -shell model space.

First, the Hamiltonian  $H$  for each interaction ( $KB3$  (6.1),  $KB3p-f$  (6.2), and  $KB3pf$  (6.3)) is generated. Then the eigenvalues and eigenvectors are calculated and the yrast states identified. Next, the matrix for the second-order Casimir operator of  $SU(3)$ , namely  $C_2 = (3L^2 + Q \cdot Q)/4$ , is generated using the shell-model code, and a moments method [74] is used to diagonalize the  $C_2$  matrix by starting the Lanczos procedure with specific eigenvectors of  $H$  for which an  $SU(3)$  decomposition is desired. Finally,  $B(E2)$  values in  $e^2fm^4$  units are calculated from one-body densities using Siegert's theorem with a typical value for the effective charge [59, 75],  $q_{eff} = 0.5$ , so  $e_p = (1 + q_{eff})e = 1.5e$  and  $e_n = (q_{eff})e = 0.5e$ .

Even though the procedure can generate the spectral decomposition of a state in terms of the eigenvectors of  $C_2$  of  $SU(3)$ , this alone is not sufficient to determine uniquely all irrep labels  $\lambda$  and  $\mu$  of  $SU(3)$ . For example,  $C_2$  has the same eigenvalue for the  $(\lambda, \mu)$  and  $(\mu, \lambda)$  irreps. Nevertheless, since for the first few leading irreps (largest  $C_2$  values) the  $\lambda$  and  $\mu$  values can be uniquely determined [76], this procedure suffices for our study.

Usually, when considering full-space calculations, a balance between computer time and accuracy has to be considered. While the Lanczos algorithm [21] is known to yield a good approximation for the lowest or highest eigenvalues and eigenvectors, it normally does a relatively poor job for intermediate states. This means, for example, that higher states, in particular high total angular momentum states, may be poorly represented or, in a worst case scenario, not show up at all when these states are close to or beyond the truncation edge of the chosen submatrix. An obvious way to maintain a good approximation is to run the code for each  $M_J$  value, that is,  $M_J = 0, 2, 4, 6, \dots$ . However, this might be a very time consuming process, but nonetheless one which could be reduced significantly if only a few  $M_J$  values

are used for each run. For the calculations of this study, we have used  $M_J = 0, 6, 10,$  and  $14$ . To maintain high confidence in the approximation of the intermediate states which have  $J = 2, 4, 8, 12, \dots$  we required that they be within the first half of all the states produced. The code output was set for 29 states. A further verification of the accuracy of the procedure is whether the energies of the same state calculated using different  $M_J$  runs are close to one another. For example, as a consistency check the energy of the lowest  $J = 6$  state in the  $M_J = 0$  run was compared to the energy of the same state obtained from the  $M_J = 6$  run.

## 6.3 Measuring Symmetry Breaking Using $C_2$ of $SU(3)$

In this section, we discuss the results of our study on the  $SU(3)$  symmetry breaking in the  $pf$ -shell. In order to identify the  $SU(3)$  structure of an yrast state, we calculate the spectral distribution of the state along the second Casimir operator ( $C_2$ ) of  $SU(3)$  as described in the previous section. From the spectral distribution, we can clearly determine whether the  $SU(3)$  symmetry is broken or not. However, a graphic or table representation of the data becomes very inelegant with growing space dimensions. Thus, we have decided to use also average quantities, such as centroid, width, and skewness of the distributions to illustrate the main points one can deduce from a complicated spectral distribution.

### 6.3.1 Spectral Distribution

The first set, Figs.6.4 and 6.5, demonstrates the recovery of the  $SU(3)$  symmetry as the single-particle spin-orbit interaction is turned off, that is, in going from the  $KB3$  to the  $KB3p\_f$  interaction. Corresponding results for the  $KB3pf$  interaction are similar to the  $KB3p\_f$  results. In each graph,  $C_2$  values of  $SU(3)$  are given on the horizontal axis with the contribution of each  $SU(3)$  state on the vertical axis. The bars within each cluster are contributions to the yrast states starting with the ground state ( $J = 0$ ) on the left. Hence the second bar in each cluster is for the  $J = 2$  yrast state, etc.

We have chosen  $^{44}\text{Ti}$  for an in-depth consideration of the fragmentation of the  $C_2$  strength in yrast states. The results for the nondegenerate  $KB3$  interaction are shown in Fig. 6.4. In this case the highest contribution (biggest bar) is more than 50% which corresponds to a  $C_2$  value of 114 for the  $J = 12$  state. The  $C_2 = 114$  value is for  $(\lambda, \mu) = (8, 2)$  which is two  $SU(3)$  irreps down from the leading one,  $(\lambda, \mu) = (12, 0)$  with  $C_2 = 180$ . The leading irrep only contributes about 10% to the  $J = 12$  yrast state. The contribution of the next to the leading irrep,  $C_2 = 144$  for  $(\lambda, \mu) = (10, 1)$ , is slightly less than 40%. Thus, for all practical purposes, the first three irreps determine the structure of the  $J = 12$  yrast state. This illustrates that the high total angular momentum  $J$  states are composed of only the first few  $SU(3)$  irreps. This is easily understood because high  $J$  values require high orbital angular momentum ( $L$ ) states which are only present in  $SU(3)$  irreps with large  $C_2$  values. The high  $J$  states may therefore be considered to be states with good  $SU(3)$  symmetry. However, this is not the case with the ground state of  $^{44}\text{Ti}$  which has very important contributions from states with  $C_2$  values 60, 72, 90, 114, 144, and 180 with respective percentages, 7.5, 25, 10,

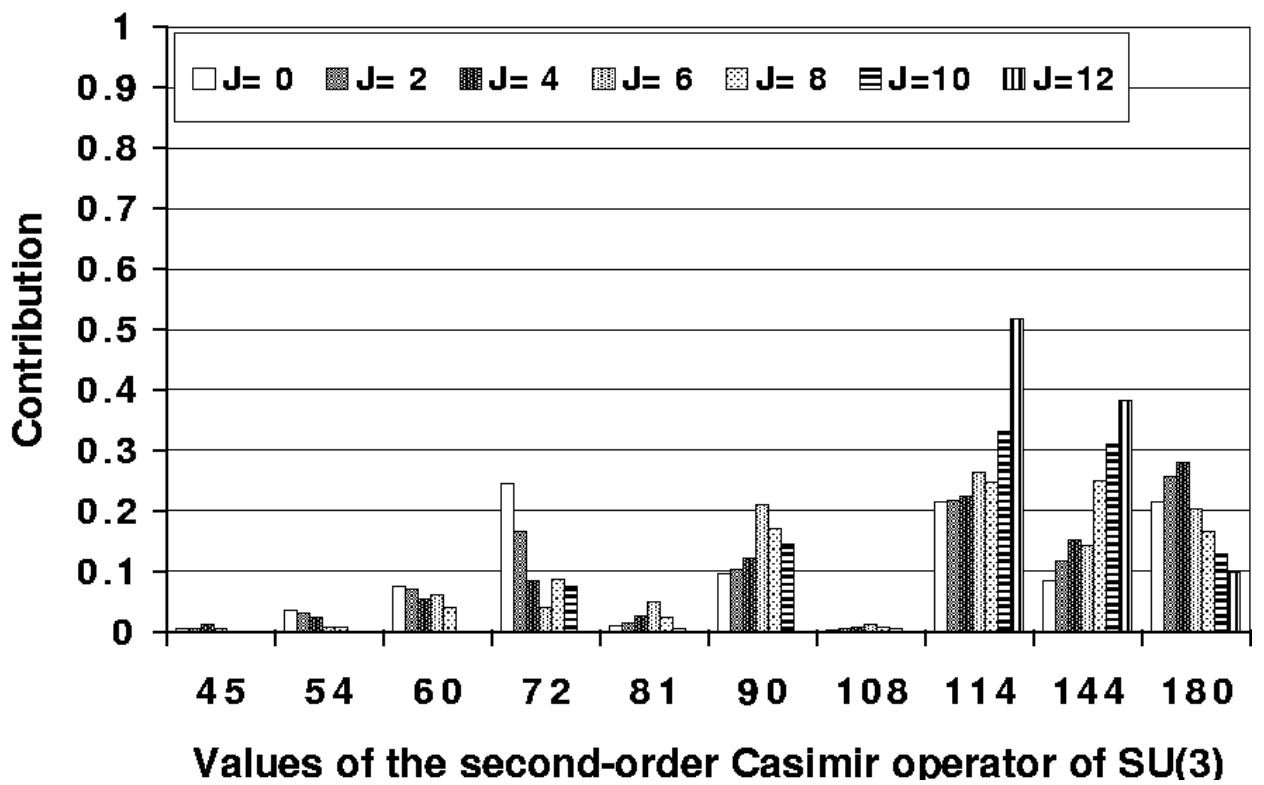


Figure 6.4: Strength distribution of  $C_2$  of  $SU(3)$  in yrast states of  $^{44}\text{Ti}$  for realistic single-particle energies with Kuo-Brown-3 two-body interaction ( $KB3$ ).

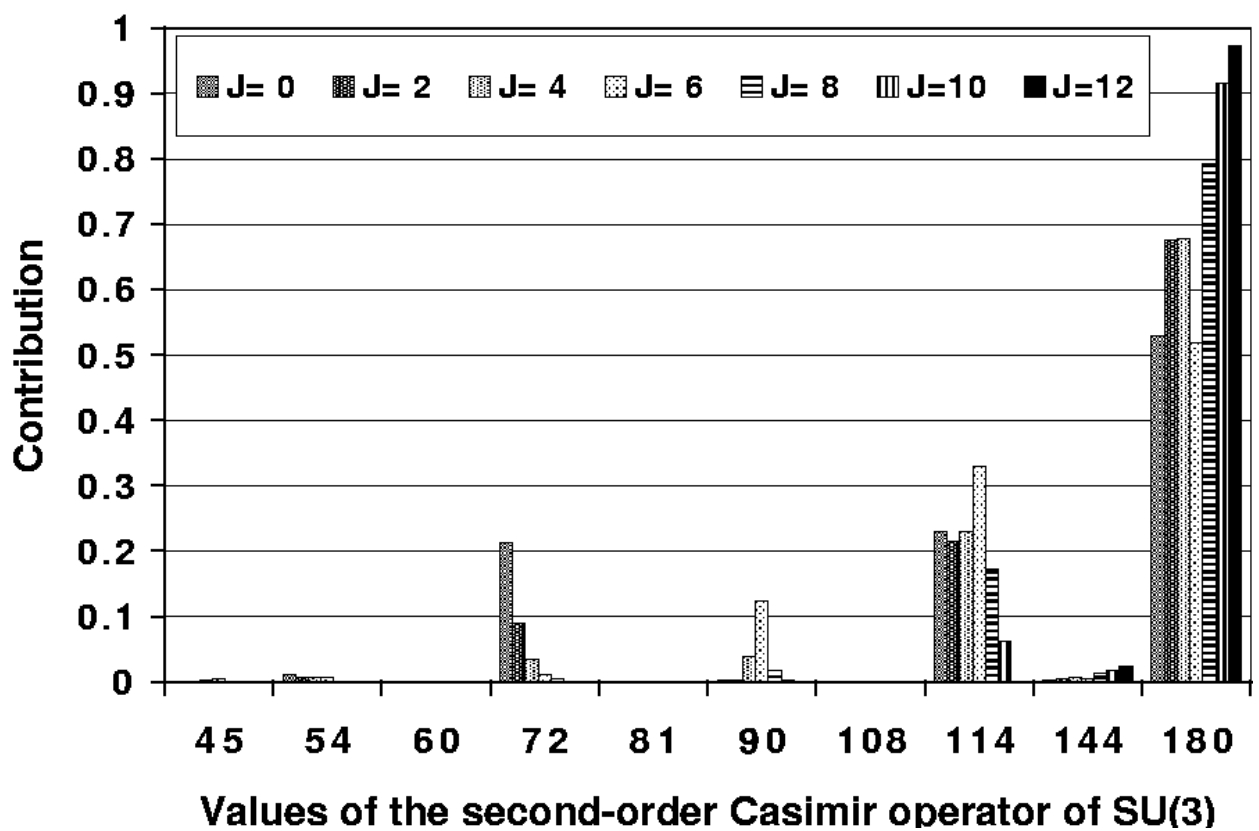


Figure 6.5: Strength distribution of  $C_2$  of  $SU(3)$  in yrast states of  $^{44}\text{Ti}$  for degenerate single-particle energies with Kuo-Brown-3 two-body interaction ( $KB3p-f$ ).

21, 8, and 21%. This shows that the leading irrep is not the biggest contributor to the  $J = 0$  ground state; there are two other contributors with about 20%, the third ( $C_2 = 114$ ) and seventh ( $C_2 = 72$ )  $SU(3)$  irrep.

When the spin-orbit interaction is turned off, which yields nearly degenerate single-particle energies since the single-particle orbit-orbit splitting is small, one has the  $KB3p-f$  interaction, and in this case the structure of the yrast states changes dramatically, as shown in Fig. 6.5. In Fig. 6.5 one can see that the leading irrep plays a dominant role as its contribution is now more than 50% of every yrast state. As in the previous case, the high total angular momentum  $J$  states have the biggest contributions from the leading irrep, for example, more than 97% for  $J = 12$ , 91% for  $J = 10$ , and 80% for  $J = 8$ . The ground state is composed of few irreps with  $C_2$  values 72, 114, and 180, but in this case the leading irrep with  $C_2 = 180$  makes up more than 52% of the total with the other two most important irreps contributing 21% [ $C_2 = 72$ ,  $(\lambda, \mu) = (4, 4)$ ] and 23% [ $C_2 = 114$ ,  $(\lambda, \mu) = (8, 2)$ ].

### 6.3.2 Moments of the Spectral Distributions.

An alternative way to show the recovery of the  $SU(3)$  symmetry is given in Fig. 6.6 and Fig. 6.7. These figures show the centroid, width, and skewness of the  $C_2$  distributions. The  $J$  values are plotted on the horizontal axis with the centroids given on the vertical axis. The width of the distribution is indicated by the length of the error bars which is just the rms deviation,  $\Delta C_2 = \sqrt{\langle (C_2 - \langle C_2 \rangle)^2 \rangle}$ , from the average value of the second-order Casimir operator  $\langle C_2 \rangle$ . The third central moment,  $\delta C_2 = \sqrt[3]{\langle (C_2 - \langle C_2 \rangle)^3 \rangle}$ , which measures the asymmetry, is indicated by the length of the error bar above,  $\Delta C_2 + \frac{\delta C_2}{2}$ , and below,  $\Delta C_2 - \frac{\delta C_2}{2}$ , the average value.

Note that the recovery of the leading irrep when the spin-orbit interaction is turned off is clearly signaled not only through an increase in the absolute values of the first centroid  $\langle C_2 \rangle$  but also through the skewness  $\delta C_2$ . For example, in  $^{44}\text{Ti}$  with the  $KB3$  interaction (spin-orbit interaction turned on) the ground state  $J = 0$  has  $\langle C_2 \rangle = 110$  and skewness  $\delta C_2 = 33$ . This changes for the  $KB3p-f$  interaction to  $\langle C_2 \rangle = 139$  and a skewness of  $\delta C_2 = -37$ , as shown in Fig. 6.6. The equivalent of the  $^{44}\text{Ti}$  graph for the  $^{48}\text{Ti}$  case is shown in Fig. 6.7. As for the  $^{44}\text{Ti}$  case, the results show the recovery of the  $SU(3)$  symmetry in  $^{48}\text{Ti}$  when the single-particle spin-orbit interaction is turned off.

### 6.3.3 Coherent Spectral Structure

We now turn to a discussion of the coherence nature of the yrast states. First, notice that the widths of the distributions as defined by  $\Delta C_2 = \sqrt{\langle (C_2 - \langle C_2 \rangle)^2 \rangle}$  are surprisingly unaffected (Fig. 6.6 and Fig. 6.7) when turning the spin-orbit interaction on and off. This effect occurs in all cases studied:  $^{44}\text{Ti}$ ,  $^{46}\text{Ti}$ ,  $^{48}\text{Ti}$ , and  $^{48}\text{Cr}$ . The more detailed graphs, Fig. 6.4 and Fig. 6.5, offer an explanation in terms of the fragmentation of the  $C_2$  distribution. As can be seen from these graphs, the irreps that are present in the structure of a given yrast

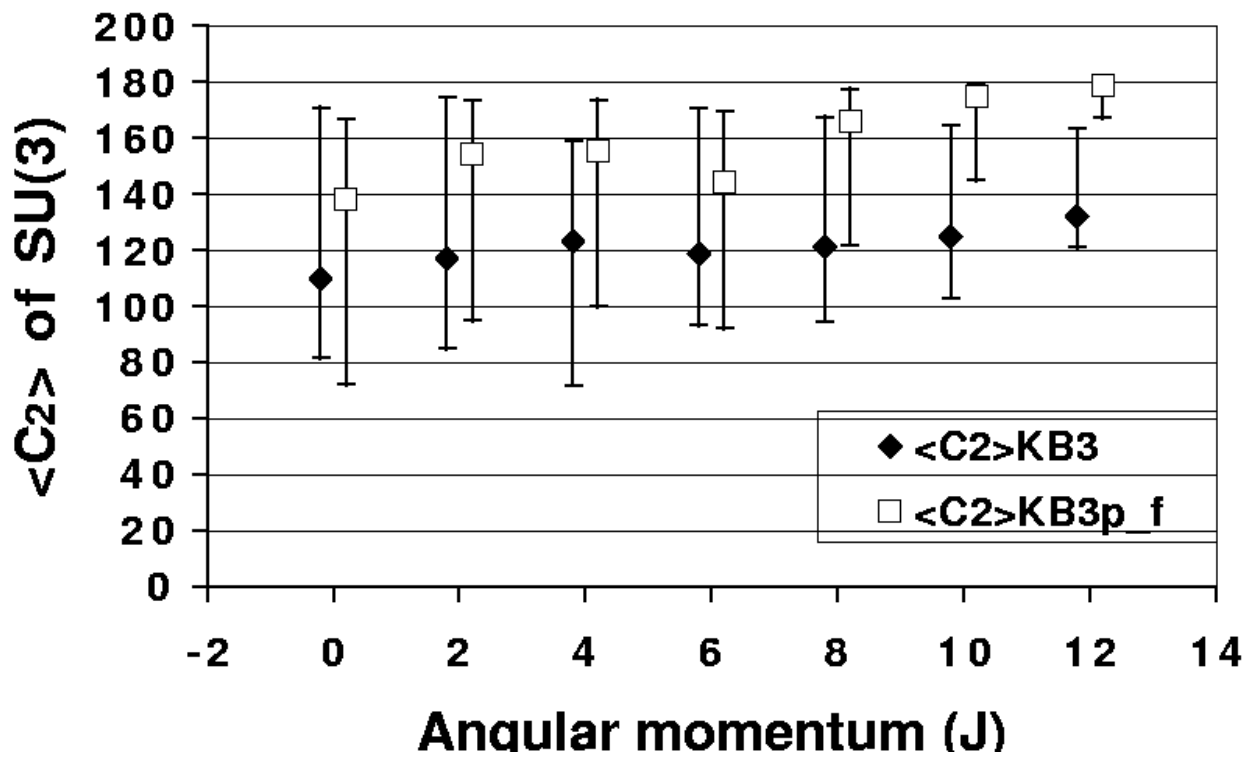


Figure 6.6: Average  $C_2$  values for  $KB3$  and  $KB3p\_f$  interactions in  $^{44}\text{Ti}$ .

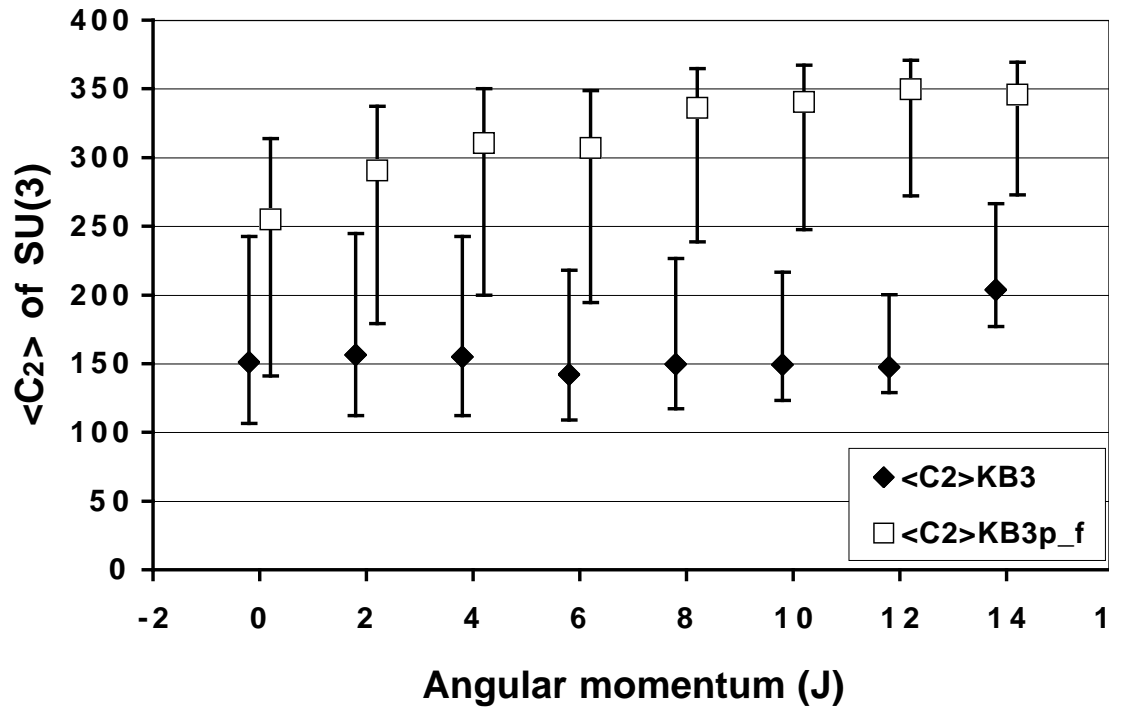


Figure 6.7: Average  $C_2$  values for  $KB3$  and  $KB3p\_f$  interactions in  $^{48}\text{Ti}$ .

state in the presence of the spin-orbit interaction (Fig. 6.4) remain present, even though with reduced strength, in the structure of the state when the spin-orbit interaction is turned off (Fig. 6.5). As a consequence,  $\Delta C_2 = \sqrt{\langle (C_2 - \langle C_2 \rangle)^2 \rangle}$  which measures the overall spread of contributing irreps, is more or less independent of the spin-orbit interaction. One can see a sharp decrease in the width of the distribution only for high spin states like  $J = 12$  in the graph for  $^{44}\text{Ti}$  in Fig. 6.6.

Fig. 6.8 demonstrates the coherent nature of the states within the yrast band. The three graphs shown give the spectrum of the second-order Casimir operator  $C_2$  of  $SU(3)$  for the  $J = 0, 2$  and  $4$  yrast states in  $^{48}\text{Cr}$ . The axes are labelled the same way as in Figs. 6.4 and 6.5, but in this case all bars are for a single yrast state. In this figure there are three peaks surrounded by smaller bars that yield a very similar enveloping shape for the given yrast states. The fragmentation and spread of  $C_2$  values is nearly identical for these states with no dominant irrep, indicative of severe  $SU(3)$  symmetry breaking.

Graphs for the  $KB3p\_f$  case, when the spin-orbit interaction is turned off, are not shown since the results are similar to the results for  $^{44}\text{Ti}$  shown in Fig. 6.5. For example, when the spin-orbit interaction is on (KB3), the leading irrep for  $^{48}\text{Cr}$  has a  $C_2$  value of 396 and this accounts for only around 10% of the total strength distribution (see Fig. 6.8), but when the spin-orbit interaction is off ( $KB3p\_f$ ), the leading irrep is the dominant irrep with more than 55% of the total strength.

We conclude the section with a discussion of the coherent structure of the yrast states by an illustration of the coherent structure of the  $^{48}\text{Cr}$  states within the spherical shell-model basis. The inset (a) of Fig. 6.9 shows the spectral structure of the lowest yrast states ( $J = 0, 2, 4,$  and  $6$ ), as calculated with the KB3 interaction, with respect to the spherical configuration basis. Notice the common spectral distribution of these states. The distribution along the energy configurations, related to excitation energies smaller than the harmonic oscillator spacing ( $< 1\hbar\omega = 10$  MeV), provides an illustration and support of the energy-based configuration truncation scheme. The bump at 12 MeV is probably related to the fact that this is only a  $pf$ -shell calculation ( $0\hbar\omega$ ) which does not include the multi-shell excitations that are at energies above  $1\hbar\omega = 10$  MeV.

### 6.3.4 Enhanced Electromagnetic Transitions.

Our results on the lower  $pf$ -shell nuclei, so far, have shown that  $SU(3)$  symmetry breaking in this region is driven by the single-particle spin-orbit splitting. However, even though states of the yrast band exhibit  $SU(3)$  symmetry breaking, the yrast band  $B(E2)$  values are insensitive to this fragmentation of the  $SU(3)$  symmetry; specifically, the quadrupole collectivity as measured by  $B(E2)$  transition strengths between low-lying members of the yrast band remain high even though  $SU(3)$  appears to be broken.

Relative  $B(E2)$  values are shown in Figs. 6.10, 6.11, and 6.12, that is,  $B(E2)$  strengths normalized to the  $B(E2 : 2^+ \rightarrow 0^+)$  value. For isoscalar transitions, the relative  $B(E2)$  strengths are insensitive to the chosen effective charges which may be used to bring the theoretical  $B(E2 : 2^+ \rightarrow 0^+)$  numbers into agreement with the experimental values. Whenever

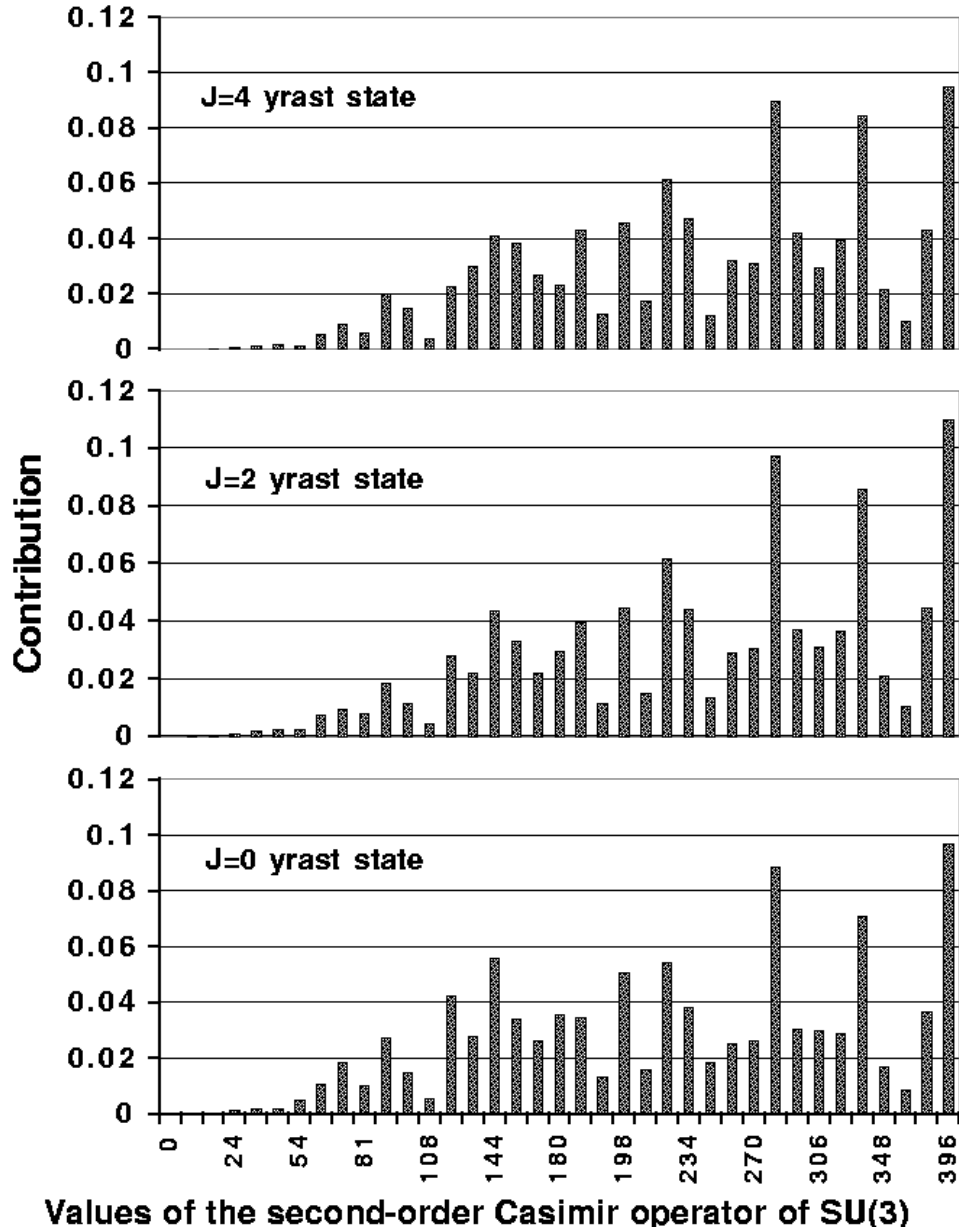


Figure 6.8: Coherent structure of the first three yrast states in  $^{48}\text{Cr}$  calculated using realistic single-particle energies with Kuo-Brown-3 two-body interaction (*KB3*). On the horizontal axis is  $C_2$  of  $SU(3)$  with contribution of each  $SU(3)$  state to the corresponding yrast state on the vertical axis.

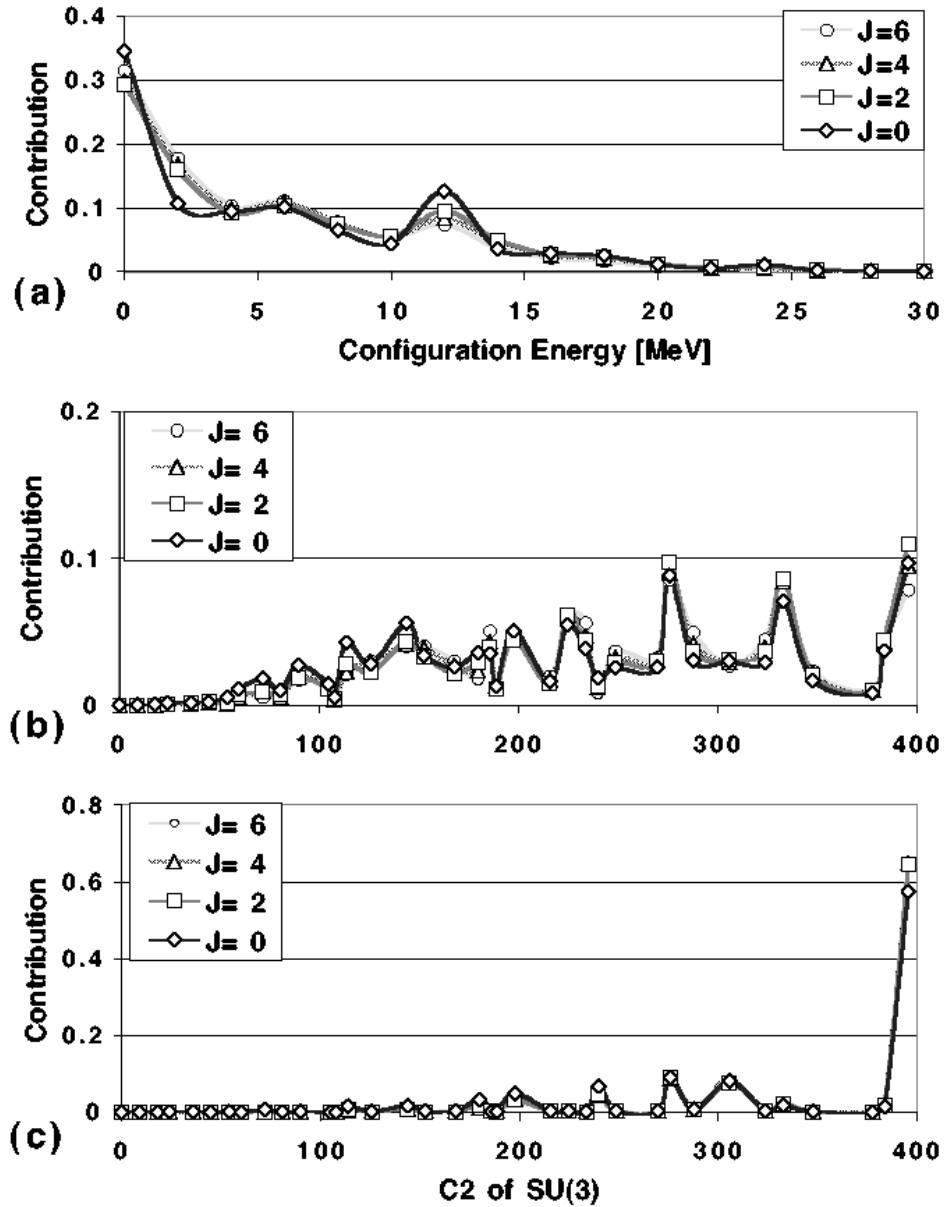


Figure 6.9: Coherent mixing and  $SU(3)$  breaking and recovery in  $^{48}\text{Cr}$ . Inset (a) demonstrates the coherent structure of the yrast states with respect to the spherical shell-model configuration basis (KB3); (b) coherent structure of the yrast states with respect to the  $SU(3)$  basis (KB3); (c) recovery of the  $SU(3)$  symmetry within the  $KB3p_f$  interaction.

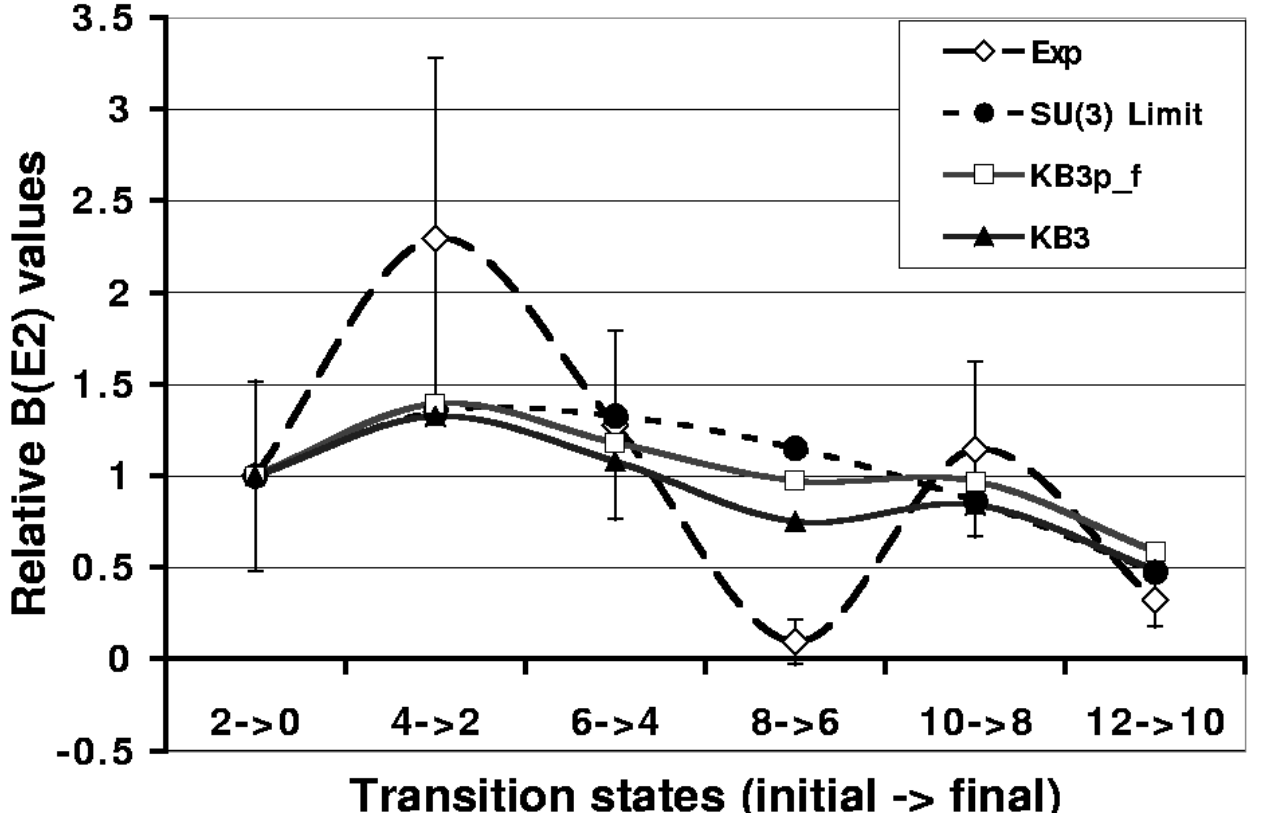


Figure 6.10: Relative  $B(E2)$  values  $\left(\frac{B(E2:J_i \rightarrow J_f)}{B(E2:2^+ \rightarrow 0^+)}\right)$  for  $^{44}\text{Ti}$ . The  $B(E2 : 2^+ \rightarrow 0^+)$  transition values are  $122.69e^2fm^4$  for the experiment,  $104.82e^2fm^4$  for the KB3 interaction, and  $138.58e^2fm^4$  for the  $KB3p\_f$  case.

absolute  $B(E2 : 2^+ \rightarrow 0^+)$  values are given, they are in  $e^2fm^4$  units and the effective charges are  $1.5e$  for protons and  $0.5e$  for neutrons ( $q_{eff} = 0.5$ ).

The first graph on relative  $B(E2)$  values (Fig. 6.10) recaps our results for  $^{44}\text{Ti}$ . Calculated relative  $B(E2)$  values for  $^{44}\text{Ti}$  corresponding to the spin-orbit interaction turned on (KB3) and spin-orbit interaction off ( $KB3p\_f$ ) are very close to the pure  $SU(3)$  limit. The agreement with experiment is very satisfactory except for the  $4^+ \rightarrow 2^+$  and  $8^+ \rightarrow 6^+$  transitions. However, the experimental data [73] on the  $8^+ \rightarrow 6^+$  transition give only an upper limit of 0.5 pico-seconds to the half-life. We have used the worse case, namely a half-life of 0.5 ps, as a smaller value would increase the relative  $B(E2)$ . For example, a half-life of 0.05 ps will agree well with the relative  $B(E2)$  value for the  $KB3p\_f$  interaction. This example supports the adiabatic mixing which seems to be present for all the yrast states of  $^{44}\text{Ti}$ .

Fig. 6.11 shows  $B(E2)$  values for  $^{46}\text{Ti}$ . In this case there are deviations from adiabatic mixing for the  $6^+ \rightarrow 4^+$ ,  $10^+ \rightarrow 8^+$ , and higher transitions. Two experimental data sets are shown in Fig. 6.11: data from the NNDC is denoted as Exp.(NNDC), and updated data

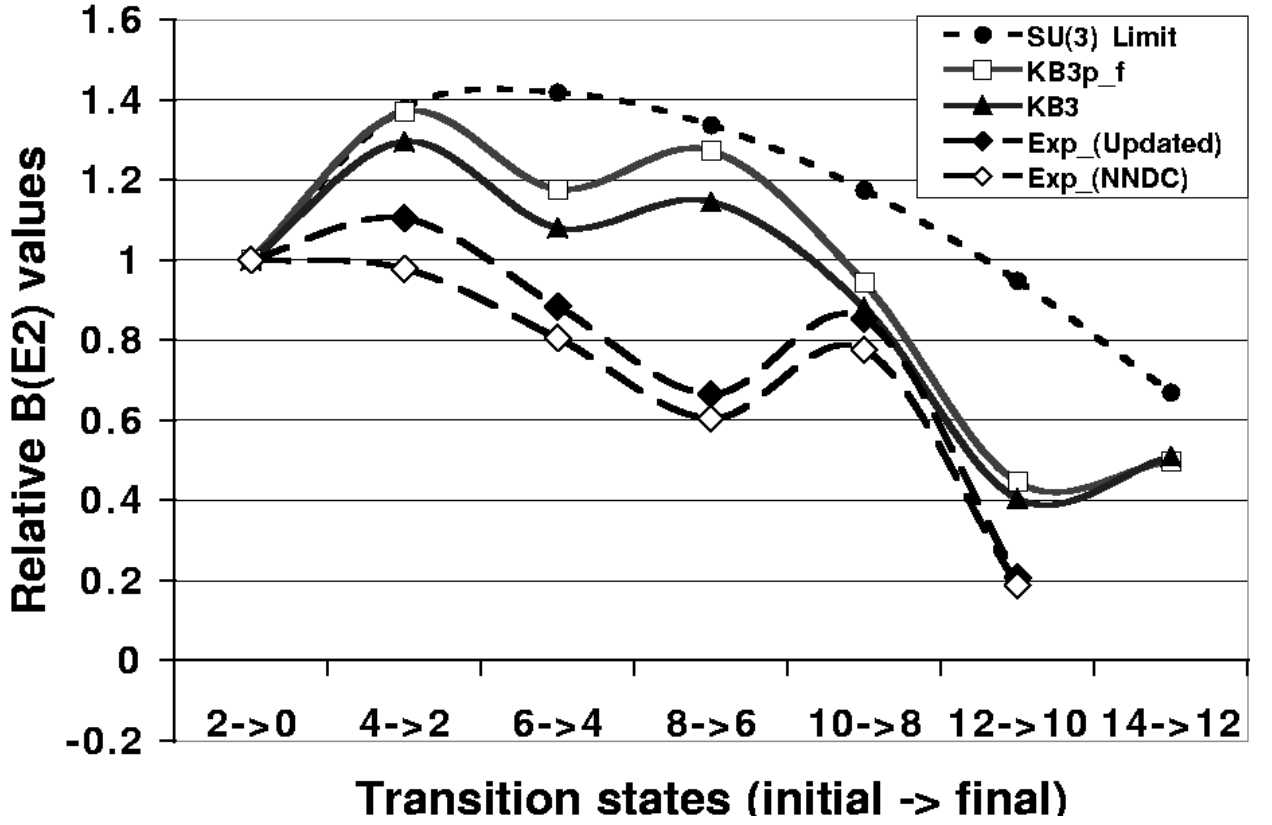


Figure 6.11: Relative  $B(E2)$  values  $\left(\frac{B(E2:J_i \rightarrow J_f)}{B(E2:2^+ \rightarrow 0^+)}\right)$  for  $^{46}\text{Ti}$ . The  $B(E2 : 2^+ \rightarrow 0^+)$  transition values are  $199.82e^2 fm^4$  for the experimental data,  $181.79e^2 fm^4$  for the updated experimental data,  $208e^2 fm^4$  for KB3 interaction, and  $299.83e^2 fm^4$  for  $KB3p\_f$ .

on  $2^+ \rightarrow 0^+$  and  $4^+ \rightarrow 2^+$  transitions from [77] is denoted as Exp\_(Updated). For  $^{46}\text{Ti}$  the agreement with the experiment is not as good as for  $^{44}\text{Ti}$ . However, the experimental situation is also less certain. The adiabatic behavior is well demonstrated for the first three yrast states  $0^+$ ,  $2^+$ , and  $4^+$  via relative  $B(E2)$  values for the KB3 and  $KB3p\_f$  interactions which are very close to the  $SU(3)$  limit.

We conclude this section by showing the recovery of the  $SU(3)$  symmetry; this time via relative  $B(E2)$  values as shown for  $^{48}\text{Ti}$  in Fig. 6.12. In Fig. 6.12 we see that for the degenerate single particle case ( $KB3p\_f$ ) the first few transitions have relative  $B(E2)$  values which follow the  $SU(3)$  limit very closely. On the other hand, the interaction involving spin-orbit splitting (KB3) is far from the  $SU(3)$  limit. The  $B(E2 : 4^+ \rightarrow 2^+)$  transition is strongly enhanced due to the adiabatic mixing which is missing in the higher than  $J = 4$  yrast states.

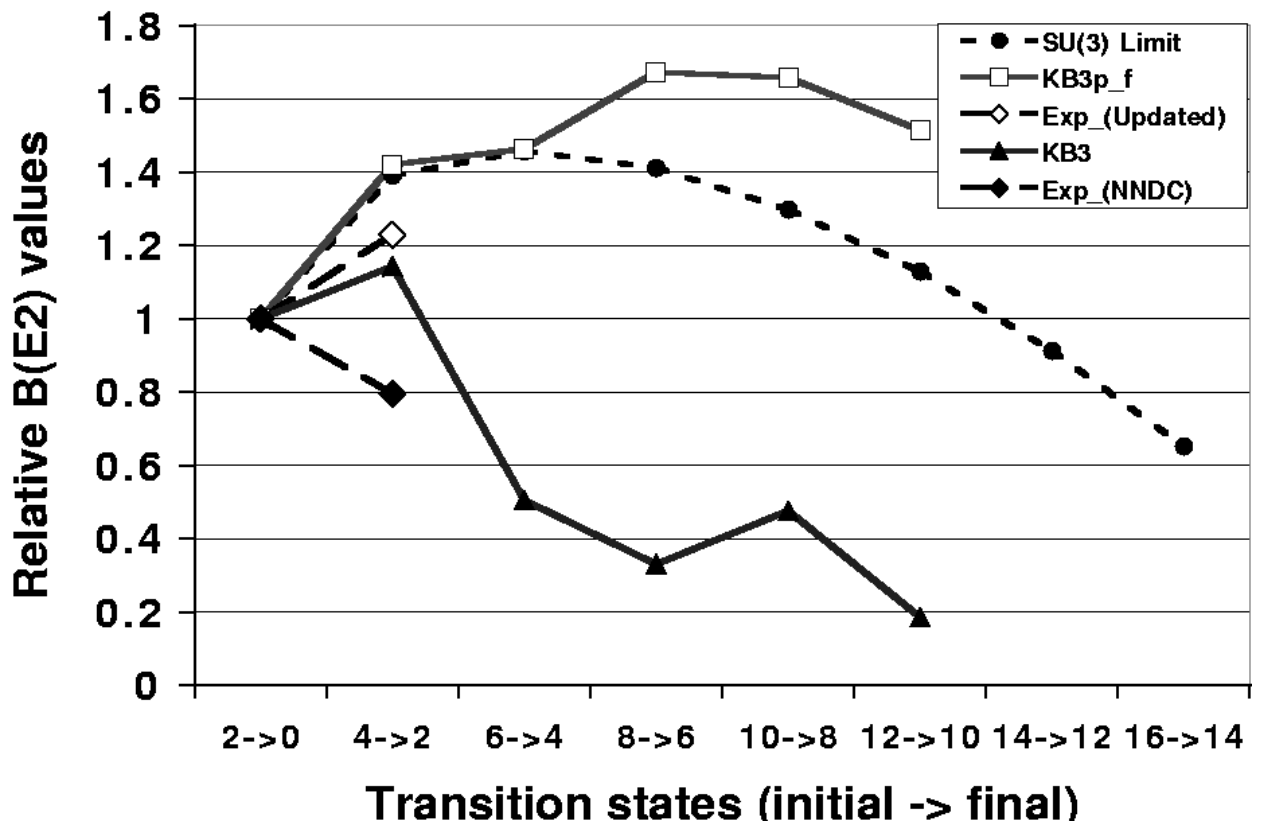


Figure 6.12: Relative  $B(E2)$  values  $\left(\frac{B(E2:J_i \rightarrow J_f)}{B(E2:2^+ \rightarrow 0^+)}\right)$  for  $^{48}\text{Ti}$ . The  $B(E2: 2^+ \rightarrow 0^+)$  transition values are  $144.23e^2fm^4$  for the experimental data,  $155.5e^2fm^4$  for the updated experimental data,  $202.4e^2fm^4$  for KB3 interaction, and  $445.32e^2fm^4$  for  $KB3p\_f$ .

# Chapter 7

## Summary and Discussions

The primary goal of the current work has been to study and apply a new method—the mixed-symmetry approach—for large shell-model calculations. Our aim was to combine two very successful computational methods: the  $m$ -scheme spherical shell model and the  $SU(3)$  shell model. In the process of this study, we have realized a new computational paradigm: an oblique-basis calculation that can be used to capture the mixed-mode structure of complex systems, such as the atomic nuclei.

The two methods, the  $m$ -scheme and  $SU(3)$ , are closely connected to the two dominant but often competing modes that characterize the structure of atomic nuclei: the single-particle shell structure underpinned by the validity of the mean-field concept, and the many-particle collective behavior manifested through the nuclear deformation. This is reflected in two dominant elements in the nuclear Hamiltonian: the single-particle term,  $H_1 = \sum_i \varepsilon_i n_i$ , and a collective two-body term  $H_2$ . The collective term  $H_2$  is dominated by the quadrupole-quadrupole interaction,  $H_{QQ} = Q \cdot Q$  which has good  $SU(3)$  symmetry. It follows that the simplified Hamiltonian  $H = \sum_i \varepsilon_i n_i - \chi Q \cdot Q$  has two exactly solvable limits and thus can be considered to be a two-mode system.

To probe the nature of such a system, we have considered a simple toy model: the one-dimensional harmonic oscillator in a box. As for real nuclei, this system has a finite volume and a restoring force whose potential is of a harmonic oscillator type. For this model, there is a well-defined energy scale which measures the strength of the potential at the boundary of the box,  $E_c = \omega^2 L^2 / 2$ . For this system, the use of two sets of basis vectors, one for each of the two limits, has physical appeal, especially at energies near  $E_c$ . One basis set consists of the harmonic oscillator states; the other set consists of basis states of a particle in a box. In the regime of strong mixing of the two modes at an energy scale compatible with  $E_c$ , there is a coherent structure expressed through a quasi-perturbational behavior of the system. Specifically, in this energy region first-order perturbation theory is not appropriate since the zeroth order approximation to the wave function is very poor; nevertheless, the first-order estimates of the energies are very close to the actual results. Even more, the structure of the exact wave functions exhibits a coherent mixing (Fig. 3.9) similar to the one observed in nuclei (Fig. 6.8).

An application of the mixed-symmetry basis calculations to  $^{24}\text{Mg}$ , using the realistic USD interaction of Wildenthal, has served to demonstrate the validity of the mixed-mode shell-model scheme. In this case, the oblique-basis consists of the traditional spherical states, which yield a diagonal representation of the single-particle interaction, together with collective  $SU(3)$  configurations, which yield a diagonal quadrupole-quadrupole interaction. The results obtained in a space that spans less than 10% of the full-space reproduce the correct binding energy, within 2% of the full-space result, as well as the low-energy spectrum, and the structure of the states within 90% overlap with the exact states. In contrast, for an  $m$ -scheme spherical shell-model calculation, one needs about 60% of the full space to obtain results comparable with the oblique basis results. Calculations for  $^{44}\text{Ti}$  also support the mixed-mode shell-model scheme, even though calculations using a few  $SU(3)$  irreps are not as good as the standard spherical shell-model calculations. And, as the results confirmed, the combined basis yields less enhancements. For example, an oblique-basis calculation in 50% of the full  $pf$ -shell space is as good as a usual  $m$ -scheme calculation in 80% of space. These results show very clearly that if the important modes can be isolated, then one can build an oblique theory that incorporates leading configurations of each mode and could get good convergence in a limited model space.

The study of the lower  $pf$ -shell nuclei  $^{44-48}\text{Ti}$  and  $^{48}\text{Cr}$ , using the realistic Kuo-Brown-3 (KB3) interaction, has shown strong  $SU(3)$  symmetry breaking due mainly to the single-particle spin-orbit splitting. When the spin-orbit splitting is reduced, the importance of the  $SU(3)$  as seen through a growth in the dominance of the leading irrep is restored. Thus the KB3 Hamiltonian is at least a two-mode system. This is further supported by the behavior of the yrast band  $B(E2)$  values that seem to be insensitive to the fragmentation of the  $SU(3)$  symmetry. Specifically, the quadrupole collectivity as measured by the  $B(E2)$  strengths remains high even though the  $SU(3)$  symmetry is rather badly broken. This has been attributed to a quasi- $SU(3)$  symmetry where the observables behave like a pure  $SU(3)$  symmetry while the true eigenvectors exhibit a strong coherent structure with respect to each of the two bases. This has been observed in all yrast states for the  $^{44}\text{Ti}$  case; while for the other nuclei studied, this coherence breaks down after the first few yrast states. In particular, even though the yrast states are not dominated by a single  $SU(3)$  irrep, the  $B(E2 : 4^+ \rightarrow 2^+)$  values remain strongly enhanced with values close (usually within 10-20%) to the  $SU(3)$  symmetry limit.

From a technical point of view, there are some other possible basis sets to be studied.<sup>1</sup> For example, one can try to use deformed Nilsson basis states, or a basis set generated from a Hartree-Fock type procedure [71]. One can even try simple cylindrical basis states with an appropriate procedure to maintain a complete set for good spin quantum numbers. If good

---

<sup>1</sup>In our study,  $SU(3)$  is shown to be good due to the 3D harmonic oscillator and the dominance of the Q.Q interaction in nuclei. The cylindrical basis is just the easiest way to construct the  $SU(3)$  states and seems to be most economical in terms of components. From computational point of view, a good total angular momentum ( $J$ ) and its third component ( $M_J$ ) for the  $SU(3)$  states are essential. However, if one can find any other basis set, besides the  $SU(3)$ -based one, with good  $J$  and  $M_J$ , then things may be as good, or even better.

rotational symmetry is to be sacrificed, then one can try a Lanczos algorithm which keeps only the big components during the iteration process.

Another further development of the theory and its application is a study of other *sd*-shell nuclei as well as *pf*-shell nuclei. Such studies will further test the theory and the codes that have been developed. In spite of the results in the lower *pf*-shell, it is expected that in the mid-shell region some sort of  $SU(3)$  collective structure is important. Thus, the oblique-basis calculation may be an important alternative for calculating structure of nuclei, such as  $^{56}\text{Fe}$  and  $^{56}\text{Ni}$ . Another possibility is to integrate the oblique basis concept into no-core calculations of the type developed by [78]. Such an extension would involve the symplectic group for multi-shell correlations rather than just  $SU(3)$  [79].

An extension of the theory to a multi-mode oblique shell-model calculation is also a possibility. An immediate extension of the current scheme might use the eigenvectors of the pairing interaction [80] within the  $Sp(4)$  algebraic approach to the nuclear structure [81], together with the collective  $SU(3)$  states and spherical shell-model states. Even the three exact limits of the IBM [2] can be considered to comprise a three-mode system.

Further, an even broader extension of the theory would involve a general procedure for the identification of dominant modes from any one- and two-body Hamiltonian along with a complementary partitioning of the model space into physically relevant subspaces with small overlaps. One can then start with eigenstates for an arbitrary subspace and constructively improve the results by including corrections from the remaining subspaces. It should be possible to do this by keeping only a small set of the calculated lowest energy states at each iteration. Hamiltonian-driven basis sets can also be considered. In particular, the method may use eigenstates of the very-near closed shell nuclei obtained from a full shell-model calculation to form Hamiltonian driven J-pair states for mid-shell nuclei [3]. This type of extension would mimic the Interacting Boson Model (IBM) [33] and the so-called broken-pair theory [3]. Nonetheless, the real benefit of this approach is expected when the system is far away from any exactly solvable limit of the Hamiltonian and the spaces encountered are too large to allow for exact calculations.

In summary, we have studied a new computational method, the oblique-basis method. The concept has been applied to a toy model, as well as to some realistic nuclear systems. For realistic nuclei, we used spherical and cylindrical single particle states to perform our mixed-symmetry calculations. We have studied  $^{24}\text{Mg}$  in the *sd*-shell and  $^{44}\text{Ti}$  in the *pf*-shell in a mixed-symmetry basis. For  $^{24}\text{Mg}$ , we have seen very promising results with respect to the energy spectra and the structures of the wave functions. When these results are translated into model space dimensions, we see that an oblique-basis calculation in 10% of the full *sd*-shell space is as good as a usual *m*-scheme calculation in 60% of the full *sd*-shell space. For  $^{44}\text{Ti}$ , the results are less pronounced due to the dominance of the one-body over the two-body part of the Hamiltonian. However, in model space dimensions, the results for  $^{44}\text{Ti}$  state that an oblique-basis calculation in 50% of the full *pf*-shell space is as good as a usual *m*-scheme calculation in 80% of the full *pf*-shell space. Through a detailed study of  $^{44}\text{Ti}$ ,  $^{46}\text{Ti}$ ,  $^{48}\text{Ti}$ , and  $^{48}\text{Cr}$  in the full *pf*-shell, we have confirmed the effect of the one-body part of the Hamiltonian, that is, the strong  $SU(3)$  symmetry breaking is due to the spin-orbit interaction

which splits the single-particle energies. For degenerate single-particle energies, we have seen that one recovers the dominance of the leading  $SU(3)$  irrep which is consistent with two-body interaction dominated by the quadrupole-quadrupole interaction. Along our study, we have seen some interesting coherent structures, such as coherent mixing of basis states, quasi-perturbative behavior in the toy model, and an enhanced  $B(E2)$  strength toward the  $SU(3)$  limit in nuclei.

In concision, the main positive outcome of this work is a prove-of-principle of the mixed-mode concept. We have shown that such calculations are doable and may yield better results and lead to a clearer understanding of complex systems. Problems yet to be solved are related mainly to the software package and its development. First of all, a routine for the complete generation of  $SU(3)$  shell model basis is needed. Basis sets other than the spherical shell-model and  $SU(3)$  shell-model basis sets are also desirable; some possible basis sets have been discussed. Another important software component is a set of commonly used physical observables and their matrix elements. The most important improvement, however, is to implement error estimate of the final results and possible extrapolation procedure for estimating the exact energy eigenvalues. Immediate further work should include a concentrated study of other  $sd$ -shell nuclei,  $pf$ -shell nuclei, and multi-shell calculations. Applications to atomic and molecular physics are also possible.

# Bibliography

- [1] J. P. Elliott, “Symmetries in physics”, ed. P. G. Dawber, Oxford University Press, New York (1979).
- [2] M. Moshinsky and Y. F. Smirnov, “The Harmonic Oscillator in Modern Physics”, Contemporary Concepts in Physics Volume **9**, ed. H. Feshbach, Amsterdam, Harwood Academic Publishing (1996).
- [3] K. L. G. Heyde, “The Nuclear Shell Model”, ed. J. M. Irvine, Springer-Verlag Berlin Heidelberg (1990)
- [4] J. P. Elliott, Proc. Roy. Soc. London, Ser. A **245**, 128 (1958); **245**, 562 (1958); J. P. Elliott and H. Harvey, *ibid* **272**, 557 (1963); J. P. Elliott and C. E. Wilsdon, *ibid* **302**, 509 (1968).
- [5] R. D. Ratnu Raju, J. P. Draayer, and K. T. Hecht, Nucl. Phys. **A202**, 433 (1973); A. Arima, M. Harvey and K. Shimizu, Phys. Lett. **B30**, 517 (1969); K. T. Hecht and A. Adler, Nucl. Phys. **A137**, 129 (1969); R. F. Casten et al, “Algebraic Approaches to Nuclear Structure”, Harwood, New York (1993); A. L. Blokhin, C. Bahri and J. P. Draayer, Phys. Rev. Lett. **74**, 4149 (1995).
- [6] S. G. Nilsson, C. F. Tsang, A. Sobiczewski, Z. Szymanski, S. Wycech, C. Gustafson, I.-L. Lamm, P. Moller, B. Nilsson, Nucl. Phys. **A131**, 1 (1969); K. H. Bhatt, C. W. Nestor Jr. and S. Raman, Phys. Rev. C **46**, 164 (1992); S. G. Nilsson and I. Ragnarsson, “Shapes and Shells in Nuclear Structure”, Cambridge University Press, U. K. (1995).
- [7] V. G. Gueorguiev, J. P. Draayer, and C. W. Johnson, “SU(3) symmetry breaking in lower fp-shell nuclei”, Phys. Rev. C **63**, 014318 (2001).
- [8] V. G. Gueorguiev, W. E. Ormand, C. W. Johnson, and J. P. Draayer, “Mixed-mode shell-model theory for nuclear structure studies”, Phys. Rev. C **65**, 024314 (2002).
- [9] T. Kuo and G. E. Brown, Nucl. Phys. **A114**, 241 (1968); A. Poves and A. P. Zuker, Phys. Rep. **70**, 235 (1981).
- [10] Maria G. Mayer, “On Closed Shells in Nuclei”, Phys. Rev. **74**, 235 (1948).

- [11] Maria Goeppert Mayer, “Nuclear Configurations in the Spin-Orbit Coupling Model. I. Empirical Evidence”, Phys. Rev. **78**, 16 (1950).
- [12] B. H. Wildenthal, Prog. Part. Nucl. Phys. **11**, 5 (1984); *wpn* interaction file from B. A. Brown via <http://www.nsl.msui.edu/~brown/database.htm>.
- [13] Maria Goeppert Mayer, “Nuclear Configurations in the Spin-Orbit Coupling Model. II. Theoretical Considerations”, Phys. Rev. **78**, 22 (1950).
- [14] O. Haxel, J. H. D. Jensen, and H. E. Suess, “On the ”Magic Numbers” in Nuclear Structures”, Phys. Rev. **75**, 1766 (1949).
- [15] J. B. French, “Multipole and Sum-Rule Methods in Spectroscopy”, in International School of Physics “Enrico Fermi”, ed. C. Bloch, Academic Press, varenna on Lake Como, Villa Monastero, Italy (1965); J. B. French, E. C. Halbert, J. B. McGrory, and S. S. M. Wong, Adv. Nucl. Phys. **3**, 237 (1969).
- [16] F. Nowacki and E. Caurier, “coupled code NATHAN”, CRN, Strasbourg (1995); F. Nowacki, Ph. D. Dissertation, Strasbourg, 1996.
- [17] C. Bahri and J. P. Draayer, “SU(3) reduced matrix element package”, Comp. Phys. Comm. **83**, 59 (1994).
- [18] S. C. Park, J. P. Draayer, S. -Q. Zheng, C. Bahri, “Numerical database system based on a weighted search tree”, Comp. Phys. Comm. **82**, 247 (1994).
- [19] B. A. Brown and B. H. Wildenthal, Annu. Rev. Nucl. Part. Sci. **38**, 29 (1988); J. B. McGrory and B. H. Wildenthal, Phys. Lett. **B103**, 173 (1981); A. De-Shalit and I. Talmi, “Nuclear Shell Theory”, Academic Press, London (1963).
- [20] G. H. Golub and C. F. Van Loan, “Matrix Computations”, The Johns Hopkins University Press, Baltimor (1989); J. K. Cullum and R. A. Willoughby, “Lanczos algorithms for large symmetric eigenvalue computations”, Birkhäuser, Boston (1985).
- [21] R. R. Whitehead, “ A numerical approach to nuclear shell-model calculations”, Nucl. Phys. **A182**, 290 (1972); R. R. Whitehead, A. Watt, B. J. Cole, and I. Morrison, “Computational methods for nuclear shell-model calculations”, Adv. Nucl. Phys. **9**, 123 (1977).
- [22] Vesselin G. Gueorguiev and Jerry P. Draayer, Rev. Mex. Fis. **44**, Suplemento **2** (October), 43 (1998)
- [23] K. T. Hecht, Nucl. Phys. **62**, 1 (1965).
- [24] J. Escher, “Electron Scattering Studies in the Framework of the Symplectic Shell Model”, Ph. D. Dissertation, Louisiana State University (1997).

- [25] T. Beuschel, “ M1 Strength Distributions in Deformed Nuclei”, Ph. D. Dissertation, Louisiana State University (1998).
- [26] C. Bahri, “Pairing and Quadrupole Interactions in the Pseudo-SU(3) Shell Model, ”, Ph. D. Dissertation, Louisiana State University (1994).
- [27] T. H. R. Skyrme, “Collective Motion in Quantum Mechanics”, Proc. Roy. Soc. London, Ser. A **239**, 399 (1957).
- [28] C. Lanczos, J. Res. Nat. Bur. Stan. B **45**, 255 (1950).
- [29] F. M. Fernandez, “Introduction to Perturbation Theory in Quantum Mechanics”, Boca Raton Crc Press (2000).
- [30] G. A. Arteca, “Large order perturbation theory and summation methods in quantum mechanics”, Springer-Verlag, New York (1990).
- [31] A. R. P. Rau, “New patterns in atomic spectra”, Nature **325**, No. 6105, 577 (1987).
- [32] A. R. P. Rau, “Astronomy-Inspired Atomic and Molecular Physics”, Kluwer Academic Publishers, Dordrecht (2002).
- [33] F. Iachello, “The interacting boson model”, Cambridgeshire University Press, New York (1987).
- [34] A. Arima and F. Iachello, Phys. Rev. Lett. **35**, 1069 (1975); Ann. Phys. **99**, 253 (1976); Ann. Rev. Nucl. Part. Sci. **31**, 75 (1981).
- [35] Cheng-Li Wu et al, Phys. Rev. C. **36**, 1157 (1987).
- [36] G. B. Armen and A. R. P. Rau, “The limitations of fixed-basis calculations in quantum mechanics”, unpublished.
- [37] K. Heyde, “ Basic Ideas and Concepts in Nuclear Physics”, IOP Publishing, Bristol UK (1994).
- [38] G. Barton, A. J. Bray, and A. J. Mckane, “The Influence of Distant Boundaries on Quantum-Mechanical Energy-Levels”, Am. J. Phys. **58**, No. 8, 751 (1990).
- [39] J. L. Marin and S. A. Cruz, “On the Harmonic-Oscillator Inside an Infinite Potential Well”, Am. J. Phys. **56**, No. 12, 1134 (1988).
- [40] R. Rosas, R. Riera, J. L. Marin and H. Leon, ”Energy spectrum of a confined two-dimensional particle in an external magnetic field”, Am. J. Phys. **68**, No. 9, 835 (2000).
- [41] J. D. Lejarreta, “The generalized harmonic oscillator and the infinite square well with a moving boundary”, J. Phys. A **32**. No. 25, 4749 (1999).

- [42] R. W. Robinett, “Wave packet revivals and quasirevivals in one-dimensional power law potentials”, *J. Math. Phys.* **41**, No. 4, 1801 (2000).
- [43] R. W. Robinett, “Visualizing the collapse and revival of wave packets in the infinite square well using expectation values”, *Am. J. Phys.* **68** (5) 410 (2000).
- [44] D. H. Berman, “Boundary Effects in Quantum-Mechanics”, *Am. J. Phys.* **59**, 937 (1991).
- [45] A. C. Tanner, “The Role of Boundary-Conditions in Separation of Variables - Quantum Oscillator in a Box”, *Am. J. Phys.* **59**, 333 (1991).
- [46] J. L. Marin and S. A. Cruz, “Enclosed Quantum-Systems - Use of the Direct Variational Method”, *J. Phys. B* **24**, No. 13, 2899 (1991).
- [47] J. L. Marin and S. A. Cruz, “On the Use of Direct Variational-Methods to Study Confined Quantum-Systems”, *Am. J. Phys.* **59**, No. 10, 931 (1991).
- [48] V. I. Pupyshev and A. V. Scherbinin, “Molecular energy level shifts in large boxes: use of the Kirkwood-Buckingham method”, *J. Phys. B* **32**, No. 19, 4627 (1999).
- [49] R. Dutt, A. Mukherjee, and Y. P. Varshni, “Supersymmetric semiclassical approach to confined quantum problems”, *Phys. Rev. A* **52**, 1750 (1995).
- [50] C. Monthus, G. Oshanin, A. Comtet, and S. F. Burlatsky, “Sample-size dependence of the ground-state energy in a one-dimensional localization problem”, *Phys. Rev. E* **54**, 231 (1996).
- [51] P. Rochford and D. J. Rowe, *Phys. Lett.* **B210**, 5 (1988); A. P. Zuker, J. Retamosa, A. Poves, and E. Caurier, *Phys. Rev. C* **52**, R1741 (1995); G. Martinez-Pinedo, A. P. Zuker, A. Poves, and E. Caurier, *Phys. Rev. C* **55**, 187 (1997); D. J. Rowe, C. Bahri, and W. Wijesundera, *Phys. Rev. Lett.* **80**, 4394 (1998); C. Bahri, D. J. Rowe, and W. Wijesundera, *Phys. Rev. C* **58**, 1539 (1998); A. Poves, *J. Phys. G* **25**, 589 (1999); C. Bahri and D. J. Rowe, *Nucl. Phys.* **A662**, 125 (2000); D. J. Rowe, S. Bartlett, and C. Bahri, *Phys. Lett.* **B472**, 227 (2000).
- [52] E. Caurier, “Computer code ANTOINE” (CRN, Strasbourg, 1989); E. Caurier, A. P. Zuker, and A. Poves, in “Nuclear Structure of Light Nuclei Far from Stability”, Proceedings of the Obernai Workshop in 1989, ed. G. Klotz, CRN, Strasbourg (1989).
- [53] B. A. Brown, A. Etchegoyen and W. D. M. Rae, “OXBASH: The Oxford-Buenos Aires-MSU shell-model code”, Michigan State University, Cyclotron Laboratory Report No. **524** (1988); A. Etchegoyen, et al, MSU-NSCL Report No. **524** (1985).
- [54] L. Fox, “An Introduction to Numerical Linear Algebra”, Clarendon Press, Oxford (1964); L. Fox and D. F. Mayers, “Computing Methods for scientists and Engineers”, Clarendon Press, Oxford (1968).

- [55] W. H. Press, S. A. Teukolsky, W. T. Vetterling, and B. P. Flannery, “Numerical Recipes in FORTRAN 77: The Art of Scientific Computing”, Volume **1**, Cambridge University Press, Cambridge (1992), <http://www.nr.com>.
- [56] J. P. Draayer, S. C. Park, and O. Castanos, *Phys. Rev. Lett.* **62**, 20 (1989).
- [57] E. Chacon, *Rev. Mex. Fis.* **12**, 57 (1963).
- [58] G. H. Lang, C. W. Johnson, S. E. Koonin, and W. E. Ormand, *Phys. Rev. C* **48**, 1518 (1993); E. Y. Loh, Jr. and J. E. Gubernatis, “Electronic Phase Transitions”, ed. by W. Hanke and Yu. V. KopaeV, Elsevier Science, New York (1992).
- [59] C. A. Ur et al, “Excited states in  $^{52}\text{Fe}$  and the origin of the yrast trap at  $I^\pi = 12^+$ ”, *Phys. Rev. C* **58**, 3163 (1998).
- [60] M. Kaluza, “Analytical Lanczos method: quantum eigenstates of anharmonic oscillators in one or more dimensions”, *Comp. Phys. Comm.* **79**, 425 (1994).
- [61] E. R Davidson, “The Iterative Calculation of a Few of the Lowest Eigenvalues and Corresponding Eigenvectors of Large Real-Symmetric Matrix”, *J. Comp. Phys.* **17**, 87 (1975).
- [62] R. F. Hausman, Jr, “The Origin of Cornelius and Vladimir” in “Strong, Weak, and Electromagnetic Interactions in Nuclei, Atoms, and Astrophysics”, AIP Conference Proceedings 242, Livermore, CA 1991, dedicated to Stew Bloom, ed. G. J. Mathews, American Institute of Physics, New York (1992)
- [63] W. C. Haxton and C. -L. Song, “Morphing the Shell Model into an Effective Theory”, *Phys. Rev. Lett.* **84**, 5484 (2000).
- [64] W. C. Haxton and T. Luu, “Perturbative Effective Theory in an Oscillator Basis?”, [nucl-th/0204072](http://nucl-th/0204072).
- [65] H. Feshbach, “A unified theory of nuclear reactions II”, *Ann. Phys.* **19**, 287 (1962).
- [66] C. Bloch and J. Horowitz, *Nucl. Phys.* **8**, 91 (1958).
- [67] Z. Pluhar, Yu F. Smirnov and V. N. Tolstoy, “A Novel Approach to the  $SU(3)$  Symmetry Calculus”, preprint, Charles University, Prague (1981).
- [68] A. Cortes, R. U. Haq, and A. P. Zuker, *Phys. Lett.* **B115**, 1 (1982).
- [69] V. Zelevinsky and A. Volya, “Randomness and collectivity in nuclear structure: Three theoretical puzzles”, Proceedings of the 7th International Spring Seminar on Nuclear Physics, Maiori, Italy, 2001, World Scientific, Singapore (2001), [nucl-th/0112014](http://nucl-th/0112014).
- [70] T. Mizusaki and M. Imada, “An extrapolation method for shell model calculations”, [nucl-th/0203012](http://nucl-th/0203012).

- [71] C. W. Johnson, I. Stetcu, J. P. Draayer, “SU(3) versus deformed Hartree-Fock”, *Phys. Rev. C* **66**, 034312 (2002), nucl-th/0207017.
- [72] E. Caurier and A. P. Zuker, A. Poves and G. Martínez-Pinedo, *Phys. Rev. C* **50**, 225 (1994); E. Caurier, J. L. Egido, G. Martínez-Pinedo, A. Poves, J. Retamosa, L. M. Robledo, and A. P. Zuker, *Phys. Rev. Lett.* **75**, 2466 (1995); G. Martínez-Pinedo, A. P. Zuker, A. Poves, and E. Caurier, *Phys. Rev. C* **55**, 187 (1997); E. Caurier, G. Martínez-Pinedo, F. Nowacki, A. Poves, J. Retamosa, and A. P. Zuker, “Full  $0\hbar\omega$  shell model calculation of the binding energies of the 1f7/2 nuclei”, *Phys. Rev. C* **59**, 2033 (1999).
- [73] Evaluated experimental nuclear structure data ENSDF, ed. by National Nuclear Data Center, Brookhaven National Laboratory, Upton, NY 11973, USA (as of May 2000). Updated experimental data were obtained via <http://www.nndc.bnl.gov/nndc/nudat/>
- [74] R. R. Whitehead and A. Watt, *J. Phys. G* **4**, 835 (1978); R. R. Whitehead et al, in “Theory and Application of Moment Methods in Many-Fermion Systems”, eds B. J. Dalton et al, Plenum Press, New York (1980); E. Caurier, A. Poves, and A. P. Zuker, *Phys. Lett* **B252**, 13 (1990); E. Caurier, A. Poves, A. P. Zuker, *Phys. Rev. Lett.* **74**, 1517 (1995).
- [75] T. de Forest, Jr and J. D. Walecka, *Adv. Phys.* **15**, 1 (1966); J. D. Walecka, *Muon Physics* **2**, 113 (1975), ed. by V. W. Hughes and C. S. Wu (Academic Press, New York, 1975); T. W. Donnelly and W. C. Haxton, *At. Data Nucl. Data Tables* **23**, 103 (1979); D. R. Bes and R. A. Sorensen, *Adv. Nucl. Phys.* **2**, 129 (1969); M. Dufour and A. P. Zuker, *Phys. Rev. C* **54**, 1641 (1996); S. Cohen, R. D. Lawson, M. H. Macfarlane, S. P. Pandya, and M. Soga, *Phys. Rev.* **160**, 903 (1967).
- [76] Jerry P. Draayer and Yorck Leschber, “Branching Rules for Unitary Symmetries of the Nuclear Shell Model”, Louisiana State University (1987).
- [77] R. Ernst et al, *Phys. Rev. Lett.* **84**, 416 (2000).
- [78] P. Navratil, J. P. Vary, and B. R. Barrett, *Phys. Rev. Lett.* **84**, 5728 (2000); P. Navratil, J. P. Vary, and B. R. Barrett, *Phys. Rev. C* **62**, 054311 (2000).
- [79] J. Escher and J. P. Draayer, *J. Math. Phys.* **39**, 5123 (1998); G. Rosensteel and D. J. Rowe, “On the Algebraic Formulation of Collective Models. III. The Symplectic Shell Model of Collective Motion”, *Ann. Phys. NY*, **126**, 343 (1980).
- [80] J. Dukelsky, C. Esebbag, and P. Schuck, *Phys. Rev. Lett.* **87**, 066403 (2001), cond-mat/0107477.
- [81] K. D. Sviratcheva, A. I. Georgieva, V. G. Gueorguiev, J. P. Draayer, and M. I. Ivanov, *J. Phys. A* **34**, 8365 (2001), nucl-th/0104051.

- [82] Ramon Munoz-Tapia, “Quantum mechanical squeezed state”, Am. J. Phys. **61**, No. 11, 1005 (1993).
- [83] S. Wolfram, “The Mathematica Book”, fourth edition, Wolfram Research, Champaign, IL (2000)

# Appendix A

## On the Wave Function Spread and Localization

In nuclear physics, we often use the three-dimensional harmonic-oscillator (3D HO) potential as a zeroth order approximation to the nuclear mean-field potential. This is usually done in the center-of-mass coordinate system, assuming that all the nucleons experience the same attractive potential,  $H_0 = \sum \left( \frac{\vec{p}_i^2}{2m} + m\Omega^2 \vec{x}_i^2 \right)$  [2]. If we assume the same localization for the nucleons, there seems to be a localization paradox since we are dealing with fermions that must obey the Pauli exclusion principle. However, this apparent paradox is resolved by using many-particle Slater determinant wavefunctions, constructed by filling the single-particle levels of the three-dimensional harmonic-oscillator potential. The Slater determinant form satisfies the Pauli principle requirements and yields different localization structure for each nucleon.

A harmonic-oscillator potential is appropriate near stable equilibrium where the interaction potential should have a local minimum. If rotational invariance applies, then the potential near stable equilibrium should actually be a three-dimensional harmonic-oscillator potential. However, because of the Pauli principle, only the closed-shell nuclei have a spherical shape, other nuclei have non-spherical ground state distributions that can be characterized as oblate, prolate or tri-axial. As a consequence, for non-closed shell nuclei, a deformed three-dimensional harmonic-oscillator potential is a more appropriate “mean field”. This idea is incorporated in the deformed Nilsson model [6]:

$$H = \frac{\vec{p}^2}{2m} + m\Omega^2 \vec{x}^2 + \varepsilon m\Omega^2 x_3^2 + v_u \vec{l}^2 + v_{ls} \vec{l} \cdot \vec{s}.$$

Here,  $\varepsilon$  is a measure of the deformation when  $\vec{l}^2$  and  $\vec{l} \cdot \vec{s}$  provide for the correct shell closures and magic numbers in nuclei.

Large scale numerical calculations usually use basis functions of the three-dimensional harmonic oscillator (3D HO). This way the wave function parameter  $\omega$  will not match the corresponding parameter  $\Omega$  in the Hamiltonian. For example,  $\Omega_z = \Omega\sqrt{1 + \varepsilon}$  may be very different from  $\omega = \Omega$  in super-deformed nuclei. It is therefore interesting to look at the

behavior of the fixed-basis calculations with respect to localization and energy scale for the one-dimensional harmonic oscillator (1D HO).

Here we fix the parameters of the 1D HO Hamiltonian to be  $m = \Omega = \hbar = 1$ . Thus, its spectrum is simple:  $E_n = n + \frac{1}{2}$ . The basis consists of displaced and scaled harmonic-oscillator wave functions,  $\Psi_n((q + \xi)/\sigma)$ ; the  $\xi = 0$  states are squeezed/stretched states, and  $\sigma = 1$  states are coherent states [82]. All the calculations are done using the default settings for Mathematica 4.1 [83].

Fig. A.1 shows the number of the fixed-basis states needed to achieve convergence to the  $10^{-4}$  in the ground-state eigenvalue and eigenvector as a function of the parameter  $\omega$ . The convergence criteria for the eigenvalues requires two successive eigenvalues to be less than the accuracy limit ( $10^{-4}$ ) apart. The convergence criteria for the eigenvectors is  $\|H\Psi - E\Psi\| <$  the accuracy limit. As expected, the eigenvalues converge much earlier than the eigenvectors.

Fig. A.2 (a) shows the first few basis states ( $\omega = 0.2$ ), the harmonic-oscillator potential ( $\Omega = 1$ ), and the true ground-state wave function. Fig. A.2 (b) shows the calculated ground-state wave functions at different dimensions of the basis states with  $\omega = 0.2$ . From these graphs, it is clear that when  $\omega < \Omega = 1$ , Fig. A.2 (a) and (b), one uses more and more basis states to produce the correct wave function behavior within the classically forbidden region. When  $\omega > \Omega = 1$ , Fig. A.2 (c) and (d), the focus is actually concentrated on getting the correct shape of the wave functions within the potential well.

Fig. A.3 is similar to Fig. A.1 but shows the convergence within the displaced (coherent states) harmonic-oscillator wave function basis ( $\Psi_n(q + \xi)$ ). Due to parity conservation, there is a good symmetry under the  $\xi \rightarrow -\xi$  transformation. An example of the basis structure and convergence path similar to Fig. A.2 is shown in Fig. A.4 for  $\xi = -2$ .

Although one should be able to solve any problem in any arbitrarily chosen orthonormal basis, the considerations presented here point to the need for properly modified basis states to reduce the model-space dimension and thus to avoid problems due to numerical noise. In the process of optimizing the basis set for a particular Hamiltonian, the orthogonality of the basis would inevitably be destroyed. In the toy model of a two-mode system, a few possible types of basis-state refinements were considered. Originally, the oblique-basis method was concerned with two or more basis sets as described in the toy model and in nuclear physics applications. However, the idea of the basis refinement can be extended in quite a general way as described in the next section.

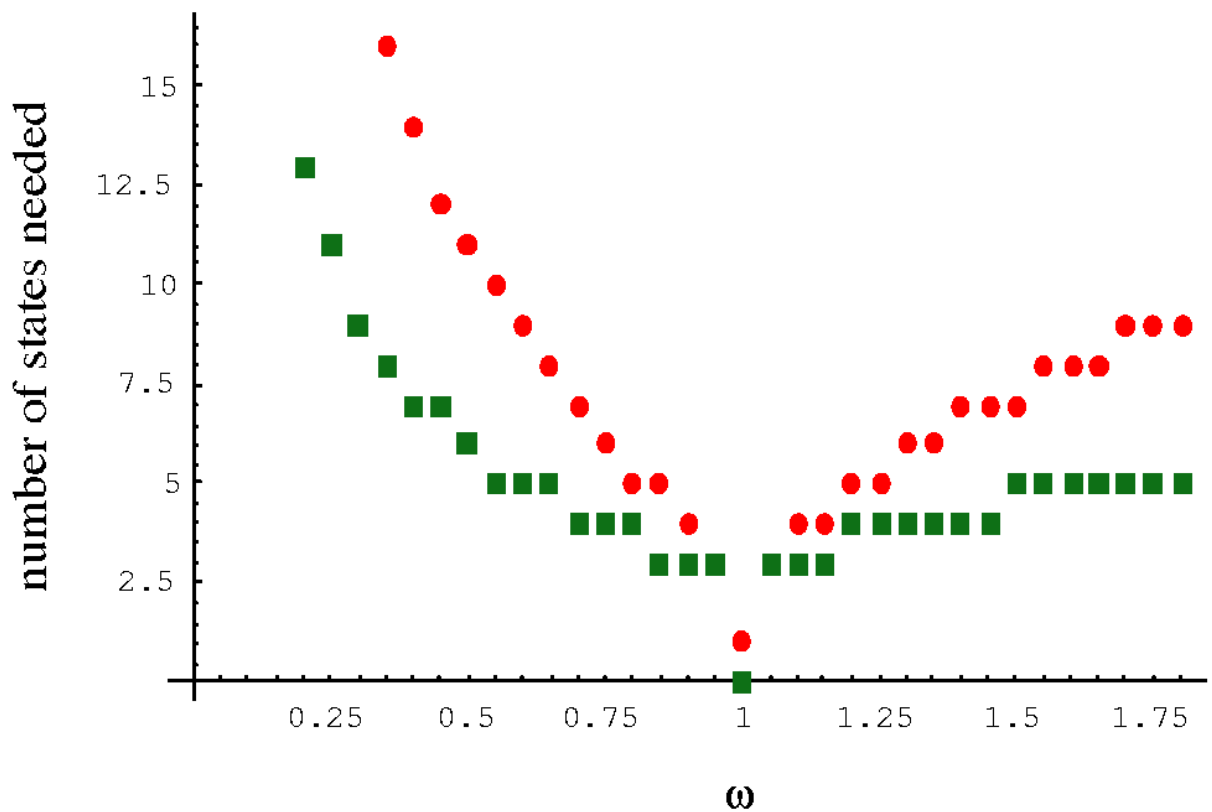


Figure A.1: Ground-state convergence for the harmonic-oscillator problem with  $\Omega = 1$  using squeezed basis states. The number of basis states needed for  $10^{-4}$  convergence accuracy of the ground-state eigenvalue is shown in green squares. The red circles are for the ground-state eigenfunction.

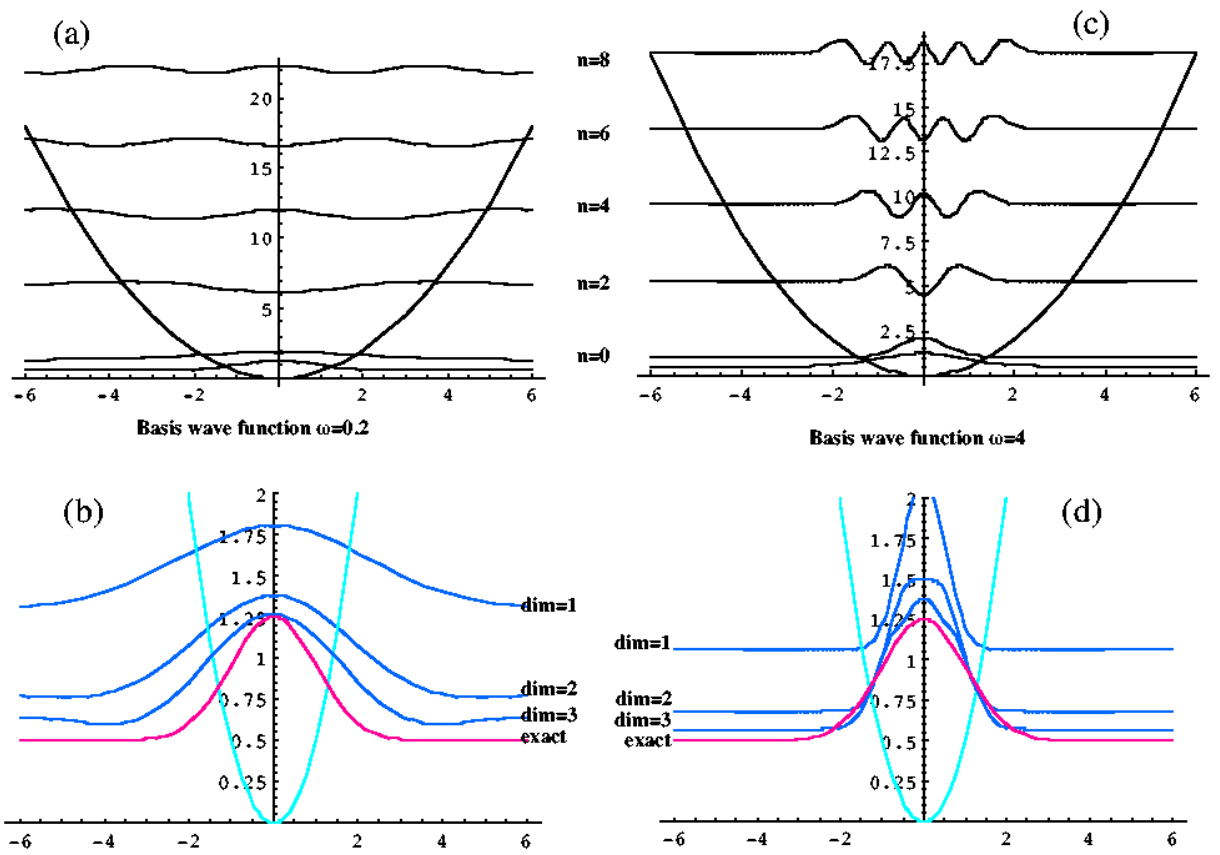


Figure A.2: Role of the wave function spread. (a) Stretched basis states with  $\omega = 0.2$  within the harmonic-oscillator potential  $\Omega = 1$ . (b) Consecutive approximations of the harmonic-oscillator ground state (red) using the stretched basis states. (c) Squeezed basis states with  $\omega = 4$  within the harmonic-oscillator potential  $\Omega = 1$ . (d) Consecutive approximations of the harmonic-oscillator ground state (red) using the squeezed basis states.

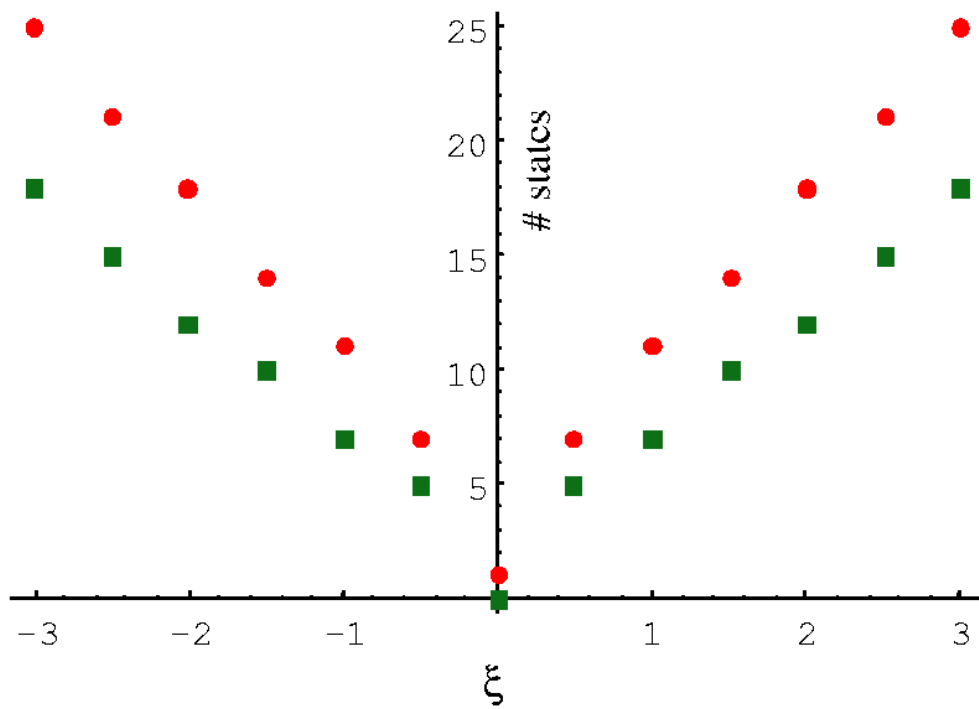


Figure A.3: Ground-state convergence for the harmonic-oscillator problem with  $\Omega = 1$  using coherent basis states. The number of basis states needed for  $10^{-4}$  convergence accuracy of the ground-state eigenvalue is shown with the green squares. The red circles are for the ground-state eigenfunction.

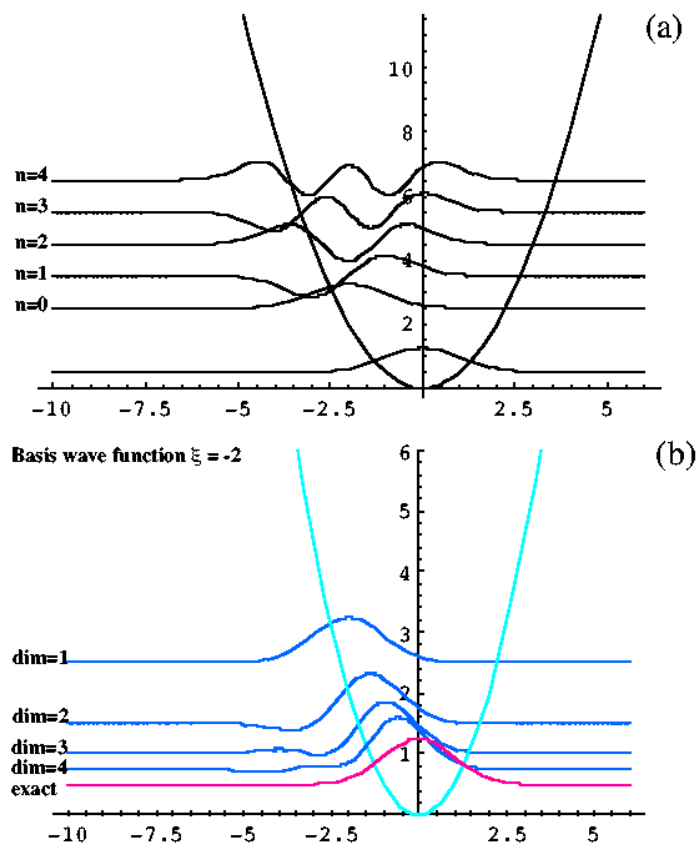


Figure A.4: Role of the wave function localization. (a) Coherent basis states with displacement  $\xi = -2$  within the harmonic-oscillator potential  $\Omega = 1$ . (b) Consecutive approximations of the harmonic-oscillator ground state (red) using the coherent basis states.

# Appendix B

## Variationally-Improved Basis Method

The usual fixed-basis method can be derived from the Rayleigh-Ritz variation principle. If one considers minimization of  $E(\vec{c})$  with respect to  $\vec{c}$  for a Hamiltonian ( $H$ ) using the basis states  $\phi_n(x; \omega)$ :

$$E[\vec{c}] = \langle \Psi | H | \Psi \rangle - \lambda(\vec{c} \cdot \vec{c} - 1), \quad \Psi(x) = \sum_n c_n \phi_n(x; \omega)$$

of a Hermitian operator  $Y(\omega)$  such that

$$Y(\omega) \phi_n(x; \omega) = Y_n \phi_n(x; \omega),$$

then  $\delta E[\vec{c}]/\delta c_n^* = 0$  is equivalent to solving the matrix eigenvalue problem  $\sum_m H_{nm} c_m = \lambda c_n$ , where  $H_{nm} = \langle \phi_n | H | \phi_m \rangle$ , and thus the set of  $\lambda$ s provides information for the eigenvalues of  $H$ . If the set  $\{\phi_n\}$  is taken to be non-orthogonal, then we have a generalized eigenvalue problem  $\sum_m (H_{nm} - \lambda \mu_{nm}) c_m = 0$  where  $\mu_{nm} = \langle \phi_n | \phi_m \rangle$ .

Notice that there is a freedom that we have not yet specified: it is the choice of  $\omega$  and  $Y(\omega)$ . Here,  $\omega$  is the set of parameters characterizing the Hermitian operator  $Y(\omega)$ . Usually one fixes  $\omega$  from experience or by simply applying Rayleigh-Ritz variation with respect to  $\omega$  in  $E[\omega] = \langle \phi_0(\omega) | H | \phi_0(\omega) \rangle$ . Thus, we have an orthonormal basis  $\phi_n$  with the same  $\omega$  for any  $n$ . One can try other procedures for fixing  $\omega$  and  $Y(\omega)$  as well [27].

All this seems fine as long as the spectrum of  $H$  is expected to be similar to the spectrum of  $Y(\omega)$ , but what if the potential for  $Y(\omega)$  does not match the “landscape” of the potential for  $H$ . For example, would the harmonic-oscillator potential wave functions be appropriate for solving an anharmonic potential problem or a double-well potential? In principle, one should be able to use any basis, but it may be at the expense of long and tedious calculations. Therefore, we may try to let  $\omega$  be a free parameter for different basis functions  $\phi_n$ . Then we can find  $\omega_n$  by variation of  $E[\omega] = \langle \phi_n(\omega) | H | \phi_n(\omega) \rangle$ .

Often  $\omega$  is related to the relevant energy scale. If we start with the correct wave function, but with the ‘wrong’ parameters, then clearly a variational approach on the parameters will give us the right answer immediately.

In the case of the harmonic-oscillator wave functions, one can argue that a calculation with a varying  $\omega$  is equivalent to a multi-shell calculation with a fixed  $\omega$  parameter. Since the harmonic-oscillator basis is a complete basis, then each function  $\phi_n(x, \omega_n)$  can be expanded in the basis associated with  $\Omega$ , for example:

$$\phi_n(x, \omega_n) = \sum_k c_n^k \phi_k(x, \Omega).$$

Therefore,  $\phi_n(x, \omega_n)$  can be viewed as the result of a multi-shell calculation with the harmonic-oscillator parameter  $\Omega$ .

Next, we discuss how in general one can refine any initial basis set so that each basis vector in the new and improved basis is the optimal one with respect to the Hamiltonian under consideration. Then, instead of refining the basis vectors, one can effectively renormalize the parameters in the Hamiltonian.

The main idea is to optimize each trial vector by applying the Rayleigh-Ritz variational principle on  $E[\Psi, A]$ :

$$E[\Psi, A] = \langle A\Psi | H | A\Psi \rangle, \quad \delta E[\Psi, A] = 0,$$

where  $A$  represents the affine group  $A$  in  $\mathbf{R}^n$ . An element  $a$  of  $A$  has a rotational component  $r$  and a translational component  $t$ , so that  $(ax)_j = r_i^j x_j + t_j$ .

If  $G$  is the symmetry group of  $H$ , then:

$$g^{-1} H g = H, \quad g \in G.$$

Therefore, the Rayleigh-Ritz variational principle should be applied with respect to the homogeneous space  $M = A/G$  that excludes the symmetry transformations  $G$ . For example, a translational symmetry of  $H$  means that scaling and rotation are the relevant transformations. Since the physical systems usually have rotational and translational symmetry, then only scaling is left as a relevant operation for constructing a variationally-improved basis:

$$\Psi(x_1, \dots, x_n) \rightarrow \Psi(sx_1, \dots, sx_n).$$

The transformation  $|\Psi\rangle \rightarrow |A\Psi\rangle$  can be defined to maintain the normalization of the states:

$$\Psi(x) \rightarrow A\Psi(x) = \sqrt{\det(r)} \Psi(rx + t).$$

However, this transformation is not a unitary transformation in general, and therefore, it will not map orthonormal states into a new set of orthogonal states. Using scaling as a variational parameter has been done previously. Specifically, in the context of the confined systems it was used by Martin and Cruz to study hydrogen and helium enclosed in a spherical shell [47], [46].

If  $\int dy = \int \det(r) dx$  is used when  $y = rx + t$ , then the variationally-improved basis can be treated as a renormalization problem for the Hamiltonian  $H$ :

$$\begin{aligned} E[\Psi, A] &= \langle A\Psi | H | A\Psi \rangle = \int \det(r) \Psi^*(rx + t) H(p, x) \Psi(rx + t) dx = \\ &= \int \Psi^*(y) H(rp, r^{-1}(y - t)) \Psi(y) dy. \end{aligned}$$

Rescaling in the above way seems to be related more to the scaling methods in condensed matter physics. For example, consider the one-dimensional harmonic oscillator:

$$H = \frac{1}{2}P^2 + \frac{1}{2}Q^2.$$

Then, the equation for the scale parameter  $s$  from  $E[\Psi, s]$  when  $\Psi(x) \rightarrow \sqrt{s}\Psi(sx)$  is:

$$\begin{aligned} E[\Psi, s] &= \frac{1}{2}s^2 \langle P^2 \rangle + \frac{1}{2} \frac{1}{s^2} \langle Q^2 \rangle, \\ \frac{\partial E[\Psi, s]}{\partial s^2} &= 0 \Rightarrow s^2 = \sqrt{\frac{\langle Q^2 \rangle}{\langle P^2 \rangle}} = \frac{\Delta q}{\Delta p}. \end{aligned}$$

Here,  $\langle Q^2 \rangle = \langle \Psi | Q^2 | \Psi \rangle$  and  $\Delta q = \sqrt{\langle Q^2 \rangle}$ . It is assumed that  $\Psi$  is such that  $\langle Q \rangle = \langle P \rangle = 0$ , which means that the localization of the wave function has been selected. Evaluating  $E[\Psi, s]$  at the extremum  $s^2 = \Delta q / \Delta p$  gives:

$$E[\Psi] = \Delta q \Delta p.$$

Finally, using  $[p, q] = -i \Rightarrow \Delta q \Delta p \geq \frac{1}{2}$ , we find that the minimum of the energy is exactly the zero point energy for the harmonic oscillator  $E_0 = \frac{1}{2}$ . Notice that quantum mechanics was only used to provide us with a constraint on the fluctuations of the observables  $q$  and  $p$ ; other than that, we can consider the system as purely statistical. Thus, different  $\Delta q \Delta p$  will give different value of  $E[\Psi]$ . Turning this argument around, we would expect  $\Delta q \Delta p \geq (n + \frac{1}{2})$  when  $\Delta q$  and  $\Delta p$  are evaluated in the space of wave functions with  $n$ -nodes.

Another interesting way to obtain the same result is to use  $H$  expressed in terms of the operators  $a^+$  and  $a$ . Then, by using coherent states as trial wave functions  $a|z\rangle = z|z\rangle$  we have  $E[z] = |z|^2 + \frac{1}{2}$  and thus  $E_0 = \frac{1}{2}$ .

# Appendix C

## On the Loss of Hermiticity

When the choice of the basis is not carried out with appropriate attention, an operator, supposedly Hermitian, may acquire a non-hermitian matrix realization within this basis. For example, a wrong basis may produce a non-Hermitian matrix for the Hamiltonian under consideration. Although this is unlikely to be encountered within the finite shell-model calculations using an occupation number representation, it is an obstacle when one wishes to use a hard core potential and a harmonic-oscillator basis [2].

Here we discuss the problem of a free particle in a one-dimensional box in the harmonic-oscillator basis. In order to proceed, we notice that the Hilbert space for the harmonic oscillator is not quite the same as for the free particle in a one-dimensional box. This is clear from the domains of the wave functions. The harmonic-oscillator wave functions are defined on the whole real axis  $\mathbf{R}^1$ , when the wave functions for a free particle in a box are defined on a finite interval  $[-L, L]$ . This discrepancy is easily fixed by projecting the harmonic-oscillator wave functions onto the interval  $[-L, L]$ , which changes the inner product for the wave functions:

$$(f, g) = \int_{-\infty}^{\infty} f^*(x) g(x) dx \rightarrow \int_{-L}^L f^*(x) g(x) dx.$$

However, in this basis the matrix corresponding to  $H$  will be nonhermitian in general.

To understand the loss of hermiticity, we look at the off-diagonal matrix elements of the momentum operator ( $P = -i\hbar \frac{\partial}{\partial q}$ ):

$$\begin{aligned} (\Psi_m, P\Psi_n) &= \int_{-L}^L \Psi_m^*(q) (P\Psi_n(q)) dq = \int_{-L}^L \Psi_m^*(q) \left(-i\hbar \frac{\partial \Psi_n(q)}{\partial q}\right) dq = \\ &= i\hbar \int_{-L}^L \frac{\partial(\Psi_m^*(q)\Psi_n(q))}{\partial q} dq + i\hbar \int_{-L}^L \frac{\partial \Psi_m^*(q)}{\partial q} \Psi_n(q) dq = \\ &= i\hbar (\Psi_m^*(q)\Psi_n(q))|_{-L}^L + \int_{-L}^L \left(-i\hbar \frac{\partial}{\partial q} \Psi_m(q)\right)^* \Psi_n(q) dq = \end{aligned}$$

$$= i\hbar (\Psi_m^*(q)\Psi_n(q))|_{-L}^L + (P\Psi_m, \Psi_n).$$

It is clear from the above expression that the *hermiticity will be maintained only when all of the basis functions are zero<sup>1</sup> at the boundary of the interval [-L,L]*. This condition is essential for solving exactly the quantization of a free particle in a one-dimensional box.

---

<sup>1</sup>Wave functions with the same value at  $\pm L$  is a necessary condition; wave functions should be zero at  $\pm L$  only for an infinite potential.

# Appendix D

## Coherent Behavior, Quasi-Symmetries and Quasi-Labels

Recently the notion of a quasi-symmetry and adiabatic mixing has been introduced in nuclear physics [51]. The toy model of a harmonic oscillator in a one-dimensional box can be used to introduce and illustrate one possible definition of a quasi-symmetry, an asymptotic label (quasi-label), and a coherent behavior associated with a quasi-symmetry.

First, we define a similarity relation of two states  $|\Phi\rangle$  and  $|\Psi\rangle$  with respect to some Hermitian operator  $\mathcal{H}$ , and denote it as:

$$|\Phi\rangle \stackrel{\mathcal{H}}{\sim} |\Psi\rangle.$$

In this approach, the operational definition of such a similarity relation uses the eigenvectors  $|\mathcal{H}; \Lambda\rangle$  and the eigenvalues  $\Lambda$  of  $\mathcal{H}$ :

$$\mathcal{H} |\mathcal{H}; \Lambda\rangle = \Lambda |\mathcal{H}; \Lambda\rangle.$$

We would say that  $|\Phi\rangle$  and  $|\Psi\rangle$  are  $\mathcal{H}$  similar ( $|\Phi\rangle \stackrel{\mathcal{H}}{\sim} |\Psi\rangle$ ), if there is a function  $f$ , eventually monotonic, that maps the distribution  $\rho_\Phi(\Lambda) = |\langle \mathcal{H}; \Lambda | \Phi \rangle|^2$  to  $\rho_\Psi(\Lambda) = |\langle \mathcal{H}; \Lambda | \Psi \rangle|^2$  so that:

$$|\rho_\Phi(\Lambda)|^2 \approx |\rho_\Psi(f(\Lambda))|^2.$$

In simple words, this means that the shape of the probability distribution  $\rho_\Phi$  is similar to the shape of the probability distribution  $\rho_\Psi$ .

If  $G$  is a symmetry group for the operator  $\mathcal{H}$ , then the eigenspace for a given  $\Lambda$  may be degenerate, and any function  $|\Phi\rangle$  obtained from  $|\Psi\rangle$  by a unitary transformation  $U \in G$  ( $|\Phi\rangle = U |\Psi\rangle$ ) will be  $\mathcal{H}$  similar to  $|\Psi\rangle$ . Thus,  $G$  defines an intrinsic symmetry for the wave functions that are similar to  $|\Psi\rangle$ . Therefore,  $|\Psi\rangle$  can be viewed as an “intrinsic state” with respect to the symmetry of  $\mathcal{H}$ .

In the case when  $\mathcal{H}$  is one of the exact limits of a Hamiltonian  $H$ , i.e.  $H = \mathcal{H} + \lambda^{-1}V$ , then one can define an adiabatic mixing of the states  $|\mathcal{H}; \Lambda\rangle$  due to the interaction  $V$ . An

asymptotic label (quasi-label)  $\Lambda$  can be assigned to each eigenvector  $|\Psi; \lambda\rangle$  of  $H = \mathcal{H} + \lambda^{-1}V$  in the limit  $\lambda \rightarrow \infty$ :

$$\mathcal{H} |\Psi; \Lambda, \lambda \rightarrow \infty\rangle = \Lambda |\Psi; \Lambda, \lambda \rightarrow \infty\rangle$$

thus,

$$|\Psi; \Lambda, \lambda\rangle \rightarrow |\mathcal{H}; \Lambda\rangle, \quad \text{when } \lambda \rightarrow \infty.$$

Assigning  $\Lambda$  by using the natural order of the levels must be done carefully by tracing the sign of each level crossing.

Once the asymptotic label  $\Lambda$  has been assigned for a state  $|\Psi\rangle$ , then a coherent behavior with respect to an observable can be defined as well. There is a quasi-symmetry  $\mathcal{H}$  for the observable  $O : |\Psi\rangle \rightarrow \mathbf{R}$ , if its value  $O [|\Psi; \Lambda, \lambda\rangle]$  does not depend much on the parameter  $\lambda$ :

$$O [|\Psi; \Lambda, \lambda\rangle] \approx O [|\mathcal{H}; \Lambda\rangle].$$

Some common functions for  $O [|\Psi; \Lambda, \lambda\rangle]$  are related to the expectation values of  $O$  :

$$\langle \Psi; \Lambda, \lambda \rightarrow \infty | O | \Psi; \Lambda, \lambda \rightarrow \infty \rangle \approx \langle \Lambda | O | \Lambda \rangle.$$

In general, a coherent behavior with respect to other quantities can be defined as well. For example, a relative transition rate from a state  $|\Psi; J\rangle$  to a state  $|\Psi; J + 2\rangle$  due to a transition operator, say  $E2$ , can be defined, say by using  $B(E2, \Psi, J)$ , where  $\Psi$  is the ‘‘intrinsic state’’ upon which the band is built. All the states within the band should actually be within the class of  $\mathcal{H}$  equivalent states. In particular, the asymptotic label  $\Lambda$  can be used as a band label.

Notice that, as in the toy model studied, it may happen that at finite  $\lambda$  the wave function  $|\Psi\rangle$  has been assigned label  $\Lambda$  while its components along the space  $|\mathcal{H}; \Lambda\rangle$  are practically missing. Following the results from the toy model, we can define some possible types of spectral structures that may exhibit such coherent behavior with respect to a Hamiltonian  $H = \mathcal{H} + V$ , and thus to specify a quasi-symmetry.

Specifically, setting  $\lambda = 1$ ,  $H = \mathcal{H} + V$  has a quasi-symmetry if:

$$\begin{aligned} H |\Psi; \Lambda_n\rangle &= E(\Lambda_n) |\Psi; \Lambda_n\rangle, \\ \mathcal{H} |\Lambda_n\rangle &= \Lambda_n |\Lambda_n\rangle, \quad \Lambda_{n+1} > \Lambda_n, \\ \Lambda_n &> \langle \Lambda_n | V | \Lambda_n \rangle > \Lambda_{n+1} - \Lambda_n, \\ E(\Lambda_n) &\approx \langle \Lambda_n | H | \Lambda_n \rangle. \end{aligned}$$

Here,  $\Lambda_n$  is the corresponding asymptotic label of the state  $|\Psi; \Lambda_n\rangle$ . The term  $\langle \Lambda_n | V | \Lambda_n \rangle > \Lambda_{n+1} - \Lambda_n$  means that  $V$  mixes strongly different  $|\Lambda_n\rangle$  states. Therefore, *perturbation theory cannot be applied in the usual small perturbation regime*. However,  $\Lambda_n > \langle \Lambda_n | V | \Lambda_n \rangle$  together with  $E(\Lambda_n) \approx \langle \Lambda_n | H | \Lambda_n \rangle = \Lambda_n + \langle \Lambda_n | V | \Lambda_n \rangle$  means that the spectral structure of  $H$  in this region is similar to the spectral structure of  $\mathcal{H}$  within a few percent:

$$\frac{E(\Lambda_n) - \Lambda_n}{E(\Lambda_n)} \approx \frac{\langle \Lambda_n | V | \Lambda_n \rangle}{\Lambda_n + \langle \Lambda_n | V | \Lambda_n \rangle} \approx \frac{\langle \Lambda_n | V | \Lambda_n \rangle}{\Lambda_n} < 1.$$

This seems to be the situation discussed in the toy model case. Since  $\Lambda_n \sim n^2$ , then  $2\Lambda_n > \Lambda_{n+1}$  gives  $(n - 1)^2 > 8$  which is always satisfied for  $n > 4$ .

# Appendix E

## Guide to the Oblique-Basis Package

Although most of the routines<sup>1</sup> in the *Oblique-Basis Package 2002* can be compiled by using the *makefile* routines provided, there is a need to follow a few simple steps in order to be able to carry out oblique-basis calculations. Here we describe some of the technical problems and their solutions that one may face in using the *Oblique-Basis package 2002*. The process of running an oblique-basis calculation consists of four main steps which are described below:

- (1) selecting and generating basis states (*nuke*, *PNGGMJ*),
- (2) preparing interaction file(s) (*IsoInt2pn*, *MakeInteractions*),
- (3) evaluating matrix elements for the chosen interactions (*su3pn*),
- (4) solving the generalized eigenvalue problem which includes: obtaining the eigenvectors of the Hamiltonian, calculating expectation values and transition probabilities for some desired operators (*GLanczos*).

In the parentheses are given the names of some relevant routines. Some current limitations of the *Oblique-Basis package 2002* are related to the single-particle basis currently employed in the computations. In its present form, the main routine *su3pn*, which is used to evaluate the matrix elements of the operators (step 3 above), is set to operate on spherical and cylindrical single-particle states. This clearly restricts the basis generation process (step 1 above) to the same type of states (spherical and cylindrical). Even though the spherical and cylindrical single-particle states are of special interest, the code could, at least in principle, be changed to operate on other desirable single-particle states, such as those one can obtain via Hartree-Fock procedure.

---

<sup>1</sup>The *Oblique Basis package 2002* is available from the author upon request.

## E.1 Generating Basis States

Since the oblique-basis idea is to combine two or more basis sets, the oblique-code package has been designed to use basis states generated and used by other shell-model packages. The two main codes in mind are: a version of the Glasgow code, which performs calculations in the spherical shell-model basis, and the SU(3) RME code, which performs calculations in the SU(3) shell-model basis using cartesian (cylindrical) single-particle states.

**Spherical Shell-Model States.** To generate spherical shell-model basis states one needs to run the Glasgow code (*nuke* located in the folder *Glasgow – code*) with the desired configuration limits and with *IBASIS* = -1 in the appropriate interaction file (*\*.int*). For more details see the example file *BasisOnly.int* and files *Glasgow.int – instructions* or *Instructions Glasgow test9.doc*. There is a script file, *RunGlasgow.sc*, which one may find useful when running *nuke*. This script file uses head files (*\*.head*) and an interaction file (*\*.int*) to construct different input files (*\*.inp*) for *nuke*.

The wave functions from *nuke* are stored in the file *fort.60* (see *Basis – states.info* for its structure). This file is used by *GlsqwBasis2Redstick*, located in the folder *Oblique – Glasgow*, to produce file *fort.35* which contains the spherical shell-model basis states and the single-particle states data. If *nuke* (Glasgow) is used to calculate the eigenvectors of a Hamiltonian, then these eigenvectors are extracted from file *fort.60* into file *fort.36*.

**Important note:** File *fort.11* is very important pre-generated file. This file (*fort.11*) is used by *nuke* and *GlsqwBasis2Redstick*. **Do not lose the file *fort.11*!**

**Tip:** In oblique runs of the *su3pn* code, consider using sorted spherical shell-model states. Such states are produced by the *EpsSorting* code located in the folder *Oblique/SphToCyl*.

**SU(3) Shell-Model States.** Even though the C. Bahri’s SU(3) RME code may provide the SU(3) highest weight states in the near future, the *Oblique -Basis package 2002* has its own highest-weight state generator for some of the most important SU(3) irreps. The SU(3) related fortran codes are in the folder *SU3Generator*.

The current highest weight state generator *SU3\_HWS\_GEN* is located in a folder with the same name. Before using *SU3\_HWS\_GEN*, one may need to run the auxiliary code *SU3Lister* which would help in the HWS selection process. The *SU3Lister* code also generates the necessary cylindrical single-particle states (file *cylin.sps*) that are needed in the evaluation of matrix elements of operators through the *su3pn* code.

**Important note:** Before doing any runs, compile file *fort.4* using *SU3GENBK* located in the folder *ProjectLibrary*.

**Tip:** By comparing the output of the *SU3Lister* with the output of the *genwsirl*, one can determine the irreps that are not generated by the generator *SU3\_HWS\_GEN*.

Once the highest weight states are created, they are stored in a file with extension *\*.hws*. This file is used as input file to the SU(3) code *PNGGMJ* located in the sub-folder *PNGGMJ*. The code *PNGGMJ* generates two files containing basis states *\*.su3* and *\*.bas*. It also generates a file *PNGGMJ-Brief-Info.log* which contains information that may be

used to set the parameters **max\_nbas\_su3** and **maxmpc** for the *su3pn* code. The *\*.su3* file has some of the SU(3) related information and is usually used in testing tools which are located in the sub-folder *ProjectTools*. The *\*.bas* file is mainly for use by the *su3pn* code.

## E.2 Generating Interaction Files

Even though there are a few the realistic interactions commonly used (KB3, Wildenthal...), their format files may differ significantly. Interactions given in the isospin format as used by the Glasgow code can be transformed into the proton-neutron format by using the code *IsoInt2pn* located in the folder *Oblique – Glasgow*.

Often used schematic interactions are also available through a package called *MakeInteractions* made by Dr. C. Johnson. *MakeInteractions* allows one to generated combinations of frequently studied nuclear interactions. The menu of the currently available interactions is:

- (0) Random noise (TBRE, two-body random ensemble),
- (1) Pairing,
- (2) Multipole-multipole (you choose L),
- (3)  $S^2$  (total spin),
- (4)  $L^2$  (total orbital angular momentum),
- (5)  $J^2$  (total angular momentum),
- (6)  $L*S$  (spin-orbit) 1+2 body.

## E.3 Running the Main Routines

**Evaluating Matrix Elements of Operators.** Usually, the running of programs takes considerable time. Thus, it is better to use a script file for such runs. Some example script files are *RunSu3pn + GLDriver.sc* and *RunSu3pnGLanzos.sc*. Basically, the input of the *su3pn* code requires the following entries to be specified:

- > name of the file containing single-particle levels with extension *\*.sps*,
- > scaling of the two-body matrix elements  $(A/B)^X$ ,
- > interaction file (*\*.int*),
- > name of the file containing cylindrical single-particle levels (*\*.sps*),
- > name of the file containing the su3 basis states (*\*.bas*)

- > name of the file containing the ssm basis states (\*.bas)
- > desired name for the output files (\*.ham and \*.ovr)

**Eigenvectors, Expectation Values and Transition Matrix Elements.** After generation of the Hamiltonian and operator matrices, and the overlap matrices (if needed), which are stored in files with extensions \*.ham and \*.ovr, one has to run the generalized Lanczos code (*GLanczos*) to obtain the eigenvalues, eigenvectors, expectation values, and transition matrix elements. There is a script file *RunGLDriver.sc* which may be used.

# Vita

Vesselin Gueorguiev was born on May 27, 1967, in Sofia, Bulgaria. He started his physics career at age 15 while attending the National Natural Science High School in Sofia, Bulgaria, where he received a diploma with a physics major as a Semiconductor Production Operator. He continued his studies in physics at the University of Sofia, St. Kliment Ohridski in Sofia, Bulgaria, where he majored in nuclear and elementary particle physics and received a master of science degree in 1992. He was then employed as a research-assistant at the Department of Theoretical Physics in the Institute of Nuclear Research and Nuclear Energy of the Bulgarian Academy of Sciences, Sofia, Bulgaria. His Doctor of Philosophy degree in nuclear physics will be awarded by Louisiana State University in December, 2002.

During his graduate school years, he attended many workshops and conferences and presented his research results at the 1998 and 2000 International Symposia in Nuclear Physics at Oaxtepec, México, the April 2000 and 2001 annual meetings of the American Physical Society, the 2000 and 2002 International Workshops on Nuclear Theory in Bulgaria, the 2001 annual meeting of the Division of Computational Physics of the American Physical Society, the 2002 Nuclear Structure Conference: Mapping the Triangle in Wyoming, and the 2002 International Colloquium on Group Theoretical Methods in Physics, Paris, France. He was a visiting scientist at the Institute for Nuclear Theory at the University of Washington in Seattle in October of 2000. He is the recipient of several awards from Louisiana State University, including a Graduate School Dissertation Fellowship, Coates Travel Award, and Graduate School Tuition Waiver. He is the author of 14 publications, including four abstracts, and three submitted papers.